INAUGURAL – DISSERTATION

zur

Erlangung der Doktorwürde

der

Naturwissenschaftlich-Mathematischen

Gesamtfakultät

der

Ruprecht-Karls-Universität

Heidelberg

Vorgelegt von:
Master of Science in Engineering Zhiyong Liu
aus: Yueyang, China

Tag der mündlichen Prüfung: June 03, 2016

THEMA

Improved Understanding of the Linkages and Interactions between Vegetation, Climate, Streamflow and Drought: Case Studies in Germany

Gutachter: Prof. Dr. Lucas Menzel (Ruprecht-Karls-Universität Heidelberg)

Gutachterin: PD Dr. Kerstin Stahl (Albert-Ludwigs-Universität Freiburg)

Summary

Global climate change has significantly impacted the terrestrial ecosystems and water cycles over the past century. This dissertation aims to further improve our knowledge of the linkages and interactions between vegetation, climate, streamflow, and drought. First, the current study investigated long-term variations in vegetation and climatic variables and their scale-dependent relationships by using Rhineland-Palatinate (Southwest Germany) as a case study area. Based upon the monthly normalized difference vegetation index (NDVI), precipitation and temperature data for six different vegetation types in two precipitation regimes (low and high precipitation regimes) of Rhineland-Palatinate, the temporal trends in the original time series of these variables and their relationships were examined. In addition, the further objectives were to evaluate which time-scale is dominantly responsible for the trend production found in the original data and find out the certain time-scales that represent the strongest correlation between NDVI and climatic variables (i.e., precipitation and temperature). A combined approach using the discrete wavelet transform (DWT), Mann-Kendall (MK) trend test and correlation analysis was implemented to achieve these goals. The trend assessment in the original data shows that the monthly NDVI time series for all vegetation types in both precipitation regimes have upward trends, most of which are significant. The precipitation and temperature data for six vegetation types in two precipitation regimes present weak downward trends and significant increasing trends, respectively. The most important time-scales contributing to the trend production in the original NDVI data are the 2-month and 8-month events. For precipitation, the most influential ones are 2-month and 4-month scales. The 4-month periodic mode predominantly affects the trends in the original temperature data. The results indicate temperature is the primary driver influencing the vegetation variability over this study area, while there is a negative correlation between NDVI and precipitation for all vegetation types and precipitation regimes. For the scale-dependent relationships between NDVI and precipitation, the 2-month

and 8-month scales generally present the strongest negative correlation. The most significant positive correlation between NDVI and temperature is obtained at the 8- and 16-month scales for most vegetation types. The results might be valuable for water resources management as well as agricultural and ecological development planning in Rhineland-Palatinate, and also offer a helpful reference for other regions with similar climate condition.

Then, this study presented a detailed regional investigation of the probabilistic and multi-scale relationships between streamflow and hydroclimatic variables (precipitation, temperature and soil moisture) and the potential links to large-scale atmospheric circulations over Baden-Württemberg, Southwest Germany. First, the joint dependence structure between seasonal streamflow and hydroclimatic variables was established using copulas. On the basis of the joint dependence structure, this study estimated the probability (risk) of hydrological droughts and floods conditioned upon two different scenarios of hydroclimatic variables for different seasons over the study area. Then, it was evaluated how the relationships between hydroclimatic forcings and streamflow vary among different temporal scales using wavelet coherence. The results reveal that the strong positive coupling between streamflow and both precipitation and soil moisture occurs at most temporal scales, particularly at decadal scales, while the multi-scale relationships between temperature and streamflow are significantly weak compared to precipitation and soil moisture. The connections between streamflow variability and large-scale atmospheric circulations were explored by using composite analysis. Although the atmospheric circulation patterns vary in different seasons, it can be found that the high streamflow anomalies for most seasons over Baden-Württemberg are related to strong westerly atmospheric circulations that play an important role in favoring the warm and moist air from the North Atlantic Ocean towards the study area and thus enhancing the precipitation. Moreover, the low streamflow anomalies are generally linked to the northerly circulations that induce the movement of cold air from northern Europe towards this study area and thus result in the reduced precipitation.

Finally, a general probabilistic prediction network was developed in this dissertation

for hydrological drought examination and environmental flow assessment. This methodology is divided into three major components. First, the joint streamflow drought indicator (JSDI) was proposed to describe the hydrological dryness/wetness conditions based on the monthly streamflow data. The JSDI relies on a high-dimensional (12-d) multivariate probabilistic model to establish a joint distribution model. In the second part, the drought-based environmental flow assessment method was introduced, which provides dynamic risk-based information about how much flow (the environmental flow target) is required for drought recovery and its likelihood under different hydrological drought initial situations. The final part involves estimating the conditional probability of achieving the required environmental flow under different precipitation scenarios according to the joint dependence structure between streamflow and precipitation. Two catchments in Germany were used to examine the usefulness of this network. The results show that the JSDI can provide an overall assessment of hydrological dryness/wetness conditions and does well in identifying both drought onset and persistence. The method also allows quantitative prediction of targeted environmental flow that is required for hydrological drought recovery and evaluates the corresponding risk. In addition, the results confirm that the general network can estimate the conditional probability associated with the required flow under different precipitation scenarios. The presented methodology offers a promising tool for water supply planning and management and for environmental flow assessment. The network has no restrictions that would prevent it from being applied to other basins worldwide.

Keywords: NDVI; climatic variables; multi-scale relationship; hydrological drought; atmospheric circulations; probabilistic prediction network; environmental flow assessment; Germany

Zusammenfassung

Der globale Klimawandel hat deutlich die terrestrischen Ökosysteme und Wasserkreisläufe im vergangenen Jahrhundert beeinflusst. Diese Dissertation zielt darauf ab, unsere Kenntnisse über die Zusammenhänge und Wechselwirkungen zwischen Vegetation, Klima, Hydrologie, und Trockenheit zu verbessern.

Der erste Teil dieser Studie untersuchte die langfristigen Veränderungen der Vegetation und der Klimavariablen und ihre maßstabsabhängigen Beziehungen in Rheinland-Pfalz (Südwest-Deutschland). Basierend auf dem monatlichen normierten Differenzvegetationsindex (NDVI), Niederschlags- und Temperaturdaten für sechs verschiedene Vegetationstypen in zwei Niederschlagsregimes (niedrige und hohe Niederschlagsregimes), untersuchte diese Studie die zeitlichen Trends in der ursprünglichen Zeitreihe dieser Variablen und ihrer Beziehungen. Darüber hinaus wurden die verschiedenen Zeithorizonte nach ihrem Einfluss auf die Trendentwicklung evaluiert, um hierdurch die stärksten Korrelationen zwischen NDVI und den Klimavariablen (u.a. Niederschlag und Lufttemperatur) zu identifizieren. Hierfür wurde ein kombinierter Ansatz aus diskreter Wavelet-Transformation (DWT), Mann-Kendall (MK) Trendtest und Korrelationsanalyse verwendet. Die Trendermittlung im ursprünglichen Datensatz zeigt, dass die monatlichen NDVI Zeitreihen für alle Vegetationstypen in beiden Niederschlagsregimen statistisch signifikante Aufwärtstrends aufweisen. Die Temperatur- und Niederschlagsdaten beider Niederschlagsregime einen schwachen Abwärtstrend bzw. eine signifikante Erhöhung des Trends auf. Die wichtigsten Zeitskalen für die Trendentwicklungn der ursprünglichen NDVI-Daten liegen im Bereich von 2 bzw. 8 Monaten. Während für den Niederschlag die 2- Monats und 4-Monats-Skalen am einflussreichsten waren, so zeigte für die Temperatur lediglich die 4-Monatsskala einen signifikanten Einfluss.

Die Korrelationsanalyse zwischen den Klimaparametern und dem NDVI zeigt für alle Niederschlagsregime und Vegetationstypen eine positive Korrelation für die Temperatur und eine negative für den Niederschlag. Betrachtet man dies auf

verschiedenen Zeitskalen, so sind die negativen Korrelationen zwischen Niederschlag und NDVI für die 2- und 8-Monatsskalen besonders stark ausgeprägt Die wichtigsten positiven Korrelationen zwischen NDVI und Temperatur zeigen die 8- bis 16-Monatsskalen für die meisten Vegetationstypen.

Die Ergebnisse der Arbeit können für das Wasserressourcenmanagement in Rheinland-Pfalz verwendet werden, und bieten eine hilfreiche Referenz für andere Regionen mit ähnlichen klimatischen Bedingungen.

Im zweiten Teil dieser Studie wurden detaillierte regionale Untersuchungen der probabilistischen und multiskalen Beziehungen zwischen Abfluss und hydroklimatischen Variablen (Niederschlag, Temperatur und Bodenfeuchte) und mögliche Verbindungen zu großräumigen atmosphärischen Zirkulationen über Baden-Württemberg, durchgeführt. Zunächst wurde die gemeinsame Abhängigkeitsstruktur zwischen saisonalem Abfluss und hydroklimatischer Variablen per Copula Methodik analysiert. Auf Grundlage gemeinsamer Abhängigkeitsstrukturn konnten in zwei verschiedenen Szenarien, die Wahrscheinlichkeiten (Risiko) für hydrologische Dürren und Überschwemmungen anhand hydroklimatischer Variablen für verschiedene Jahreszeiten geschätzt werden. Im Anschluss wurden die Beziehungen zwischen hydroklimatischem Antrieb und Abflussänderung bei unterschiedlichen Zeitskalen-Wavelet-Kohärenzen untersucht. Die Ergebnisse zeigen, dass starke positive Kopplungen zwischen Abfluss und sowohl Niederschlag als auch Bodenfeuchte auf sämtlichen Zeitskalen aber besonders stark in der dekadischen Zeitskal existieren. Im Gegensatz hierzu sind die multiskalen Beziehungen zwischen Temperatur und Abfluss deutlich schwächer ausgeprägt.

Im dritten Teil dieser Arbeit wurden die Verbindungen zwischen Abflussschwankungen und großräumigen atmosphärischen Zirkulationen anhand von Verbundanalysen untersucht. Als Untersuchungsgebiet diente Baden-Württemberg, da hier die Datenverfügbarkeit größer war als im ursprünglichen Untersuchungsgebiet. In der Regel werden Abflussanomalien mit hohen Abflüssen mit Großwetterlagen mit westlicher Strömung in Zusammenhang gebracht, die warme, feuchte Luftmassen aus dem Nordatlantik in Richtung Untersuchungsgebiet bringen und somit zu starken

Niederschlagsereignissen führen können. Abflussanomalien mit niedrigen Abflüssen sind hingegen mit nördlichen Strömungen n verbunden, die kalte und trockene Luft aus Nordeuropa ins Untersuchungsgebiet bringen unzu geringen Niederschlägen führen.

Im letzten Teil der Dissertation wurde ein allgemeiner probabilistischer Vorhersageansatz zur Vorhersage von hydrologischen Dürren entwickelt. Dieser Ansatz wurde in drei Hauptkomponenten unterteilt. Erstens wurde ein "joint streamflow drought indicator" (JSDI) entwickelt um die hydrologischn Trocken/Feucht Bedingungen basierend auf monatlichem Abflussdaten zu beschreiben. Der JSDI beruht auf einem hochdimensionalen (12-d) multivariaten Wahrscheinlichkeitsmodell. Zweitens wurde eine dürrebasiert Bewertungsmethode eingeführt, welche dynamische risikobasierte Informationen darüber bietet, wieviel Abfluss für eine Minderung bzw. Erholung von einer hydrologischen Dürre benötigt wird. Der dritte Teil schätzt die bedingte Wahrscheinlichkeit, ob die erforderlichen Abflüsse zur Minderung der hydrologischen Dürre in unterschiedlichen Niederschlagsszenarien eintreten werden. Für die Analysen wurden zwei Flusseinzugsgebiete in Deutschland verwendet, um die Anwendbarkeit dieses Ansatzes zu evaluieren.

Die Ergebnisse zeigen, dass die JSDI zur Gesamtbeurteilung der hydrologischen Trocken/Feucht Bedingungen geeignet ist und bei der Identifizierung von Trockenheitbeginn und –dauer gute Ergebnisse erzielen kann. Das Verfahren ermöglicht zudem quantitative Vorhersagen für die benötigten klimatischen Rahmenbedingungen zur Erholung von hydrologischen Dürren. Darüber hinaus bestätigen die Ergebnisse, dass der Ansatz die bedingte Wahrscheinlichkeit mit der erforderlichen atmosphärischen Strömung unter verschiedenen Niederschlagsszenarien schätzen kann. Die vorgestellte Methode bietet ein vielversprechendes Werkzeug für die Planung und das Management der Wasserversorgung. Es bestehen keine Restriktionen, die eine Anwendung auf andere Flussgebiete verhindern würde.

Acknowledgment

Completion of this doctoral dissertation was under the support of some important people in my life. I would like to express my heartfelt gratitude to all of them.

First of all, I would like to gratefully and sincerely thank my supervisor Prof. Dr. Lucas Menzel for his guidance, patience, and support during my graduate studies in Heidelberg. I appreciate all his contributions of work, time, and ideas to make my doctoral study fruitful and stimulating, as well as the chance to learn from his research expertise. Prof. Menzel encouraged me to not only grow as a hydrologist but also as an independent thinker. He granted me the opportunity to develop my own individuality with such independence, and provided me valuable suggestions, feedback, and consistent encouragement throughout my research work.

I am very thankful to my colleagues: Matthias Stork, Chunyu Dong, Benjamin Kopp, Stefanie Minderlein, Munkhdavaa Munkhjargal, and Tobias Törnros for their time, constructive feedback, valuable discussions and accessibility. I was inspired a lot through their academic interactions and advices at various aspects of my research topic.

I would like to deeply thank my family (parents, my sister, my little niece and nephew) for their love, sacrifices, encouragement, and support.

Moreover, I would like to thank the China Scholarship Council for the financial support to my doctoral study.

Table of contents

List of figures

List of tables

Mathematical and physical notations

wavelet

ψ	mother wavelet
γ	translation factor (time step) of the wavelet
s	wavelet scale (scale factor)
s_0	specified fixed dilation step
γ_0	location parameter
$W_\psi(j,k)$	wavelet coefficient. j and k are integers that control the wavelet dilation (scale factor) and translation, respectively
R_n	wavelet coherence
$\Im$	smoothing operator determined by the wavelet type
$W_n^X(s)$	wavelet transform functions of time series X
$W_n^{XY}(s)$	cross-wavelet spectrum of X and Y

Mann-Kendal (MK) test

S	statistic of MK test
Z	standardized test statistic of MK test
t_j	the number of data in the jth (tied) group
x_k and x_i	variables
e_r	relative error

copula

C	copula function
$F_{X,Y}(x,y)$	bivariate distribution
$F_X(x)$	cumulative distribution function (CDF) of X
S_n	Cramér-von Mises statistics
C_{emp}	empirical copula

C_θ	parametric copula
$F_{X \le x \mid Y=y}$	conditional non-exceedance distribution of $X \le x$ given $Y= y$
$F\ (x_1,...,,x_n)$	*n*-dimensional multivariate joint distribution function
H	multivariate CDF
F_i	CDF of the *i*th margin
F_i^{-1}	the corresponding inverse function
ϕ	generator of the copula
ϕ^{-1}	inverse of generator
f_k	marginal densities
$c_{i,i+j\mid 1:(i-1)}$	bivariate copula densities

Abbreviations

AIC	Akaike information criterion
AMS	American meteorological society
CCF	cross-correlation function
CDF	cumulative distribution function
chi2	chi-squared
CPC	climate prediction center
CPs	circulation patterns
CZI	China-Z index
CWT	continuous wavelet transform
DWD	Deutscher Wetterdienst
DWT	discrete wavelet transform
ENSO	El Niño–Southern Oscillation
EOF	empirical orthogonal function
GIMMS	global inventory modeling and mapping studies
IPCC	intergovernmental panel on climate change
JDI	joint deficit index
JSDI	joint streamflow drought indicator
K-S	Kolmogorov-Smirnov
LVBW	Landesverband Baden-Württemberg
MK	Mann-Kendall
MRE	mean relative error
MSDI	multivariate standardized drought index
MVC	maximum value compositing
NAO	North Atlantic Oscillation
NASA	national aeronautics and space administration
NCEP/NCAR	national centers for environmental prediction/national center for atmospheric research
NDVI	normalized difference vegetation index
NOAA	national oceanic and atmospheric administration
PCs	principal components
RAI	rainfall anomaly index
SRI	standardized runoff index
SSI	standardized streamflow index
SWSI	surface water supply index
VCI	vegetation condition index
WTC	wavelet coherence

Chapter 1: Introduction

1.1 General introduction

Changes in climate have resulted in the altered water cycles on regional and global scales, thus directly impacting the ecosystems and socio-economic activities humans depend on. It has been widely recognized that vegetation, climate and streamflow are crucial components in the water cycle and they are dynamically affected by each other. In general, there exists a strong connection between climate and vegetation zones on a global scale, such as the dry subtropics related with subtropical deserts, zones of temperate climate with temperate/boreal forests, and the humid tropics with the tropical forests (Brovkin, 2002). Vegetation covers a major part of the Earth and includes all plants from trees to bushes and grass which play a significant role in the water cycle. Climate determines the primary types of terrestrial vegetation, e.g., coniferous forest, grassland, and desert. Terrestrial vegetation could act as a sensitive indicator of climatic and environmental changes at various spatial regions (Chuai et al., 2013; Zhang et al., 2003). In turn, vegetation also exerts some degree of impact on climate and weather through evapotranspiration, water conductivity, albedo, atmospheric gas composition, and physical feature of land surfaces (Brovkin, 2002). It is thus desirable to investigate the relationship between vegetation and climate in order to provide better understanding of future ecosystem dynamics under varying climate conditions, especially considering the disparity in various vegetation types.

Climate variability also affects the sustainability and availability of the water resources on both global and regional scales. Climatic variables can directly be used as a significant indictor in capturing the timing and variability of streamflow (Intergovernmental Panel on Climate Change (IPCC), 2008). For most watersheds, the main impact factor on streamflow is precipitation including the rainfall and snowfall. Changes in temperature could also have an important effect on the magnitude and temporal characteristics of streamflow, thus impacting the water resources management (Luce and Holden, 2009; Ma et al., 2010; Nijssen et al., 2001). Moreover,

the climate variability may reduce or enhance the influence of human-involved pressures on river and groundwater systems. For instance, extreme low-precipitation events may drive human to pump more water from river for agricultural irrigation, drinking water supply and other water demands. Thus, in addition to the investigation of vegetation-climate connections, the estimation of the potential linkages between climate variability and streamflow is also important for efficient water resources management.

Due to climate variation, the development in agriculture and industry and the increasing of population, there is a significant increase in the water demand from rivers and hydrological drought has become a serious environmental, social and economic issue in most regions of the world (Mishra and Singh, 2010). Hydrological droughts generally correspond to water deficit in the hydrological cycle such as the below-normal discharges in rivers and below-normal water levels in groundwater, lakes, and reservoirs (Van Loon, 2015). Hydrological droughts may affect the drinking water supply, irrigation, hydropower generation, water quality, disturbed riparian habitats, species composition and structure, and other socio-economic sectors. Within these issues, there is increasing demand to develop an appropriate indicator or methodology for hydrological drought identification and drought-based environmental flow assessment, particularly providing the estimation of drought risk and the recovery.

The general goal of this dissertation is to further improve our knowledge of the linkages and interactions between vegetation, climate, streamflow, and drought. The study areas of the dissertation are located in Germany including Rhineland-Palatinate State, Baden-Württemberg State, and two catchments in Germany. The present study would be helpful for better water resources management, reasonable agriculture/forest strategies, as well as preparations for potential hydrological drought disasters in the study areas. Moreover, it has a great potential for providing a valuable reference for other regions worldwide.

1.2 Objectives of the research

Therefore, the major objectives of the dissertation are:

- to identify long-term variations in vegetation and climatic variables and their scale-dependent relationships (a case study in Rhineland-Palatinate);
- to explore the probabilistic and multi-scale correlations between streamflow and hydroclimatic variables and the possible linkages to large-scale atmospheric circulations (a case study in Baden-Württemberg);
- to propose a copula-based overall drought indicator to describe the hydrological dryness/wetness conditions and assess the environmental flow.

1.3 Structure of the dissertation

This dissertation is divided into six chapters. This chapter (Chapter 1) presents a general introduction with specific objectives of the study. Chapter 2 gives an overall introduction about vegetation, climate factors, streamflow, and drought. Chapter 3 focuses on investigating long-term variations in vegetation and climatic variables (precipitation and temperature) and their scale-dependent relationships in Rhineland-Palatinate. Chapter 4 provides a detailed regional examination of the probabilistic and multi-scale connections between streamflow and hydroclimatic variables (precipitation, temperature and soil moisture) and the potential links to large-scale atmospheric circulations over Baden-Württemberg. In Chapter 5, this dissertation proposes a general probabilistic prediction network to identify the hydrological drought and drought recovery with environmental flow assessment. Chapter 6 gives overall conclusions and perspectives about the present research work.

Chapter 2: Introduction of vegetation and hydroclimatic variables

2.1 Vegetation

Vegetation is normally described as the overall characteristics of plant cover in an area. On one hand, vegetation plays a very important role in terrestrial ecosystem and is affected by a variety of environmental factors (e.g., climate, geomorphic process, and biotic process) and human disturbances (Ichii et al., 2002; Piao et al., 2010; Tourre, Jarlan et al., 2008; Wang et al., 2011; Zhou et al., 2014). The impact of climate on vegetation changes includes rainfall, drought, wind, snow avalanches and drifts, glaze storm, fires by lighting, as well as long-term climate variations (Burrows and Colin, 1990). Geomorphic process includes soil erosion driven by water and wind, soil movements due to gravity, flooding, and the spatial characteristics of topography (e.g., plains, hills, deserts, rivers, and lakes) (Burrows and Colin, 1990). The influence of biotic process on vegetation changes generally refers to the mutual effect between different plants, plant disease, and insects. Moreover, the vegetation is also strongly impacted by human disturbances. For instance, agricultural lands are planted based on an annual plan. The variability in agricultural lands or forests may be disturbed by the management strategies taken, e.g., irrigation, adaptation policies, and afforestation. On the other hand, vegetation is able to regulate climate via the exchange of energy, water vapor, and momentum between land surface and atmosphere (Pielke et al., 1998). Vegetation also has a significant impact on atmospheric CO_2 and absorbs around one-third of anthropogenic fossil fuel emissions to the atmosphere by vegetation photosynthesis.

2.2 Temperature and precipitation

Temperature is a key factor in climate system. Numerous scientific evidences have shown that the global warming is increasing (IPCC, 2007). Based on the global temperature analysis carried out by national aeronautics and space administration (NASA)’s scientists, the average global temperature has increased by 0.8 °C since

1880. More importantly, two-thirds of this increase has taken place since 1975 (Hansen et al., 2010). According to IPCC's report based on climate model projections, the global surface temperature during the 21st century is probably to rise a further 0.3 to 1.7 °C even under their lowest emissions scenario (IPCC, 2013). Although climate warming and the relevant impacts may vary from different areas, some direct results may include extreme climate events (e.g., drought, food, heavy snow, and heat waves), rising sea levels, precipitation patterns, as well as changing glaciers, permafrost and sea ice. Moreover, the effects are on vegetation growth and species extinctions. For humans, significant impacts may include the food security, migration because of the rising sea levels, and indirect mitigation and adaptation policies due to warming.

Precipitation is a major component in the Earth's water cycle, and connects the atmosphere, lands, and oceans. It is in the form of rain, freezing rain, sleet, and snow, but most precipitation falls as rain. As we know, precipitation is unevenly distributed over different regions of the Earth. The spatial distribution of precipitation is impacted by large-scale atmospheric circulations. In general, the Earth's atmosphere has zones with large-scale rising air and other zones with declining air, which varies by latitude. Rising air dominates near the equator and in the multitudes where tend to be wet regions, while the declining air is mainly observed in poles and subtropics where tend to be dry regions (Rodgers and Streluk, 2003). Moreover, the spatial patterns of precipitation are also influenced by topography and large bodies of water (e.g., lakes and oceans). In addition to the spatial variation, precipitation also varies over time. The temporal variability in global precipitation is strongly connected to the seasonal changes in the Earth's heating and its influence on the movement of global pressure systems and air masses (Ritter and Michael, 2006). Also, precipitation has interannual variations. It has been well known that the El Niño–Southern Oscillation (ENSO) is a significant driver for the interannual variations in global and hemispheric precipitation patterns (Arkin, 1982; Bjerknes, 1969). New et al. (2000) documented that ENSO contributes around 38% of the interannual variance in globally-averaged land precipitation. Moreover, some other climate indices also significantly affect the temporal characteristics of precipitation on both local and global scales, e.g., Pacific

North American index (PNA) and North Atlantic Oscillation (NAO).

2.3 Streamflow

The water from the oceans returns to the Earth in the form of precipitation. Due to gravity, a part of the precipitation is taken into the ground as infiltration, and the other part directly runs downhill as surface runoff (Horton, 1933). The term "streamflow" generally refers to the amount of water flowing in a stream or river. The major effect on streamflow variability is precipitation in a basin. The short-term variability in streamflow is typically driven by seasonal climatic characteristics and patterns and weather conditions in a basin (Gleick, 1993). The streamflow also has a long-term trend. The long-term trend in streamflow may lead to permanent changes in ecosystem including the plants and animals relying on the river. The natural impacts on streamflow include precipitation (e.g., rainfall and snowfall), snowmelt, glaciers, permafrost, transpiration by plants, evaporation from soil and water bodies, groundwater, etc. Also, there are an amount of human-related impacts, such as agricultural and industrial uses, dam construction, water resources plans, and alterations of the natural streamflow channels. Moreover, the global warming also indirectly impacts the streamflow variability in different rivers.

2.4 Drought

Drought simply means the absence of water for a certain long period at a region where it is "not normal" as compared to "normal" condition. Drought is a slow-onset natural disaster and may last for a few days, months or years. It could take place in all climate regions, but its characteristics and influences vary greatly among different areas. The main characteristics include the beginning, termination, frequency, severity, and duration for a given return period (Mishra and Singh, 2010; Tatli and Türkes, 2011). Drought has negative impacts on agriculture, industry, water supply and management, ecosystem and social-economical sectors. The definition of drought varies among different variables that include hydroclimatic variables (e.g., temperature, precipitation, streamflow, and soil moisture), agricultural variables and socioeconomic factors. According to different definitions, droughts are commonly classified into five

types including meteorological, agricultural, hydrological, and socio-economic droughts. Meteorological drought usually refers to below-precipitation over a region during a period. Hydrological drought is described as lacking surface and subsurface water resources in a hydrological system, including the abnormally low flows in rivers and abnormally low levels in groundwater, lakes, and reservoirs (Van Loon, 2015). Streamflow data are commonly used for hydrological drought system. Agricultural drought is the drought affecting crop growth or the ecology of the range. It is generally linked to the declining soil moisture. Socio-economic drought is that a water resources system fails to meet water demands for an economic good or social uses.

In order to examine drought characteristics, drought indices are commonly developed for different drought classes, e.g., rainfall anomaly index (RAI; van Rooy, 1965), standardized precipitation index (SPI; McKee et al., 1993), the modified standardized precipitation index (MSPI; Türkes¸ and Tatli, 2009), surfacewater supply index (SWSI; Shafer and Dezman, 1982), crop-specific drought index (CSDI; Meyer and Hubbard, 1995), Palmer drought severity index (PDSI; Palmer, 1965), soil moisture drought index (SMDI; Hollinger et al., 1993), China-Z index (CZI; Wu et al., 2001), vegetation condition index (VCI; Liu and Kogan, 1996), and joint deficit index (JDI, Kao and Govindara, 2010).

Chapter 3: Identifying long-term variations in vegetation and climatic variables and their scale-dependent relationships: a case study in Rhineland-Palatinate

3.1 Introduction

It has been well understood that terrestrial vegetation acts as a sensitive indicator of climatic and environmental changes at various spatial scales, from regional to global (Chuai et al., 2013; Zhang et al., 2003). In recent decades, monitoring vegetation dynamics and detecting their responses to climate fluctuations have received a significant attention and become an essential aspect of climate change research, particular with the help of the satellite-based normalized difference vegetation index (NDVI) that is generally used as a proxy of vegetation productivity (Forkel et al., 2013; Horion et al., 2013; Mao et al., 2012; Miao et al., 2013; 2015; Rees et al., 2001; Running and Nemani, 1988; Vicente-Serrano et al., 2008). For instance, Ichii et al. (2002) pointed out that there was a strong relationship between NDVI and both temperature and precipitation in northern and southern semiarid regions of the Earth during the period 1982–1990. They also compared the global NDVI trends and found that increasing NDVI trends in the mid- and high latitudinal zones of the Northern Hemisphere were connected to the upward temperature trends, while the decreasing NDVI trends in southern semiarid regions were attributed to the declining trends in precipitation. Several studies suggested that there is an increase in vegetation variability during the past two decades in the mid- and high latitudinal regions of East Asia dominantly due to the lengthened growing season (Kawabata et al., 2001; Park and Sohn, 2010; Zhou et al., 2003). He et al. (2012) examined relationships between vegetation (NDVI) and climatic factors on seasonal and inter-annual scales over Canadian ecosystems and revealed that temperature was the dominant driver for seasonal variability in NDVI and the correlation between precipitation and NDVI is weaker but still significant. Udelhovena et al. (2009) evaluated the lag-time

correlation between precipitation and NDVI in Spain for the period from 1989 to 1999. They presented that a significant lagged correlation between rainfall and NDVI was observed in most areas of Spain at 1-month lag time. This study focuses on investigating the trends of vegetation and climatic variables as well as their relationships in Southwest Germany with the selection of Rhineland-Palatinate state as the study area. Rhineland-Palatinate is a typical humid area and this investigation may also provide a reference for other regions with close climate features.

The geographic time series (e.g., NDVI and climatic variables) are generally non-stationary and contain different frequency components, e.g., seasonal variations, long-term and short-term fluctuations (de Beurs and Henebry, 2005; He et al., 2012). Such components could provide detailed multi-scale information that contributes to the trend production in different geographic time series and affects their correlations. The wavelet transform (WT), which can provide a time–frequency representation of a signal, is a quite useful tool to determine multi-scale and non-stationary processes in a time series (Martínez and Gilabert, 2009). To date, the WT technique has been commonly applied to analyze the non-stationary trends and periodicities in hydroclimatic time series (Pisoft et al., 2004). For instance, Jung et al. (2006) identified the trends in climatic factors (i.e., temperature and precipitation) over South Korea by employing the wavelet-based methods. They found a warming linear trend in the winter temperature at decadal and inter-decadal scales. Partal (2010) combined WT and the Mann-Kendall (MK) trend test to examine potential trends in streamflow data in Turkey. Nalley et al. (2012) used the discrete wavelet transform (DWT) and MK test to detect trends in streamflow and precipitation over Canada.

In order to better understand the temporal variations in vegetation and climatic variables over Rhineland-Palatinate (Southwest Germany) and the potential impacts of climatic change on vegetation, this study aims to explore the multi-scale trends in NDVI and climatic variables and their scale-dependent relationships, particularly with different vegetation types and precipitation regimes considered. Therefore, the main aims of this chapter are: (1) to examine the trends in monthly NDVI temperature and precipitation data at different time-scales for different vegetation types and

precipitation regimes in Rhineland-Palatinate, by co-utilizing the DWT technique and MK trend test; (2) to determine which time-scale is predominantly responsible for the possible trend production in these original time series; (3) to investigate the scale-dependent relationships between NDVI and climatic variables for various vegetation types and precipitation regimes.

3.2 Study area and materials

3.2.1 Study area

Rhineland-Palatinate state is situated at Southwest Germany (between 48° 57' –50° 59' N and 6° 5' –8° 31' E), covering an area of 19,853 km^2 (Fig.3.1). It has an average elevation between 400 and 600 m. The largest river is the Rhine River which runs through this state from the southeast to the northeast. The northern part of this study area is composed of woodlands and cultivated fields which are crossed by deeply eroded river valleys. Several mountain chains in north Rhineland-Palatinate are separated from each other by some tributaries of the Rhine River. The southeastern portion includes Rhine River valley, which is also the main agricultural and cultivated area in this state. Rhineland-Palatinate is characterized as a mild temperature humid climate with warm summers and no dry season. This region is mainly dominated by frequently changing low pressure systems and anticyclones (Dong and Menzel, 2016). The state's mean annual total precipitation varies from 540 mm in the central part (Rhine valley) to 1,100 mm on the higher regions. The mean annual temperature ranges from 6°C (the higher regions) to 10°C (lower valleys). The state is dominated by forestland (covering approximate 50% of the entire state), followed by cropland, grassland, urban and water area (Hellebrand et al., 2009).

3.3.2 Meteorological and remote sensing datasets and data pre-processing

The gridded monthly total precipitation and mean temperature dataset (during 1982–2006) across Rhineland-Palatinate (1 km×1 km spatial resolution) was obtained from Germany's national meteorological service (Deutscher Wetterdienst, DWD) (https://werdis.dwd.de/werdis/start_js_JSP.do). This continuous gridded dataset was derived from daily observations in the station network of the DWD with high quality.

The geographic distribution of the precipitation and temperature stations over this study area is showed in Fig. 3.1a.

The NDVI data were extracted from global inventory modeling and mapping studies (GIMMS) dataset derived by the advanced very high resolution radiometer (AVHRR) sensor aboard national oceanic and atmospheric administration (NOAA) satellites (NOAA-7, 9, 11, 14, 16 and 17) (http://glcf.umd.edu/data/gimms/). This dataset has been widely used since 1981 (Townshend 1994; Tucker et al., 2005; Julien and Sobrino, 2010). The NDVI dataset is given with a spatial resolution of 8 km and is available from July 1981 to December 2006 (the period from January 1982 to December 2006 was considered in this study). The monthly NDVI data used in the current study were produced from processed 15-day (13–16 days) NDVI composites, using the maximum value compositing (MVC) method (Borak et al., 2000; Holben, 1986; Martínez and Gilabert, 2009; Zhu et al., 2013).

A landuse/vegetation map in 2000 for Rhineland-Palatinate (the landuse was not significantly changed during the past three decades) was applied to identify different vegetation types, with a spatial resolution of 1 km (Fig. 3.1b). Six vegetation types (i.e., cropland, orchard, grassland, deciduous forest, coniferous forest and mixed forest) in this vegetation map were considered in this study excluding the urban land and water. To be in agreement with the gridded metrological map and vegetation map, the AVHRR-NDVI dataset was simply resampled into a spatial resolution of 1 km.

To assess the variations of NDV and climatic factors and their relationships in different precipitation conditions, this study area was separated into two precipitation regimes: the high and low precipitation, based on the mean annual total precipitation (828 mm) over this study area (based on the data from 1982 to 2006) (Fig. 3.1c). It can be found that the low precipitation regime is dominantly located in valleys and low lands and the high precipitation regime is mainly concentrated in up lands. According to the vegetation type and precipitation regime maps, NDVI, temperature and precipitation values during 1982–2006 for each vegetation type in two precipitation regimes were extracted. The spatially-averaged monthly time series of NDVI, total precipitation and mean temperature, corresponding to six different

vegetation types in two precipitation regimes, were then generated over the period 1982–2006, respectively.

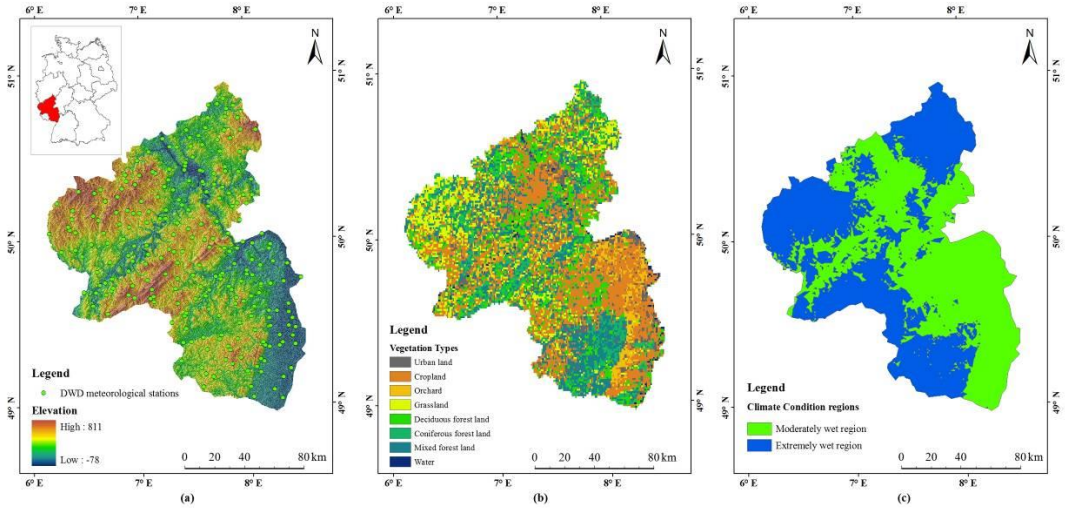

Figure 3.1 Locations of DWD meteorological stations and elevation in Rhineland-Palatinate, southwestern Germany (a). The map of vegetation types in Rhineland-Palatinate (b). The map of two precipitation regimes in Rhineland-Palatinate (c).

3.3 Methods and data processing

3.3.1 Wavelet transform and discrete wavelet transform

The wavelet transform is a mathematical technique that can decompose a signal into multiple lower resolution levels by controlling the scaling and shifting factors of a single wavelet function (mother wavelet) (Torrence and Compo, 1998). The wavelet transform of a signal produces a number of wavelet coefficients for different resolution levels (scales) and detect the periodic components in a signal (Nalley et al., 2012; 2013). The higher resolution levels (scales) refer to the stretched version of a wavelet, and the corresponding wavelet coefficients provide the information about the low-frequency components of the signal. The lower resolution levels (scales) are the compressed version of a mother wavelet and aim to capture the high-frequency components of the signal. Since the wavelet transform can separate the time series into short, medium, and long periodic components, it can be used to identify the main

components which contribute to producing the trend in a time series (Kim, 2004). The wavelet transform generally involves two techniques: continuous wavelet transform (CWT) and the discrete wavelet transform (DWT).

The CWT operates on smooth continuous functions and is able to identify and decompose signals at all scales (Kulkarni, 2000; Nalley et al., 2012; Partal and Küçük, 2006). By contrast, the DWT operates on scales which have discrete number and the scales and locations in the DWT are generally based on the integer powers of two (a dyadic arrangement). This can simplify the process of transformation (decomposition) and reduce flexibility when compared to CWT which generates too much redundant information and is more difficult to implement (Percival, 2008). DWT is commonly applied in dealing with the signal containing jump or shifts. The wavelet function of DWT is expressed as:

$$\psi_{(j,k)}(\frac{t-\gamma}{s}) = \frac{1}{s_0^{j/2}}\psi(\frac{t-k\gamma_0 s_0^j}{s_0^j}) \tag{3.1}$$

where ψ represents the mother wavelet; j and k are integers that determine the wavelet dilation (scale factor) and translation, respectively; t represents time and γ is the translation factor (time step) of the wavelet over the time series; the variable s indicates the wavelet scale (scale factor); s_0 is a specified fixed dilation step greater than 1; γ_0 denotes the location parameter greater than zero (Mallat, 1989). For a discrete time series x_t, when occurring at a discrete time t (t =0, , 2, . . ., *N-1*, and N is an integer power of 2), the corresponding wavelet coefficient ($W_\psi(j,k)$) for the DWT is defined as:

$$W_\psi(j,k) = \frac{1}{2^{j/2}}\sum_{t=0}^{N-1} x_t \psi(\frac{t}{2^j} - k) \tag{3.2}$$

here, the wavelet coefficient for the DWT is evaluated at scales $s = 2^j$ and locations $\gamma = 2^j k$.

Although the CWT has some disadvantages mentioned above, it can locate certain events in a signal and is therefore desirable to detect and determine the possible

seasonality characteristics (annual cycle) in the times series. The details of the calculations and properties of the CWT can be found in Torrence and Compo (1998).

3.3.2 Mann-Kendal (MK) test and seasonal Mann-Kendal (MK) test

The Mann-Kendall (MK) test is a non-parametric technique and widely used for the trend test in geographic time series (Helsel and Hirsch, 1992; Zhang et al., 2006). It does not need the time series to be normally distributed, and is simple to calculate (Gan, 1998; Kendall, 1975; Mann, 1945; Qin et al., 2010; Petrow et al., 2009).

The standardized test statistic Z is calculated by:

$$Z = \begin{cases} \dfrac{S-1}{\sqrt{Var(S)}}, S > 0 \\ 0 \qquad\quad , S = 0 \\ \dfrac{S+1}{\sqrt{Var(S)}}, S < 0 \end{cases} \tag{3.3}$$

$$S = \sum_{i=1}^{n-1} \sum_{k=i+1}^{n} \mathrm{sgn}(x_k - x_i) \tag{3.4}$$

$$\theta = x_k - x_i \tag{3.5}$$

$$\mathrm{sgn}(\theta) = \begin{cases} 1, & \theta > 0 \\ 0, & \theta = 0 \\ -1, & \theta < 0 \end{cases} \tag{3.6}$$

$$Var(S) = \frac{1}{18}[n(n-1)(2n+5) - \sum_{j=1}^{m} t_j(t_j-1)(2t_j+5)], \tag{3.7}$$

where the statistic S is distributed approximately normally, n is the amount of tied groups, t_j is the amount of data in the jth (tied) group, and x_k and x_i are variables. The null hypothesis is rejected at the α=0.05 significance level if $|Z| > Z_{\alpha/2}$, where $Z_{\alpha/2}$ is the standard normal deviate, indicating that Z is statistically significant (Gan, 1998). However, the main disadvantage of the original MK test is that it does not consider the seasonality patterns which are usually found in the monthly geographic time series and could result in inaccurate interpretations of the MK test. To overcome this weakness, a modified Mann–Kendall test (an improved version of original MK test)

proposed by Hirsch et al. (1982) is able to account for seasonality and serial correlation factors in the data. Previous documents have provided the specific introduction about these two MK tests and their formulations (Gan, 1998; Hamed and Rao, 1998; Hirsch and Slack, 1984; Qin et al., 2010).

The trend's significance is evaluated by comparing the *Z* value (the statistic of the MK test) with the standard normal variate at the pre-specified significance level. In this study, the absolute value of this Z-value is compared to the critical two-tailed *Z*-value. The *Z* values in a two-tailed test for α of 5% are $\pm$ 1.96. This means that the absolute Z-value from the MK calculation greater than 1.96 shows that the trends are significant (Choi et al., 2011; Nalley et al., 2012).

3.3.3 Data processing

In DWT, decomposing the signals generates two kinds of coefficients, i.e., the details indicating the high-frequency components (noise) of the original signal, and approximation indicating the low-frequency components of the original signal. Also, the higher detail levels have lower frequencies (Dong et al., 2008; Partal, 2010; Sang et al., 2009).

Wavelet choice, decomposition level, and extension mode (border conditions) are the important issues which should be carefully considered when performing the DWT (Liu et al., 2014; 2015b; Sang et al., 2013). In this study, the Daubechies (db) wavelets, as the widely-used mother wavelets for the DWT analysis in hydroclimatic data, were applied, because they have specific characteristics for localizing events in time series (Daubechies, 1988; Popivanov and Miller, 2002).

The maximum decomposition level should be determined based on the specified time series (Sang et al., 2012). According to de Artigas et al. (2006) and Nalley et al. (2012), the highest decomposition level (*J*) for monthly series was assessed using:

$$J = \frac{Log(\frac{N}{2k-1})}{Log(2)} \tag{3.8}$$

where *N* is the number of data in monthly series and *k* is the number of vanishing moments of a db wavelet. In this study, there are 300 data points for the monthly

series for the period of 25 years. Daubechies wavelets (db5–db10) were tried for each monthly time series. The maximum levels for different Daubechies wavelets (db5–db10) were between 3.9 and 5.1 (for monthly time series). Hence, both four and five levels were considered in this study.

In addition, the extension modes (border conditions) should also be considered in DWT analysis. Three common extension modes are: zero-padding, periodic extension, and symmetrization (Misiti et al., 1997). All modes have individual advantages and disadvantages (de Artigas et al., 2006) and were taken into consideration and tried.

Thereby, for monthly series, four and five levels of decomposition were tried for each db wavelet (db5–db10) in three different extension modes. Two criteria were employed to determine the appropriate maximum levels, mother wavelets and the extension modes to be used in the data analysis for each series.

The mean relative error (MRE) was firstly used (de Artigas et al., 2006). It is given as:

$$MRE = \frac{1}{N}\sum_{i=1}^{N}\left|\frac{a_i - x_i}{x_i}\right| \tag{3.9}$$

here, N is the length of a given signal (x_i), a_i is the approximation values of x_i after decomposition. Furthermore, Nalley et al. (2012) introduced a criterion by using the relative error of the MK Z-values between the approximation and original data (e_r). The relative error (e_r) was computed as:

$$e_r = \left|\frac{Z_a - Z_0}{Z_0}\right| \tag{3.10}$$

where Z_0 is the MK Z-value of the original data and Z_a is the MK Z-value of the last approximation for the decomposition level.

For all monthly time series of NDVI, precipitation and temperature regarding six vegetation types in two precipitation regimes considered in this study, lower MREs were obtained for four decomposition levels. Taking precipitation time series as an example, the MERs for four and five levels were 0.41–0.45 and 0.69–0.72, respectively. Thus, four decomposition levels were applied in the DWT. However, the MREs did not show significant difference among the different border conditions and db wavelet types used in four decomposition levels. The relative error (e_r) was further

used to assess the border conditions and db types. The border conditions and db wavelet types for these original time series of NDVI, precipitation and temperature for six vegetation types in two precipitation regimes were determined by their lowest e_r, but this value varies from one time series to another. For instance, the lowest value for the NDVI time series of deciduous forest in the high precipitation regime was produced when using the periodic border extension with db5 wavelet (e_r: 0.49), while the lowest value for the precipitation time series of coniferous forest in the low precipitation regime was obtained when zero-padding border with db8 wavelet used (e_r: 0.34).

To examine the most dominant periodicities for trend production in a time series, the MK Z-value for each of the detail components (Ds) with the corresponding approximation (A) added (Ds+A) were compared to the MK Z-value of the original data for checking whether they are close (Nalley et al., 2012).

3.4 Results and discussion

3.4.1 Wavelet decomposition of original data

Each original time series of spatially-averaged monthly NDVI, total precipitation and mean temperature for two precipitation regimes and six vegetation types was decomposed into four details (D1–D4) and an approximation (A4), by using the DWT approach. D1, D2, D3, and D4 correspond to the 2-month, 4-month, 8-month, and 16-month scales, and A4 represents the approximation component of the original time series. The examples of applying the DWT approach on monthly NDVI, precipitation and temperature series are illustrated in Figs. 3.2, 3.3 and 3.4, respectively. Only the time series with deciduous forest in the high precipitation regime are presented due to the space limitation.

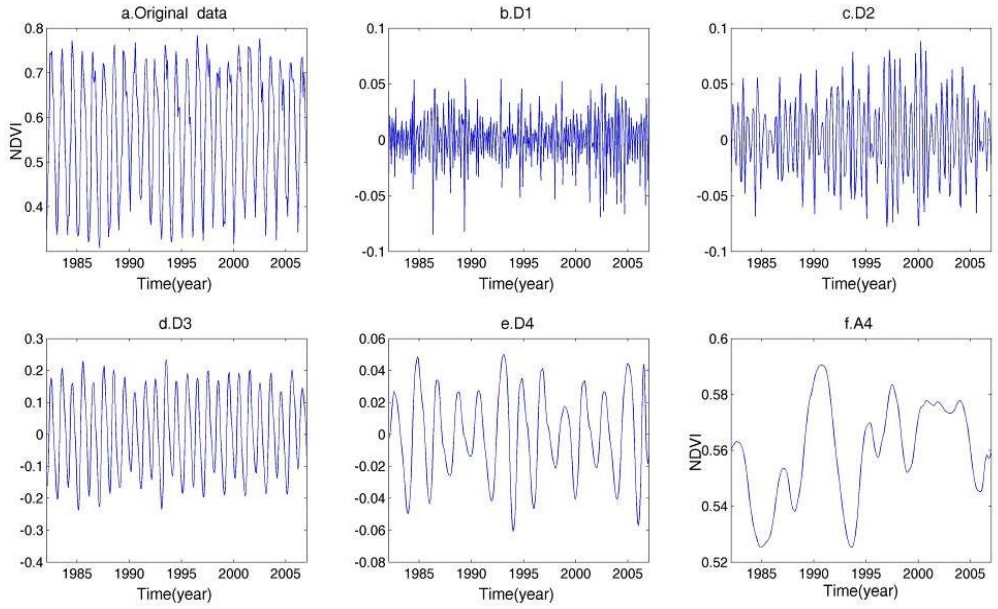

Figure 3.2 The original monthly NDVI time series for deciduous forest in the high precipitation regime and its transforms into four decomposition levels (i.e., D1–D4) and an approximation (A4) via DWT.

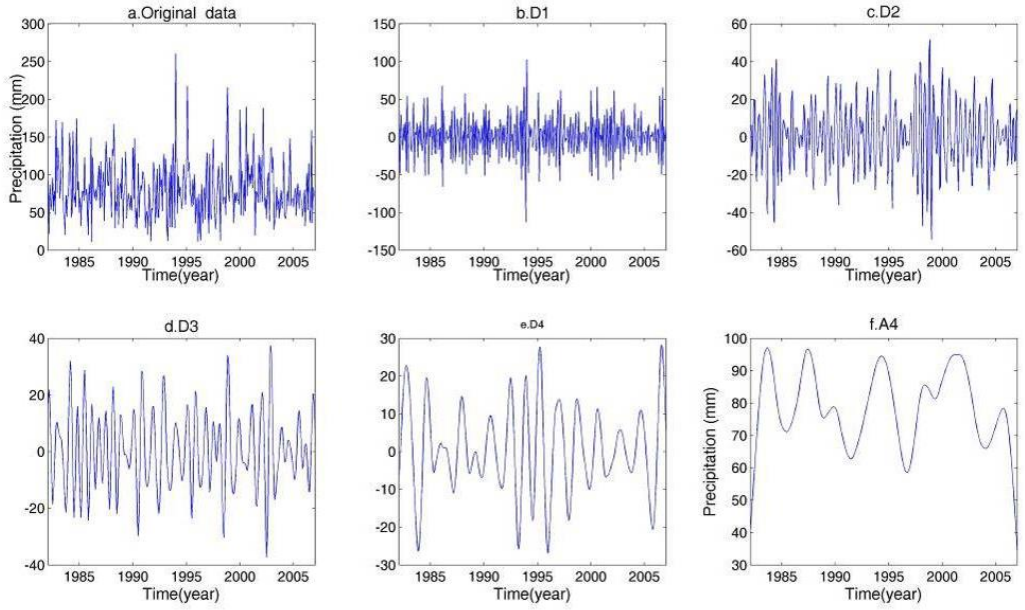

Figure 3.3 The original monthly precipitation time series for deciduous forest in the high precipitation regime and its transforms into four decomposition levels (i.e., D1–D4) and an approximation (A4) via DWT.

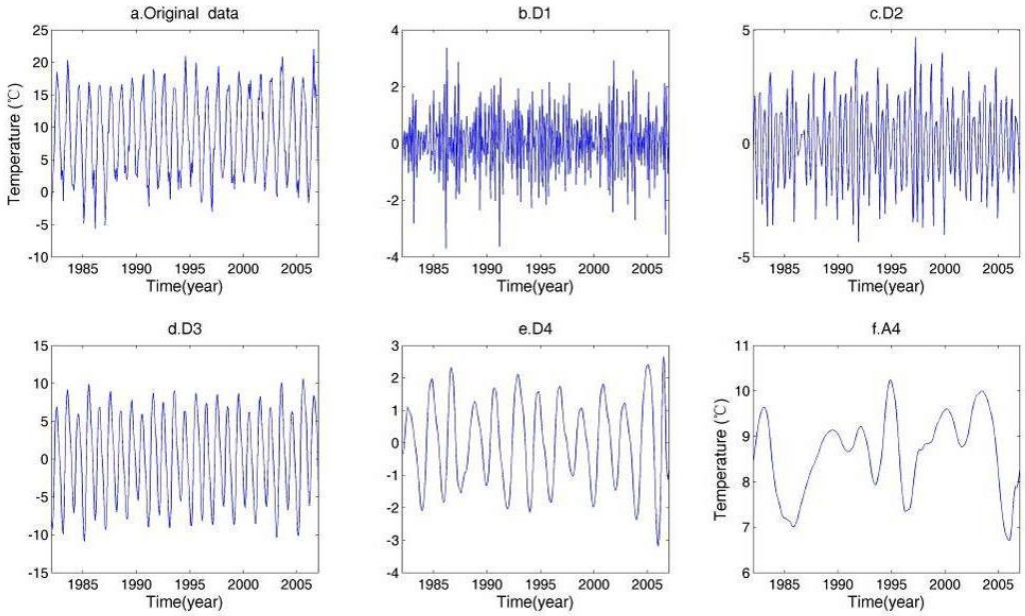

Figure 3.4 The original monthly temperature time series for deciduous forest in the high precipitation regime and its transforms into four decomposition levels (i.e., D1–D4) and one approximation (A4) via DWT.

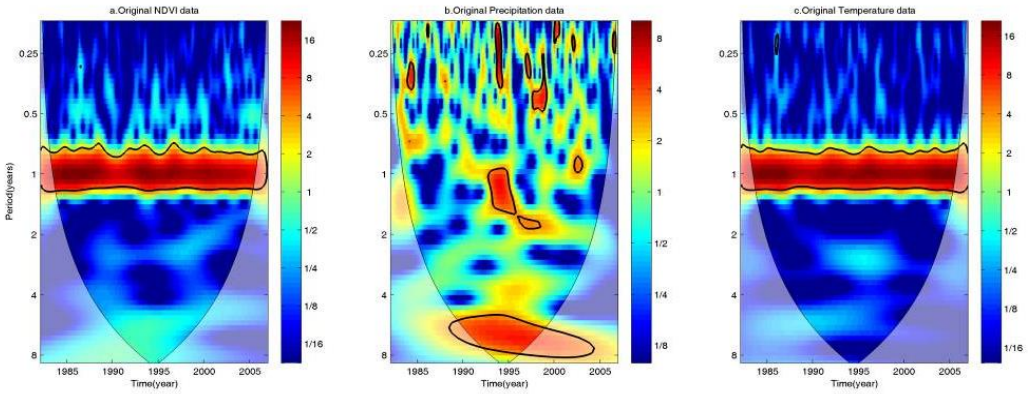

Figure 3.5 Continuous wavelet power spectrum for detecting seasonality patterns in the monthly time series of original NDVI (a), precipitation (b) and temperature (c) for deciduous forest in the high precipitation regime. The low wavelet power is shown in blue and high power in red and orange. The thick contours indicate the 5% significance level. The black line indicates the cone of influence (COI) (to reduce the edge effect).

To identify the seasonality patterns in monthly NDVI, mean temperature and total precipitation time series, the CWT approach was used. According to CWT analysis, significant seasonality patterns may exist in a time series when it presents a stably and

consistently significant (at the 5% significance level) 1-year cycle (annual cycle) during 1982–2006. In addition to these original time series, the time series of wavelet components (details and approximations) of original data via the DWT decomposition may also present seasonality patterns (Choi et al., 2011). Hence, the seasonality patterns of those wavelet components (Ds and A4) and the combinations of the detail components with the approximation added (Ds+A4) were also detected by employing CWT analysis. A strong and consistent annual cycle is found in the time series of original NDVI and temperature, their D3 components and A4+D3 combinations. The rest of time series including the original precipitation data do not exhibit an evident annual cycle. Examples of applying of the CWT analysis to detect the seasonality patterns in the time series are indicated in Fig. 3.5.

In order to examine trends in the original data (i.e., NDVI, temperature and precipitation) and the time series of the different wavelet components and the combinations (Ds+A4) obtained from the DWT decomposition, two MK tests as mentioned above were employed in this study. The original MK test was applied when the time series dose not reveal seasonality patterns and the modified MK test was used for the time series with strong seasonality.

3.4.2 Wavelet-based trend analysis for NDVI, precipitation and temperature

3.4.2.1 Monthly NDVI

The MK Z-values of the original NDVI data, their wavelet components (Ds and A4), and the combinations (Ds+A4) for six vegetation types and two precipitation regimes are shown in Table 3.1. With respect to the original NDVI data, upward trends can be found in the monthly time series for all vegetation types in the high precipitation regime and three forest types show statistically significant MK Z-values (at the 5% significance level): deciduous forest, coniferous forest, and mixed Forest. The original NDVI time series for all vegetation types in the low precipitation regime indicate significant increasing trends over the 25 years (1982–2006). It is noticeable that the cultivated areas (cropland and orchard) in the low precipitation regime (accounting for the major part of agricultural areas and irrigated areas in this state) present the

strongest positive trends. The results of the MK test on the detail components (D1–D4) of each NDVI series indicate that all individual detail components reveal a mixture of non-significant positive and negative trends. The detail components reflect the abrupt fluctuations which are considered as the noise of the original signal. Although their trend directions are ambiguous, these details still imply the basic (detailed) information of the trend in the monthly NDVI data at different time-scales (Nalley et al., 2012; Partal and Küçük, 2006). When the approximations (A4) were added to the detail components (the combinations of Ds+A4), the MK Z-values become higher, many of them being statistically significant. Also, the trend directions of the combinations are consistent with those of their corresponding original data. This may be attributed to the high Z-values of the A4 components. This study focused on the detail components with the approximation added which can provide clear information to determine the most predominant periodic components responsible for the primary trend production in the original data, by comparing the closeness of their MK Z-values with those of the original data (Nalley et al., 2012). As shown in Table 3.1, although the predominant periodic components are not consistent for different vegetation types in both precipitation regimes, the most common one contributing to the trend production in the observed data is the D3 plus A4 (D3+A4). This means that the trends in the monthly NDVI time series over the study area are mainly affected by 8-month periodic event. Additionally, D1 (2-month) component (with A4) for the grassland and deciduous forest in the high precipitation regime and coniferous and mixed forests in the low precipitation regime is observed to be the most influential component to affect the trends in the original data. D4 (16-month) component (with A4) for mixed forest in the high precipitation domain is found to be the most influential one.

Table 3.1 Mann-Kendall trend values of all NDVI time series for six vegetation types in the high and low precipitation regimes, including original time series, approximations (A4), details (D1–D4), and combinations of the details and the corresponding approximations.

Series	Cropland	Orchards	Grassland	Deciduous forest	Coniferous forest	Mixed forest
(a) High precipitation regime						
Original	0.351	1.835	1.707	3.811*	4.155*	3.952*
D1	0.055	0.489	0.533	0.615	-0.051	0.467
D2	0.423	-0.067	-0.075	-0.098	0.264	-0.026
D3	0.061	1.315	1.288	1.476	0.681	1.517
D4	1.735	-0.308	-0.356	-0.310	0.790	-0.310
A4	0.373	1.710	1.354	6.056*	7.977*	7.490*
D1+A4	1.193	1.086	**1.566**	**4.007***	5.361*	4.671*
D2+A4	0.788	0.597	0.720	2.753*	3.540*	3.419*
D3+A4	**0.317**	**2.232***	2.056*	4.241*	**4.268***	4.807*
D4+A4	2.111*	0.527	0.756	3.188*	6.370*	**4.029***
(b) Low precipitation regime						
Original	2.838*	3.034*	2.292*	2.420*	2.367*	2.090*
D1	0.154	0.075	0.453	0.253	0.274	0.335
D2	0.070	0.058	-0.003	0.027	-0.058	-0.003
D3	1.032	0.937	1.045	0.829	1.045	1.099
D4	-0.134	-0.050	-0.253	-0.304	-0.317	-0.348
A4	3.290*	3.000*	2.801*	3.161*	3.089*	2.743*
D1+A4	2.153*	1.940	1.916	2.081	**1.876**	**1.820**
D2+A4	1.812	1.715	1.354	1.614	1.389	1.299
D3+A4	**3.108***	**3.149***	**2.501***	**2.690***	3.027*	2.515*
D4+A4	1.885	1.693	1.453	1.809	1.511	1.437

The most influential periodic components for trends in the original data are shown in bold.

*. The trend is significant at the 5% significance level.

3.4.2.2 Monthly total precipitation

In two pre-defined precipitation regimes, the original monthly total precipitation time series for each vegetation type present a negative MK Z-value, but none of them are statistically significant. This suggests that the precipitation may experience a decreasing trend in entire Rhineland-Palatinate during 1982–2006. In addition, there is no significant difference regarding the trend values in six vegetation types for both high and low precipitation regimes. It can be observed that the absolute MK Z-values of the A4 components are relatively high and the statistically significant values are

obtained in some cases of vegetation types, particularly for the high precipitation regime (Table 3.2). This also indicates that the trends in decomposed components (via DWT) of the original data might reflect some significant characteristics even though the original series does not present the significant trends.

Table 3.2 Mann-Kendall trend values of all precipitation time series for six vegetation types in the high and low precipitation regimes, including original time series, approximations (A4), details (D1–D4), and combinations of the details and the corresponding approximations.

Series	Cropland	Orchards	Grassland	Deciduous forest	Coniferous forest	Mixed forest
(a) High precipitation regime						
Original	-0.880	-0.886	-0.879	-0.831	-0.632	-0.815
D1	-0.302	-0.189	-0.191	-0.242	-0.272	-0.298
D2	-0.132	-0.236	0.040	-0.196	-0.132	-0.149
D3	0.042	0.119	0.352	0.003	0.036	0.072
D4	-0.238	-0.111	-0.949	-0.298	-0.180	-0.150
A4	-1.911	-1.680	-2.125*	-1.928	-1.285	-1.873
D1+A4	**-1.053**	-1.002	-1.143	**-1.044**	**-0.809**	**-0.989**
D2+A4	-1.104	**-0.996**	**-0.915**	-1.223	-0.873	-1.107
D3+A4	-1.526	-1.198	-1.422	-1.698	-1.285	-1.514
D4+A4	-1.890	-1.370	-2.603*	-1.911	-1.414	-1.749
(b) Low precipitation regime						
Original	-0.796	-0.532	-0.872	-1.044	-0.731	-0.907
D1	-0.255	-0.189	-0.224	-0.247	-0.253	-0.246
D2	-0.224	-0.291	-0.192	-0.222	-0.204	-0.251
D3	0.014	0.109	-0.043	-0.096	0.047	-0.031
D4	-0.223	-0.142	-0.173	-0.246	-0.143	-0.181
A4	-1.863	-1.220	-2.038*	-2.430*	-1.477	-2.075*
D1+A4	-1.129	-0.803	-1.075	-1.319	-0.943	-1.200
D2+A4	**-0.894**	**-0.526**	**-0.960**	**-1.302**	**-0.674**	**-1.059**
D3+A4	-1.141	-0.611	-1.367	-1.528	-1.052	-1.420
D4+A4	-1.706	-1.254	-1.697	-2.083*	-1.273	-1.789

The most influential periodic components for trends in the original data are shown in bold.

*. The trend is significant at the 5% significance level.

It is clear to notice that the trend directions of individual detail components become consistent with those of their corresponding original data after the addition of the approximations (A4). Table 3.2 also shows that the most predominant periodic components influencing the production of trends in the monthly total precipitation data for different vegetation types are not consistent in the high precipitation regime.

Most of the precipitation trend production are determined by the D1 component (with A4), except for orchards and grassland where the D2 (with A4) is found as the most predominant component. This shows that the prominent periodic components influencing the trend production in the original precipitation series are the 2- to 4-month scales. In the low precipitation regime, the most influential component for all vegetation types is the 4-month scale.

Table 3.3 Mann-Kendall trend values of all temperature time series for six vegetation types in the high and low precipitation regimes, including original time series, approximations (A4), details (D1–D4), and combinations of the details and the corresponding approximations.

Series	Cropland	Orchards	Grassland	Deciduous forest	Coniferous forest	Mixed forest
			(a) High precipitation regime			
Original	3.607*	3.843*	3.432*	3.647*	3.459*	3.620*
D1	0.082	0.126	0.060	0.117	0.090	0.074
D2	-0.192	-0.127	-0.185	-0.166	-0.169	-0.151
D3	2.757*	2.609*	2.731*	2.677*	2.757*	2.731*
D4	-0.017	0.011	-0.081	-0.012	-0.065	0.009
A4	3.957*	4.014*	3.839*	3.976*	3.847*	3.997*
D1+A4	1.780	1.914	1.665	1.738	1.688	1.809
D2+A4	1.173	1.248	1.068	1.147	1.079	1.188
D3+A4	**4.065***	**4.295***	**3.958***	**4.065***	**4.038***	**4.187***
D4+A4	2.027*	2.249*	1.915	2.016	1.925	2.040*
			(b) Low precipitation regime			
Original	3.418*	3.593*	3.607*	3.418*	3.553*	3.459*
D1	0.125	0.133	0.101	0.125	0.098	0.111
D2	-0.134	-0.117	-0.139	-0.124	-0.138	-0.115
D3	2.542*	2.501*	2.650*	2.569*	2.609*	2.663*
D4	0.001	-0.010	-0.022	-0.005	0.009	-0.016
A4	3.598*	3.731*	3.894*	3.688*	3.594*	3.810*
D1+A4	1.469	1.603	1.681	1.534	1.469	1.595
D2+A4	0.866	0.962	1.044	0.957	0.896	1.013
D3+A4	**3.877***	**4.038***	**4.106***	**3.931***	**3.931***	**4.025***
D4+A4	1.823	1.962*	1.979*	1.869	1.834	1.943

The most influential periodic components for trends in the original data are shown in bold.

*. The trend is significant at the 5% significance level.

3.4.2.3 Monthly mean temperature

For the monthly mean temperature data, the original time series for all vegetation

types in two different precipitation regimes show statistically significant ascending trends (all MK Z-values greater then 3.4) and the difference of their MK Z-values is not apparent. This suggests that the significantly increasing trends could occur across the entire study area.

Table 3.3 shows that the Z-values of individual detail components for six vegetation types and two precipitation regimes become higher and the trend directions become stable (positive values) and consistent with the respective original temperature data after adding approximations (A4). As illustrated in Table 3.3, the D3 component (plus A4), representing the 8-month scale is observed to be the most important periodic component in impacting the trend production of the original temperature data.

3.4.3 Lag-times and scale-dependent (wavelet) correlations between NDVI and climatic variables

3.4.3.1 NDVI and precipitation

To evaluate the response of vegetation dynamics to regional climatic fluctuations in Rhineland-Palatinate during the period 1982–2006, this study examined the relationships between the NDVI and climatic variables for different vegetation types and precipitation regimes. In both precipitation regimes, a statistically significant negative correlation (at the 1% level) between NDVI and precipitation (original data) can be found in all vegetation types (Table 3.4). It can be inferred that the available moisture in both high and low precipitation regimes is sufficient for the vegetation growth. However, redundant precipitation or consistent rainy days may decrease the temperature, which is not beneficial for the growth of plants and even will prohibit the growth (Chuai et al., 2013; Gitelson, 2004; Piao et al., 2006). Moreover, precipitation could cause more clouds and thus result in the reduction of incident radiation which would hinder photosynthesis of vegetation. These may partially accouter for the negative relationship between NDVI and precipitation for most vegetation cases over both precipitation regimes. What is more, the significant inverse relationships observed in the cultivated vegetation (cropland and orchards) may also be related with

the influencing of human disturbance, e.g., the cultivated measures and strategies. To detect the potential lagged response of NDVI to climatic variables, the cross-correlations between original monthly time series of these variables for six vegetation types and two precipitation regimes were carried out at five different monthly lags (i.e., 0- to 4-month lags). For each vegetation type in the high precipitation regime, the cross-correlations between NDVI and precipitation are dominated by slightly negative correlations at most lags and the highest negative cross-correlation function (CCF) values for all vegetation types are seen at lag zero months (0-month) (Fig. 3.6). Additionally, the precipitation occurred in previous one month still has negative influence on vegetation variation in the high precipitation regime, although the absolute CCF values are lower than the current month (0-month lag) and not statistically significant. With respect to vegetation types in the low precipitation regime (Fig. 3.7), the lag-time effect of precipitation on NDVI is quite similar to the higher precipitation region.

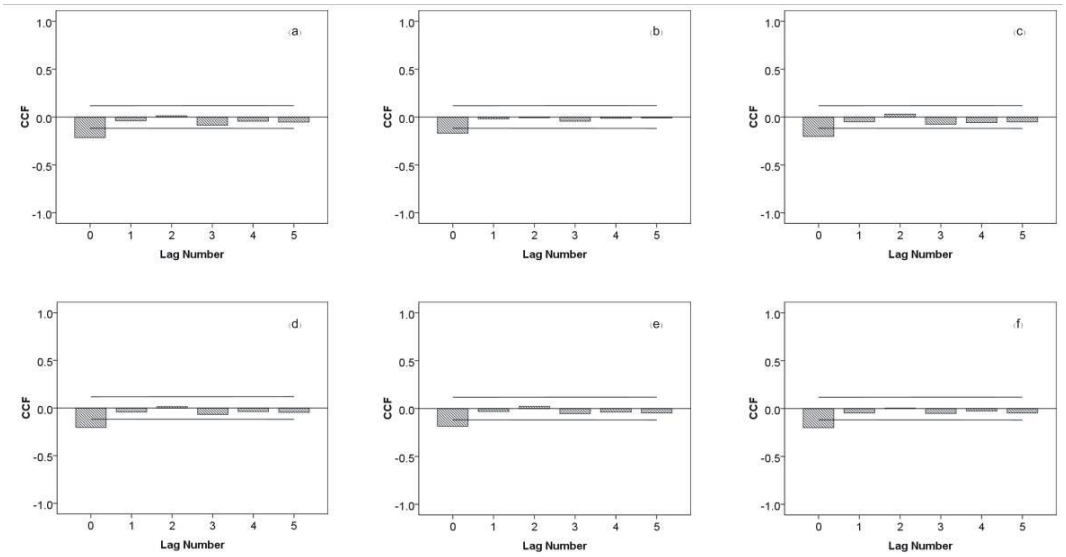

Figure 3.6 Cross-correlation between NDVI and precipitation for six vegetation types, i.e., cropland (a), orchard (b), grassland (c), deciduous forest (d), coniferous forest (e) and mixed forest (f) in the high precipitation regime. The CCF values represent cross-correlation function values and lag number is by one month. The two solid lines represent the upper and lower confidence intervals (95%). The effect of autocorrelation has been corrected.

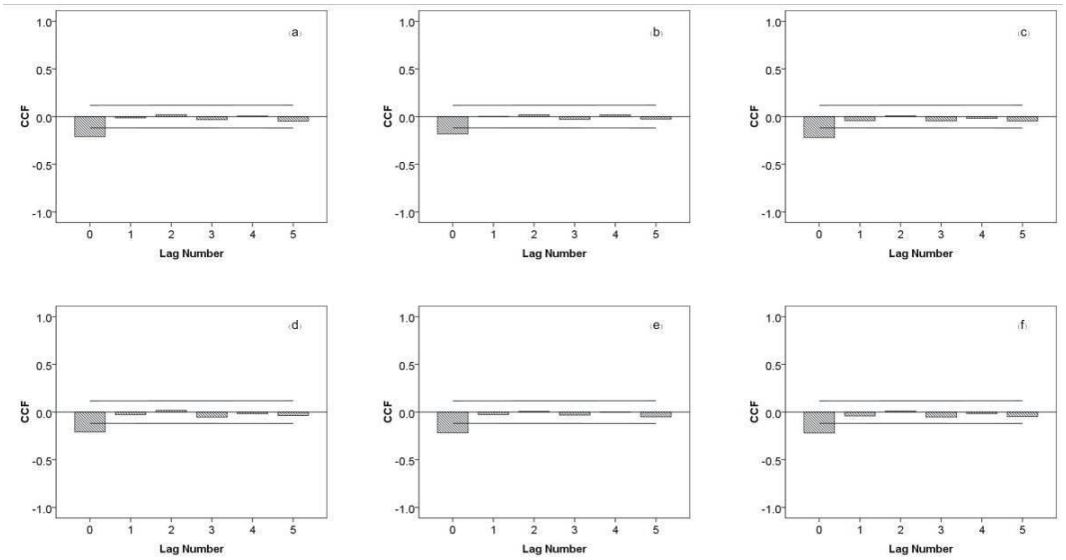

Figure 3.7 Cross-correlation between NDVI and precipitation for six vegetation types, i.e., cropland (a), orchard (b), grassland (c), deciduous forest (d), coniferous forest (e) and mixed forest (f) in the low precipitation regime. The CCF values represent cross-correlation function values and lag number is by one month. The two solid lines represent the upper and lower confidence intervals (95%). The effect of autocorrelation has been corrected.

The scale-dependent relationships between NDVI and climatic variables were further investigated by means of DWT technique and Pearson's correlation analysis, in order to determine which periodic component (the detail components with the corresponding approximation added) shows the strongest correlation (highest absolute Pearson's correlation coefficients). Table 3.4 shows there is a statistically significant negative relationship between NDVI and precipitation for six vegetation types in the high precipitation regime at four time-scales. Although the *R*-values for each vegetation types vary from one time-scale to another, the most significant periodic components are generally found at 2- and 8-month scales (the D1 and D3 components with their A4 added), except for the cropland. In the low precipitation regime (Table 3.4), all scale-dependent correlations between NDVI and precipitation are dominated by negative correlation coefficient for each vegetation type (Table 3.4). The D1 component, indicating the 2-month scale, has the highest negative *R*-values among those periodic components for most vegetation types, except for the deciduous forest.

Table 3.4 Scale-dependent correlation coefficients between NDVI and precipitation for various vegetation types in the high (a) and low (b) precipitation regimes, the original time series the combinations of the details (D1–D4) and the corresponding approximations (A4). The effect of autocorrelation has been corrected.

Series	Cropland	Orchards	Grassland	Deciduous Forest	Coniferous forest	Mixed Forest
			(a) High precipitation regime			
Original	-0.215**	-0.170**	-0.203**	-0.203**	-0.185**	-0.199**
D1+A4	-0.287**	**-0.254****	-0.308**	-0.271**	**-0.290****	**-0.277****
D2+A4	-0.058	-0.065	-0.318**	-0.065	-0.194**	-0.064
D3+A4	-0.286**	-0.197**	**-0.339****	**-0.323****	-0.163**	-0.235**
D4+A4	**-0.377****	-0.172**	-0.269**	-0.301**	-0.191**	-0.228**
			(b) Low precipitation regime			
Original	-0.210**	-0.182**	-0.220**	-0.209**	-0.217**	-0.219**
D1+A4	**-0.282****	**-0.265****	**-0.282****	-0.282**	**-0.275****	**-0.283****
D2+A4	-0.051	-0.048	-0.056	-0.056	-0.057	-0.057
D3+A4	-0.178**	0.002	-0.238**	**-0.306****	-0.124*	-0.267**
D4+A4	-0.147*	0.032	-0.200**	-0.267**	-0.100	-0.232**

The strongest correlation coefficients among different scales are shown in bold.

**. Correlation is significant at the 1% level (2-tailed).

*. Correlation is significant at the 5% level (2-tailed).

3.4.3.2 NDVI and temperature

The correlations between NDVI and temperature in all vegetation types are strong and statistically significant at the 1% level in both high and low precipitation regimes over the period 1982–2006 (Table 3.5). It can be concluded that the effect of temperature is mainly responsible for vegetation variation for all different vegetation types in this study area as compared to precipitation. In general, higher temperature provides more adequate heat condition which contributes to accelerating the photosynthesis and respiration of vegetation and also has positive effect on the length of the growing season, which is thereby beneficial for the vegetation growth (Wang et al., 2001; Weiss et al., 2004). This result is in agreement with some other studies in humid regions, which also found that the temperature is the main driver for the variation of NDVI (Cui and Shi, 2010; Guo, 2003). Additional cross-correlation analyses were also applied to determine the strength of the lag-time effect on the relationship between NDVI and temperature. As shown in Figs. 3.8 and 3.9, it is clear that the

most significant lag is obtained at zero months across all vegetation types and precipitation regimes considered, suggesting that NDVI provides the strongest positive correlation with temperature when no lag-time is involved. In addition, it can be found that the vegetation greenness in this study area is also positively sensitive to the temperature 1–3 months ahead.

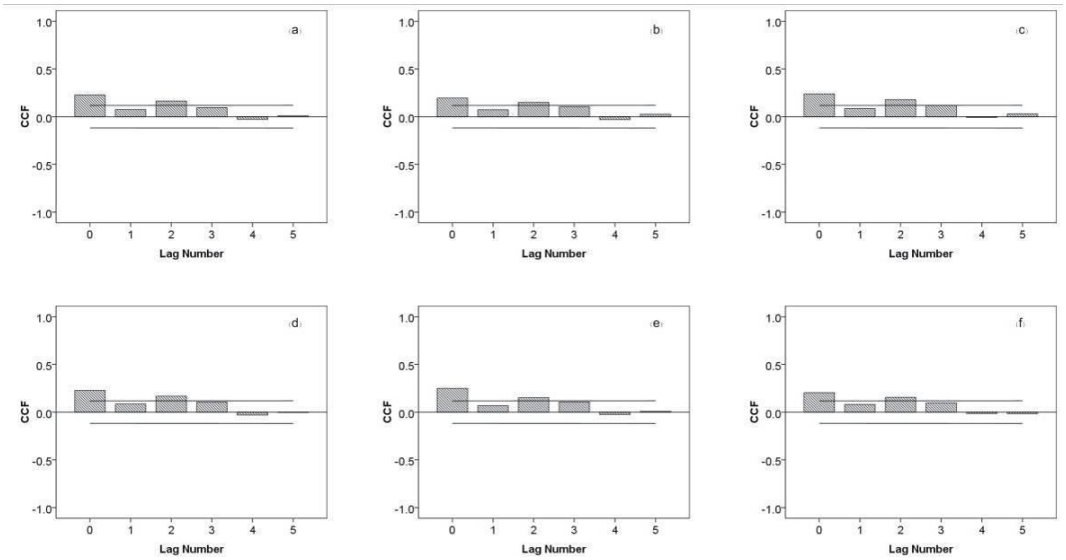

Figure 3.8 Cross-correlation between NDVI and temperature for six vegetation types, i.e., cropland (a), orchard (b), grassland (c), deciduous forest (d), coniferous forest (e) and mixed forest (f) in the high precipitation regime. The CCF values represent cross-correlation function values and lag number is by one month. The two solid lines represent the upper and lower confidence intervals (95%). The effect of autocorrelation has been corrected.

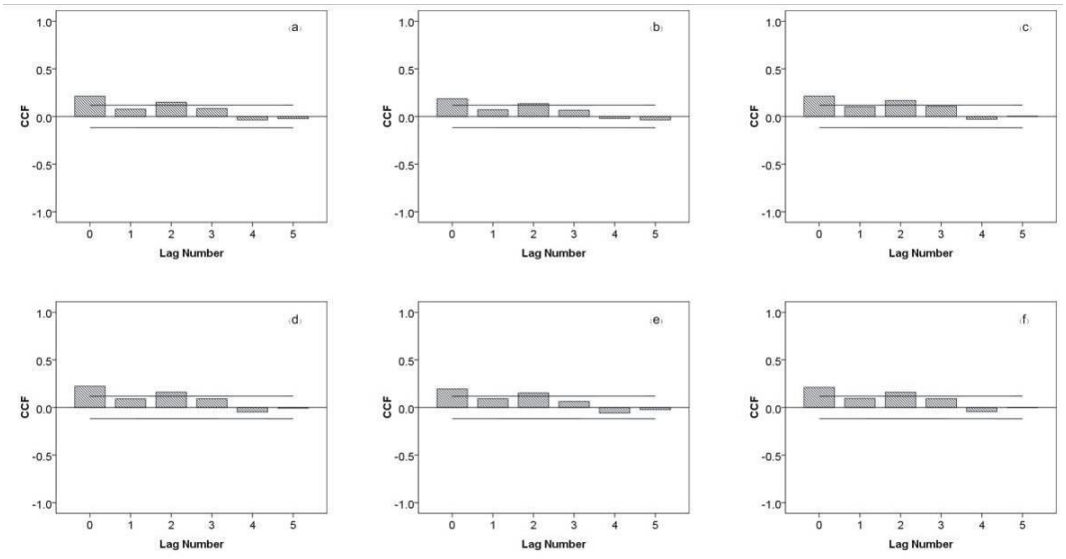

Figure 3.9 Cross-correlation between NDVI and temperature for six vegetation types, i.e., cropland (a), orchard (b), grassland (c), deciduous forest (d), coniferous forest (e) and mixed forest (f) in the low precipitation regime. The CCF values represent

cross-correlation function values and lag number is by one month. The two solid lines represent the upper and lower confidence intervals (95%). The effect of autocorrelation has been corrected.

The wavelet correlations between NDVI and temperature were also assessed over time-scales ranging from 2- to 16-month for different vegetation types and precipitation regimes. The scale-dependent correlations between NDVI and temperature are shown in Table 3.5. The strongest positive correlation for different vegetation types and precipitation regimes is generally obtained at 8- and 16-month scales (D3 and D4 component with approximation added) in the high precipitation regime, except for the cropland. There is an apparent increment in *R*-values for higher time-scales when compared to the lower time-scales for most vegetation types. For low precipitation regime, the strongest positive correlations between NDVI and temperature are generally at the higher periodic modes (i.e., the 8-month or 16-month) for most vegetation types.

Table 3.5 Scale-dependent correlation coefficients between NDVI and precipitation for various vegetation types in the high (a) and low (b) precipitation regimes, the original time series the combinations of the details (D1–D4) and the corresponding approximations (A4). The effect of autocorrelation has been corrected.

Series	Cropland	Orchards	Grassland	Deciduous Forest	Coniferous forest	Mixed Forest
			(a) High precipitation regime			
Original	0.229**	0.196**	0.239**	0.228**	0.249**	0.204**
D1+A4	**0.225****	0.166**	0.186**	0.181**	0.267**	0.177**
D2+A4	-0.162**	0.450**	0.470**	0.464**	0.027	0.444**
D3+A4	0.223**	**0.530****	0.500**	**0.618****	0.497**	**0.631****
D4+A4	0.216**	0.507**	**0.515****	0.597**	**0.538****	0.597**
			(b) Low precipitation regime			
Original	0.213**	0.187**	0.214**	0.223**	0.194**	0.211**
D1+A4	0.170**	0.143*	0.153**	0.166**	0.165**	0.157**
D2+A4	0.350**	0.345**	0.419**	0.384**	0.444**	0.419**
D3+A4	**0.510****	**0.539****	0.504**	**0.524****	0.505**	0.495**
D4+A4	0.492**	0.507**	**0.510****	0.521**	**0.512****	**0.504****

The strongest correlation coefficients among different scales are shown in bold.

**. Correlation is significant at the 1% level (2-tailed).

*. Correlation is significant at the 5% level (2-tailed).

3.5 Conclusions

This chapter examined the temporal trends of NDVI, precipitation and temperature for six vegetation types in two precipitation regimes of Rhineland-Palatinate (southwest Germany) and their relationships at different time-scales, by jointly utilizing DWT, MK tests and correlation analysis. The spatially-averaged monthly NDVI data for all vegetation types in both high and low precipitation regimes reveal upward trends during the period 1982–2006, most of which show statistically significant (at the 5% significance level) increasing trends except for the cultivated vegetations (i.e., cropland and orchard) and grassland. The observed monthly precipitation and temperature data for each vegetation types in two precipitation regimes indicate weak downward trends and statistically significant positive trends respectively. Wavelet-involved trend analysis was further conducted to examine the changing characterization and trend structures in the NDVI, precipitation and temperature data at various time-scales, and to determine the most dominant and effective periodic modes which could mainly affect the trends found in the original data. It can be found that the trend analysis based on wavelet decomposition clearly present the basic structures of trend in the original NDVI, precipitation and temperature data for different vegetation types of two precipitation regimes. Despite that the periodic modes producing the original trends vary among different vegetation types and precipitation regimes, some general conclusions could still be obtained. For instance, the 2-month and 8-month periodic modes are seen to be the most prominent time-scales in affecting the trends of the NDVI data for different vegetation types in both high and low precipitation regimes. For the precipitation data, the most influential periodic modes are 2-month and 4-month scales for different vegetations in high precipitation regime, and the most important mode is the 4-month event for all vegetation types in less precipitation region. The trend production in the observed temperature data for each vegetation type over this study area is predominantly affected by 8-month periodic event.

Additionally, the investigation of relationships between NDVI and climatic variables

reflects that the original NDVI data of all vegetation types in both high and low precipitation regimes exhibit statistically significant negative correlation with precipitation. By contrast, there is a statistically significant positive relationship between NDVI and temperature for all vegetation types over the study area. It can therefore be speculated that the change in temperature plays a more important role in affecting the vegetation variability in Rhineland-Palatinate in comparison with precipitation. The analyses of cross-correlation present that the lag-times have a limited influence on the correlations between NDVI and both precipitation and temperature. The scale-dependent correlations between NDVI and climatic variables for different vegetation types in two precipitation regimes were also identified at various time-scales using DWT approach. For the NDVI-precipitation relationship, the most common time-scales with strongest negative correlation are the 2-month and 8-month time modes. The best correlation between NDVI and temperature is found at higher time-scales (i.e., the 8-month and 16-month) in most vegetation cases.

Chapter 4: Investigating the probabilistic and multi-scale relationships between streamflow and hydroclimatic variables and the possible linkages to atmospheric circulations: a case study in Baden-Württemberg

4.1 Introduction

Climatic variables such as precipitation and temperature have been widely recognized as key parameters in the hydrological cycle. Also, soil moisture affects the process of precipitation into streamflow and infiltration and thus largely determines the streamflow behavior and variability (Aubert et al., 2003). Understanding the linkages between hydroclimatic variables (e.g., precipitation, temperature, and soil moisture) and streamflow is significant for water resources planning and adapting appropriate practices to deal with the drought and flood risk under extreme conditions, and the knowledge obtained may also assist the improvement of hydrological modeling. In the past decades, numerous studies have focused on investigating the relationships between the variability in streamflow and changes in the hydroclimatic driving phenomena over different parts of the world. On the one hand, some researchers focused on employing deterministic correlation coefficient and linear statistical approaches such as multiple linear regressions to examine the influence of regional hydroclimatic variables on streamflow and the potential links between them (Brocca et al., 2008; Cayan, 1993; Cunderlik and Burn, 2004; Ficklin et al., 2009; Kletti and Stefan, 1997; Penna et al., 2011; Stewart et al., 2005). On the other hand, many scholars investigated the hydrological response to climate and environment variability based on conceptual or physically-based hydrological models, and also assessed the sensitivity of the streamflow to changes in the hydroclimatic drivers (Hamlet et al., 2007; Jha et al., 2004; Zehe et al., 2010; Zhang et al., 2011). However, few studies have focused on building up the joint probabilistic dependence between streamflow and hydroclimatic factors and identifying the conditional risk of floods and

streamflow deficit events under varying hydroclimatic scenarios, particularly regarding the seasonal variation. This risk-based information would be of great value for water resources planning and drought and flood prevention. To identify the joint probabilistic dependence between streamflow and hydroclimatic variables, copulas would be an ideal tool. They have the advantage of allowing the dependence to be constructed independently from the marginal distributions, and thus it is possible to join different marginal distributions without any transformations (Genest and Favre, 2007). There have been increasing applications of copulas in hydrological fields during the past decade such as flood and frequency analysis, return periods of hydrological events, forecasting of drought events, and geostatistical interpolation (Bárdossy and Li, 2008; Genest and Favre, 2007; Madadgar and Moradkhani, 2013; Salvadori and De Michele, 2004; Zhang and Singh, 2007). The joint probability model can pave a way to developing a conditional risk assessment of droughts and floods under various hydroclimatic forcings.

In addition, it would also be beneficial for hydrological prediction to explore the temporal variation in the relationships between streamflow and hydroclimatic variables at different time scales. This investigation would help to understand how these multi-scale relationships evolve over time and at which time scales the hydroclimatic drivers may impact the variability in streamflow. The patterns of multi-scale relationship between different signals can be detected by various signal filtering techniques. Among them, wavelet analysis has recently been reported to be an effective way to capture the periodic behaviors within a time series and identify the coherence between different time series at various time scales (Mengistu et al., 2013; Özger et al., 2009; Sang et al., 2013; Torrence and Compo, 1998).

In Baden-Württemberg (Southwest Germany), water resources management has been and continues to be an important environmental issue. For more effective water resources management in Baden-Württemberg, it is necessary to understand how streamflow responds to climate change and how streamflow and hydroclimatic factors are related, particularly focusing on the risk of flood and low flow under different hydroclimatic conditions. Several studies have focused on this topic in the past as a

basis for linking the streamflow variability to hydroclimatic changes over some specific regions or basins (in Baden-Württemberg) of interest (e.g., Huang et al., 2015; Schröter et al., 2013; Warrach-Sagi et al., 2008). However, few efforts have been made to identify the probabilistic dependence between streamflow and hydroclimatic forcings and the conditional risk of streamflow deficit events and floods under different hydroclimatic conditions. Moreover, there remains a lack of insight into the question how hydroclimatic factors may impact the changes in streamflow at inter-annual and longer-term scales.

Atmospheric circulations are known to strongly affect precipitation variability and the changes in streamflow. There have been many studies focusing on changes in atmospheric dynamics and their links to regional hydrological processes and extreme flow events in Europe. Jacobeit et al. (2003) detected the connections between flood events and atmospheric circulation patterns for the past 500 years in central Europe. They described how some specific atmospheric circulation modes (as a dynamic factor) significantly influence the incidence of flood events. Bárdossy and Filiz (2005) identified the flood-producing atmospheric circulation patterns (CPs) by means of large-scale pressure fields over some meso-scale catchments in France and Spain. Bouwer et al. (2006) quantitatively assessed the impact of variation in atmospheric circulations on the changes in winter streamflow over northwest Europe. They reported that the frequency of the western atmospheric circulation over Europe could be a useful reference for investigating climate change impacts on streamflow in northwest Europe. Ionita et al. (2012) examined the streamflow in the Rhine River and the links to large-scale climate anomaly patterns in spring and autumn using composite analysis, and concluded that the variability of the atmospheric circulation pattern significantly affects the precipitation fluctuations and Rhine streamflow variability in both seasons. This study also seeks to explore the possible connections between streamflow in Baden-Württemberg and large-scale atmospheric circulations. This analysis may provide additional information to understand the streamflow variability based on prior knowledge from varying atmospheric circulation patterns.

Therefore, the objectives of the study in this chapter are threefold. First, the current

study aims to quantify the seasonal probabilistic dependence structure between streamflow and hydroclimatic factors including precipitation, temperature and soil moisture over Baden-Württemberg by using copulas. The established dependence structure allows the evaluation of the risk of streamflow deficit events and floods conditioned on different hydroclimatic scenarios. Second, this study examines the coupling of streamflow and hydroclimatic forcings at different temporal scales based on wavelet coherency analysis. Third, this study further identifies the potential links between streamflow variability and large-scale atmospheric circulations in various seasons.

4.2 Methodology

4.2.1 Probabilistic measures of the dependence between streamflow and different hydroclimatic variables

In this chapter, copulas are used to describe the probabilistic relationships between different variables. A copula is simply described as a joint distribution function from multiple variables (Laux et al., 2011; Madadgar and Moradkhani, 2013; Sklar, 1959). Based on Sklar's theorem (Sklar, 1959), a bivariate distribution $F_{X,Y}(x, y)$ for variables X and Y can be expressed by a copula that satisfies:

$$F(x, y) = C(F_X(x), F_Y(y)) = C(u_1, u_2) \tag{4.1}$$

C called a copula is the joint cumulative distribution function (CDF) and its form reflects the joint dependence structure ($u_1 = F_X(x)$ and $u_2 = F_Y(y)$).

Modeling the joint dependence structure requires a well-fitted marginal distribution of each variable. To determine the best-fit distribution of the variables, five common theoretical probability distributions were compared: normal, gamma, Weibull, lognormal and exponential. The parameters of each distribution were estimated by the maximum likelihood method (Gyasi-Agyei, 2013). To determine the appropriateness of the theoretical distributions and discriminate between them, the chi-square goodness-of-fit was employed (Madadgar and Moradkhani, 2013; Massey, 1951). This test returns the p value, which should be greater than the significance level (5%)

to accept the null hypothesis. The most appropriate distribution was determined by the smallest statistics (the corresponding *p* value should be greater than the significance level as well) from the chi-squared test.

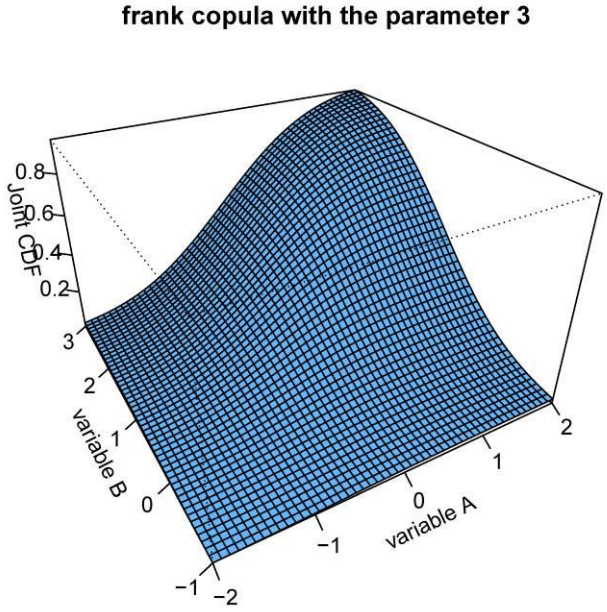

Figure 4.1 The joint CDF of variable A fitted by a Frank distribution with the specific parameters (i.e., mean = 0, standard deviation = 1) and variable B fitted by normal (Gaussian) distribution with the specific parameters (i.e., mean = 1, standard deviation = 0) using frank copula with the parameter ($\theta = 3$).

After obtaining the best-fitted marginal distributions, an approximate bivariate copula is expected to join the margins and construct the joint dependence. In this study, one copula from the elliptical copula family (Gaussian) and two copulas (Clayton and Frank) from the Archimedean copula family were considered. The details of these copulas used in the current study are given in Appendix A. As an illustration, Fig. 4.1 depicts the joint CDF of two different variables using a Frank copula.

To select the copula that best models the dependence of the given data, a parametric bootstrapping goodness-of-fit test was used (Genest and Remillard, 2008; Madadgar and Moradkhani, 2013). The goodness-of-fit test is called the Cramér-von Mises test which computes the Cramér-von Mises statistic S_n as a measure of the distance

between the empirical and parametric copulas, given by:

$$S_n = \int_{[0,1]^k} \Delta C(u)^2 \, dC(u) \; u = (u_1, u_2, ...u_k) \in [0,1]^k \tag{4.2a}$$

$$\Delta C = \sqrt{n}(C_{emp} - C_\theta) \tag{4.2b}$$

where C_{emp} and C_θ are the empirical and parametric copulas fitted to the given data with the size of *n*. The *p* values associated with the test statistics were calculated by the bootstrap sampling procedure using the Monte Carlo approach (Genest and Favre, 2007). The null hypothesis ($H_0 : C_{emp} \in C_\theta$) is accepted when the *p* value is above a predefined significance level of 5%; otherwise, it is rejected and the copula would not be a good selection for the considered significance level. Among several copulas, the one with the smallest S_n and highest *p* value (greater than the significant level as well) will be considered the best-fitted copula (Madadgar et al., 2013).

Once the copula-based joint distribution has been obtained, the conditional distributions of *X* under given *Y* can be generated and thus the conditional distribution can be computed. The conditional non-exceedance distribution of $X \leq x$ given $Y = y$ can be given as follows (Zhang, 2005):

$$F_{X \leq x|Y=y}(x \mid y) = \frac{\partial C_{X,Y}(x, y)}{\partial F_Y(y)} \tag{4.3}$$

Given the conditional probability, one can also gain the probability of attaining the required streamflow (or the risk of streamflow deficit or flood) under the given conditions of hydroclimatic variables. In fact, an $F_X(x)$ event could be defined as "dangerous" if $F_X(x)$ exceeds (or never exceeds) a certain threshold (Salvadori and De Michele, 2004). The current study deems streamflow to be under a "streamflow deficit risk" (i.e., the streamflow drought threshold) if the corresponding streamflow value (here the streamflow PC1 value as introduced in Section 4.3) is less than the 20th percentile of streamflow, denoted as $F_X(x)_{drought} \leq 20\%$. Also, it is possible to obtain the conditional exceedance distribution of $X > x$ given $Y = y$ by

computing $F_{X>x|Y=y}(x \mid y) = 1 - \frac{\partial C_{X,Y}(x, y)}{\partial F_Y(y)}$. This study considers streamflow to be under "flood risk" when the corresponding streamflow value is greater than the 80th percentile of streamflow, denoted as $F_X(x)_{flood} \geq 80\%$. This study focused on three given scenarios of hydroclimatic variables: events at the 30th, 60th and 90th quantiles of hydroclimatic variables, denoted as $F_Y(y) = 30\%$, $F_Y(y) = 60\%$ and $F_Y(y) = 90\%$. It should be mentioned that one could conduct any scenarios of interest for hydroclimatic variables with self-defined streamflow deficit thresholds as long as the copula-based joint distribution has been constructed. Based on the joint distribution, one can use the probabilistic difference between streamflow and hydroclimatic variables to describe the sensitivity of streamflow to different hydroclimatic variables. The probabilistic difference is given as follows:

$$Difference = \int (F_{X|Y=y_1}(x \mid y) - F_{X|Y=y_2}(x \mid y))dx \tag{4.4}$$

4.2.2 Wavelet coherence

Wavelet analysis provides a method to identify the information about the time series for different frequency intervals and is a powerful tool to analyze a nonstationary time series (Özger et al., 2009; Sang et al., 2013; Torrence and Compo, 1998). Wavelet coherence (WTC) is able to evaluate the relationships between different time series by identifying frequency bands and time intervals where two time series are related (Grinsted et al., 2004; Torrence and Webster, 1999). The WTC R_n of two time series is written as:

$$R_n^2(s) = \frac{\left|\Im(s^{-1}W_n^{XY}(s))\right|^2}{\Im(s^{-1}\left|W_n^X(s)\right|^2) \cdot \Im(s^{-1}\left|W_n^X(s)\right|^2)} \tag{4.5}$$

where $\Im$ is a smoothing operator determined by the wavelet type used. $W_n^X(s)$ and $W_n^Y(s)$ are the wavelet transform functions of two time series X and Y. $W_n^{XY}(s)$ is the cross-wavelet spectrum of X and Y. The statistical significance level (5%) is estimated using Monte Carlo methods (Grinsted et al., 2004). The term "coherence"

refers to the squared WTC, ranging from 0 to 1 (1 being the strongest coherence). More details of the WTC method can be in from Grinsted et al. (2004).

4.3 Study area and data sets

Baden-Württemberg is a federal state located in Southwest Germany with an area of 35,752 km^2. The geography varies greatly across this state and it has Germany's largest continuous forest area, i.e., the Black Forest located in west Baden-Württemberg. The main rivers include the Rhine, Neckar (a tributary of the Rhine) and the Danube. The Black Forest is the main mountain range of the state and the Swabian Alps is another important mountain range extending from southwest to northeast. In Baden-Württemberg, the mean annual temperature is around 8.1 °C with a range between 3.3°C in the highest part of the Black Forest and about 10 .4 °C in the Rhine valley. The mean annual precipitation is between 660–2200 mm.

The monthly streamflow anomalies from 37 streamflow gauges in Baden-Württemberg during the period 1948–2003 were provided by Landesverband Baden-Württemberg (LVBW). Table 4.1 shows the statistical information of the streamflow data. The locations of hydrological stations are shown in Fig. 4.2. The dominant patterns of the variability of monthly streamflow anomalies over Baden-Württemberg were examined using the empirical orthogonal function (EOF). The EOF can identify spatiotemporal modes which are ordered by considering their representations of data variance (Liu et al., 2013; Lorenz, 1956). The output of EOF analysis includes spatial patterns (EOFs), temporal coefficients (principal components, PCs), and eigenvalues (Liu et al., 2013). This analysis is an effective approach to examine the spatial and temporal variability of time series covering an area. Table 4.2 indicates that first five EOF loadings of streamflow anomalies from 37 hydrological stations. It can be seen that the first EOF of streamflow has explained around 80% of the total variance. The corresponding monthly time series (PC1) of the first EOF were used to represent the time series of streamflow anomalies over Baden-Württemberg.

Table 4.1 Basic statistical information for the streamflow data.

Station	Mean	Max	Min	Std.	Period
MengenAddAblach	3.206	12.341	0.740	1.664	1948-2003
PfaeffingenAmmer	0.955	3.863	0.152	0.560	1948-2003
GiessenArgen	19.709	64.377	2.587	11.513	1948-2003
HammereisenbachBreg	4.840	21.167	0.522	3.917	1948-2003
BergDonau	38.446	152.744	6.103	24.812	1948-2003
BeuronDonau	11.944	71.572	0.245	12.850	1948-2003
HundersingenDonau	25.704	115.705	2.577	19.922	1948-2003
KirchenHausenDonau	13.041	58.849	1.275	10.130	1948-2003
EbnetDreisam	5.899	23.579	0.111	4.503	1948-2003
MosbachElz	2.011	15.389	0.205	2.101	1948-2003
PforzheimEnz	18.165	100.184	4.223	13.121	1948-2003
RiederichErms	2.982	11.105	0.489	1.627	1948-2003
PlochingenFils	9.390	55.619	0.530	7.424	1948-2003
HopfauGlatt	4.112	28.084	0.449	3.753	1948-2003
DoerzbachJagst	10.199	68.324	0.473	10.071	1948-2003
JagstzellJagst	3.042	19.504	0.160	2.907	1948-2003
UntergriesheimJagst	16.472	107.168	1.730	14.745	1948-2003
HoelzlebruckJosbach	1.408	5.818	0.165	1.028	1948-2003
SchwaibachKinzig	23.360	111.164	2.440	18.030	1948-2003
KocherstettenKocher	16.287	100.754	1.100	14.326	1948-2003
SteinKocher	23.713	134.983	2.971	19.502	1948-2003
RiegelLeopoldskanal	13.987	74.679	0.002	13.577	1948-2003
RotenfelsMurg	15.679	65.115	2.892	10.947	1948-2003
HorbNeckar	14.243	82.322	1.122	11.478	1948-2003
OberndorfNeckar	7.494	41.537	0.613	5.693	1948-2003
PlochingenNeckar	47.471	238.673	4.921	33.552	1948-2003
UntermuenstertalNeumagen	1.662	6.069	0.180	1.123	1948-2003
BerghausenPfinz	1.855	8.703	0.333	1.252	1948-2003
NeustadtRems	6.352	34.525	0.795	4.474	1948-2003
NiederkirchRiss	4.424	11.270	1.464	1.542	1948-2003
UnterschmeienSchmeie	1.574	6.318	0.168	1.098	1948-2003
GerbertshausSchussen	10.908	40.013	2.417	6.045	1948-2003
SennfeldSeckach	2.311	11.153	0.499	1.576	1948-2003
BadMergentheimTauber	6.213	43.925	0.552	5.938	1948-2003
ZellWiese	7.778	29.797	0.387	5.765	1948-2003
PforzheimWuerm	2.804	23.907	0.489	2.121	1948-2003
OberlauchringenWutach	8.912	44.699	0.575	7.015	1948-2003

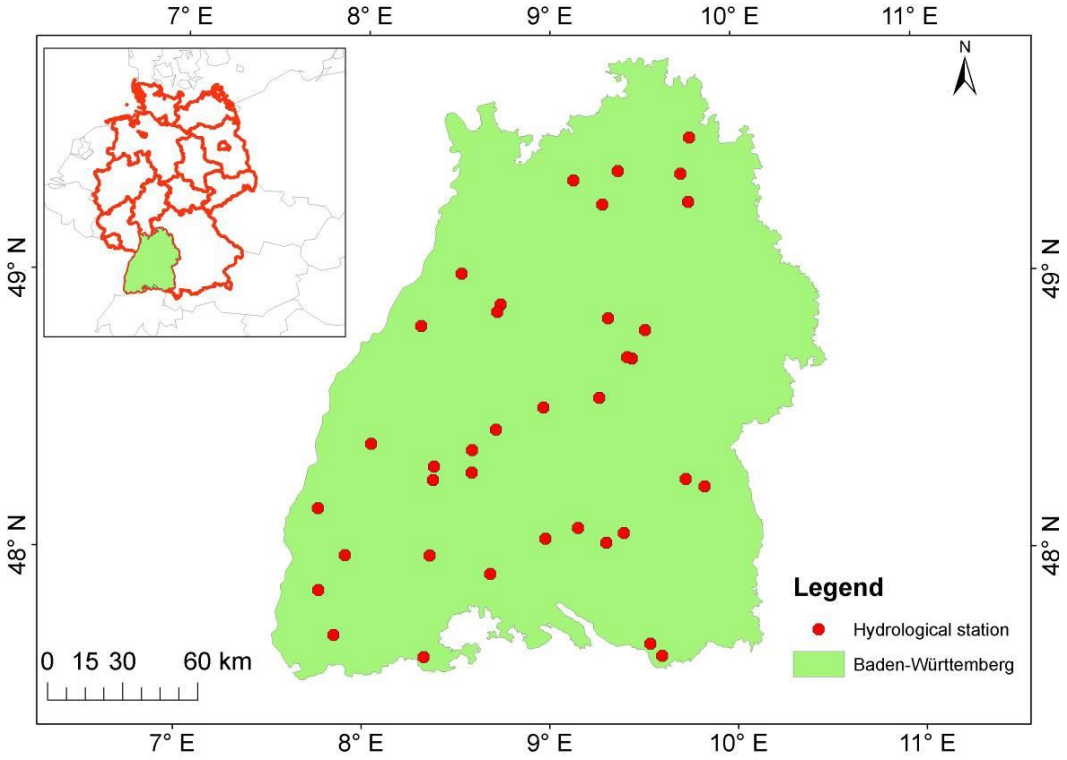

Figure 4.2 Locations of 37 hydrological stations over Baden-Württemberg.

Table 4.2 First five EOF loadings of monthly streamflow anomalies from 37 stations.

Mode	PC1	PC2	PC3	PC4	PC5
Percent variance explained (%)	79.949	5.161	3.015	2.452	1.554
Cumulative variance (%)	79.949	85.110	88.125	90.577	92.131

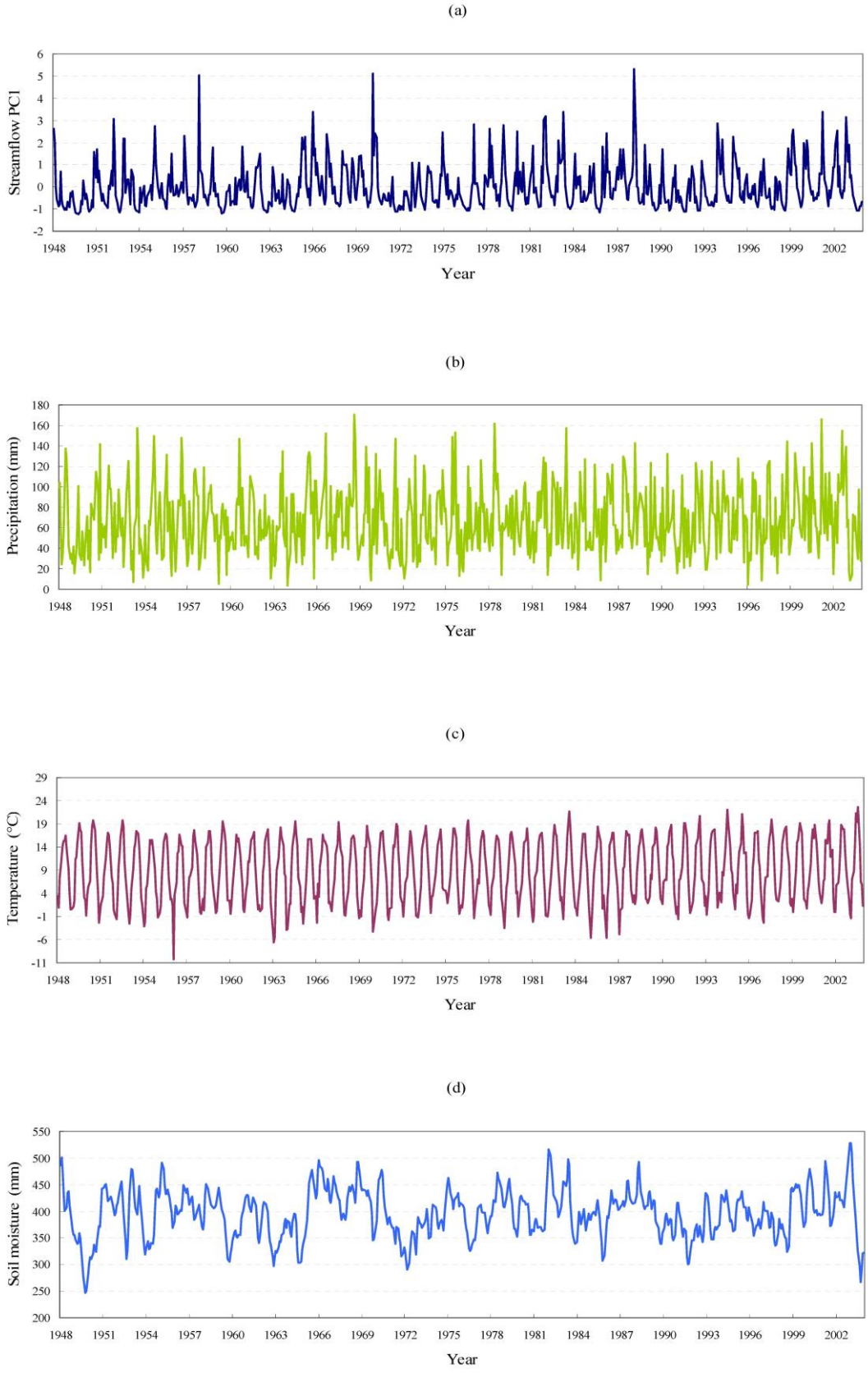

Figure 4.3 The monthly time series of streamflow PC1 (a), precipitation (b), temperature (c) and soil moisture (d).

The monthly precipitation, monthly temperature, and modeled monthly soil moisture were derived from climate prediction center (CPC) datasets with a spatial resolution of 0.5° (available from https://data.noaa.gov/dataset). These gridded products have been widely used for many regional hydroclimatic applications (e.g., Fan and van den Dool, 2008; Fujinami et al., 2015; Syed et al., 2014; Zhang et al., 2012). The time series of temperature, precipitation and soil moisture for Baden-Württemberg were gained by spatially averaging the grids over the study area. The monthly anomalies of temperature, precipitation and soil moisture were gained by subtracting their corresponding monthly means. For the analysis of atmospheric circulation, this study used the geopotential height anomalies (Z850), the zonal and the meridional wind (U- and V-wind) components at 850 hPa on a $2.5° \times 2.5°$ grid during the period 1948–2003, from the national centers for environmental prediction/national center for atmospheric research (NCEP/NCAR) R1 dataset (Kalnay et al., 1996). The time series of these variables are plotted in Fig. 4.3.

4.4 Results

4.4.1 Probabilistic relationships between streamflow and hydroclimatic variables

In this section, this study first examined the joint dependence structure between streamflow (PC1 values) and hydroclimatic variables. Then the study identified the conditional probability of streamflow under different scenarios of hydroclimatic variables based on the established dependence structure. The joint dependence structure between streamflow and hydroclimatic variables in different seasons was constructed by a proper bivariate copula function through joining their marginal distributions. The Cramér-von Mises test was used to test the goodness-of-fit of the copulas, as mentioned in Section 4.2.1. Table 4.3 gives the goodness-of-fit statistics (S_n) of the Cramér-von Mises test for the dependence between streamflow and other hydroclimatic variables (i.e., precipitation, temperature, and soil moisture) in each season. Although the best-fitted copula varies in different cases, the Normal copula tends to be more appropriate to fit the joint dependence between streamflow and both precipitation and soil moisture for most seasons. The Frank copula seems to better

join streamflow and temperature. Based on the best-fitted copula, it is also possible to obtain the joint CDF of streamflow and different hydroclimatic variables in four seasons as illustrated in Fig. 4.4. Once the dependence structure is built up, the conditional distributions of streamflow conditioned upon two scenarios (i.e., $F_Y(y) = 30\%$ and $F_Y(y) = 70\%$) of explanatory variables (e.g., precipitation, temperature and soil moisture) can be obtained using Equation (4.3).

Table 4.3 The Cramér–von Mises statistics (S_n) of different copulas (2-dimendional) for the dependence between streamflow and precipitation, temperature and soil moisture in each season. The S_n statistics that are accepted by the Cramér–von Mises test at the significance level of 0.05 are shown in bold. The one with smallest S_n statistics is the most appropriate copula among others, indicated by *.

Variables	Copula	Spring	Summer	Autumn	Winter
Precipitation	Normal	**0.028**	**0.016***	**0.020***	**0.018***
	Clayton	0.148	**0.030**	0.095	0.061
	Frank	**0.027***	**0.021**	**0.034**	**0.034**
Temperature	Normal	**0.035**	**0.044**	**0.037**	**0.015**
	Clayton	**0.065**	0.256	**0.066**	**0.066**
	Frank	**0.030***	**0.042***	**0.031***	**0.015***
Soil moisture	Normal	**0.017***	**0.016***	**0.033**	**0.014***
	Clayton	0.071	**0.052**	**0.029***	**0.049**
	Frank	**0.023**	**0.025**	0.041	**0.025**

Fig. 4.5 indicates the conditional distributions of streamflow under two given scenarios of the hydroclimatic variables in different seasons. In addition, it is also possible to gain the probability (the intersections between the dashed line and two solid curves) of streamflow deficit events regarding a certain streamflow threshold ($F_X(x)_{drought} \leq 20\%$) given the two precipitation conditions in Fig. 4.5. This value helps to know about the risk of occurring streamflow deficit occurring for the given streamflow thresholds, and smaller values mean a lower deficit risk. For precipitation, the risk of streamflow deficit in different seasons is generally around 20–50% under the low-precipitation scenario ($F_Y = 30\%$). The increment of precipitation (i.e., under the precipitation scenario $F_Y = 70\%$) indeed has a positive effect on reducing the streamflow deficit risk (lower than 10%). This difference between the two curves of

conditional distributions also suggests that streamflow in this study area is very sensitive to the precipitation in each season. It can be noted that in spring and summer the risk of streamflow deficit is weak for the given low-temperature condition. However, when the temperature shifts towards a higher condition, the streamflow deficit risk turns to be higher, particularly in summer. The streamflow seems insensitive to the temperature variability in autumn but the higher temperature results in a low streamflow deficit risk in winter, as shown in Fig. 4.5. The soil moisture presents a similar pattern of the conditional distribution as compared to precipitation. In general, the streamflow deficit risk drops to some extent under the high soil moisture conditions. Fig. 4.6 provides the occurrence probability for the given flood threshold ($F_X(x)_{flood} \geq 80\%$) conditioned on two given hydroclimatic scenarios. Under scarce precipitation and soil moisture conditions, the risk of floods occurring is relatively low (below 10%) for each season. The risk apparently increases to some extent (between 20–40%) when precipitation and soil moisture become sufficient, particularly in autumn. Regarding temperature, the flood risk is below 20% for both high and low temperature conditions in most seasons with the exception of winter when the risk is around 30% under the high temperature scenario.

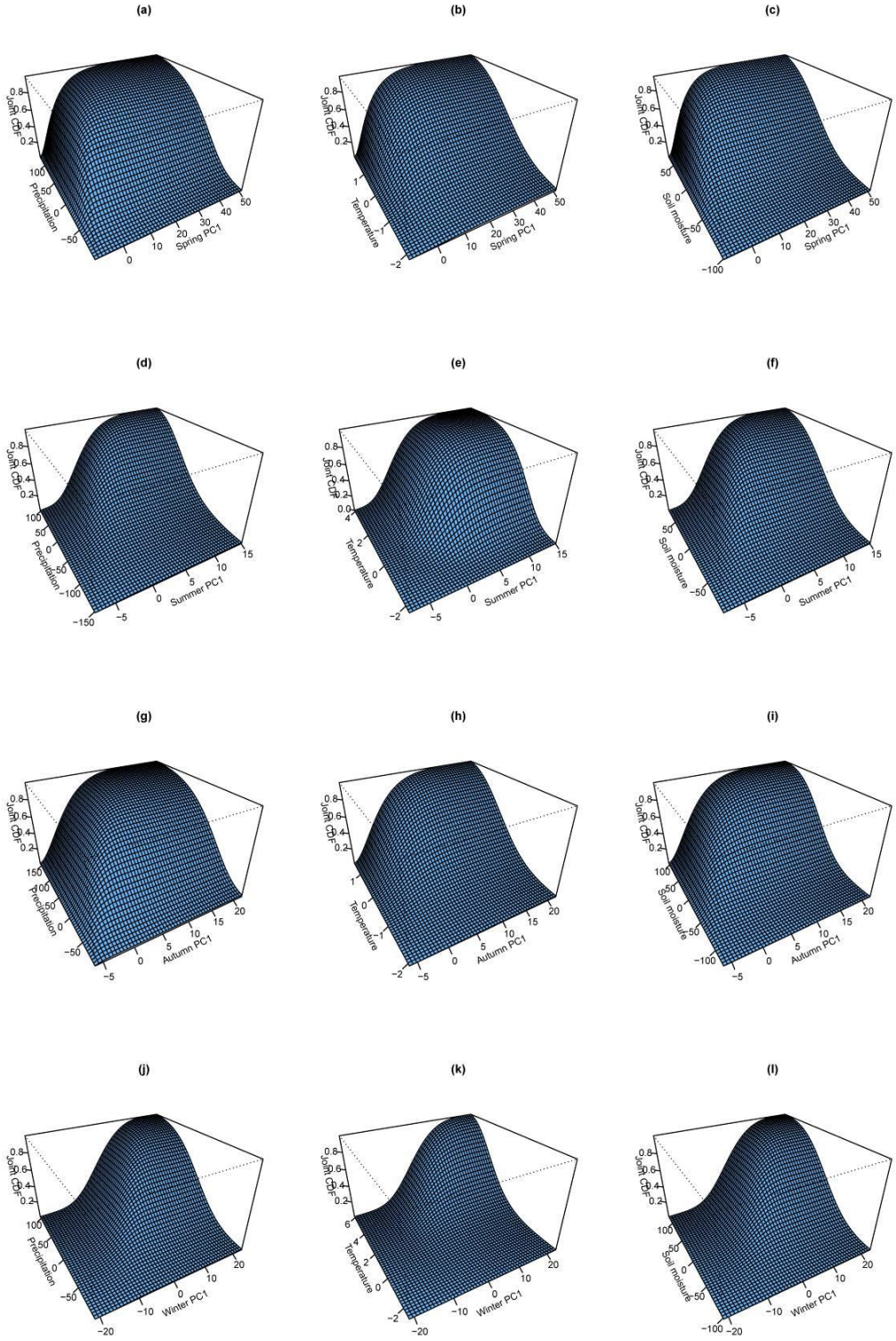

Figure 4.4 The joint CDF of streamflow PC1 values and different hydroclimatic variables in four seasons.

Additionally, this study also examined the probabilistic relationships between

streamflow and hydroclimatic variables across different seasons using Equation (4.4). As shown in Fig. 4.5, it is evident that the precipitation and soil moisture generally present stronger positive probabilistic relationships with streamflow than others in each season. There is an inverse probabilistic relationship between streamflow and temperature in spring and summer, while the relationship seems to be very weak in autumn and turns positive in winter.

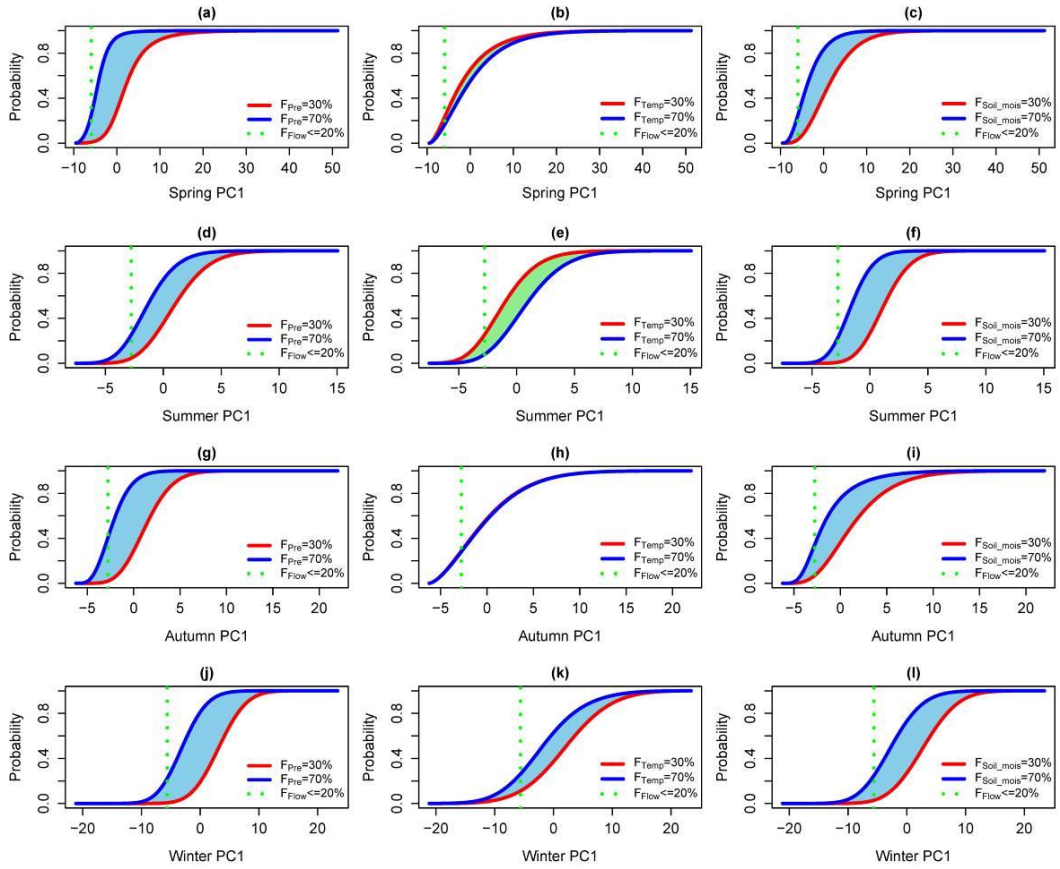

Figure 4.5 The conditional non-exceedance distribution of streamflow for different seasons under two hydroclimatic scenarios: $F_Y(y)$ = 30% (red line) and $F_Y(y)$ = 70% (blue line), as well as risk (the intersections between the dashed line and two solid curves) of streamflow deficit events concerning a certain streamflow threshold ($F_X(x)_{drought} \leq 20\%$). The blue areas indicate the positive probabilistic relationship, while the green areas indicate the inverse probabilistic relationship. The bigger the area, the stronger the probabilistic relationship.

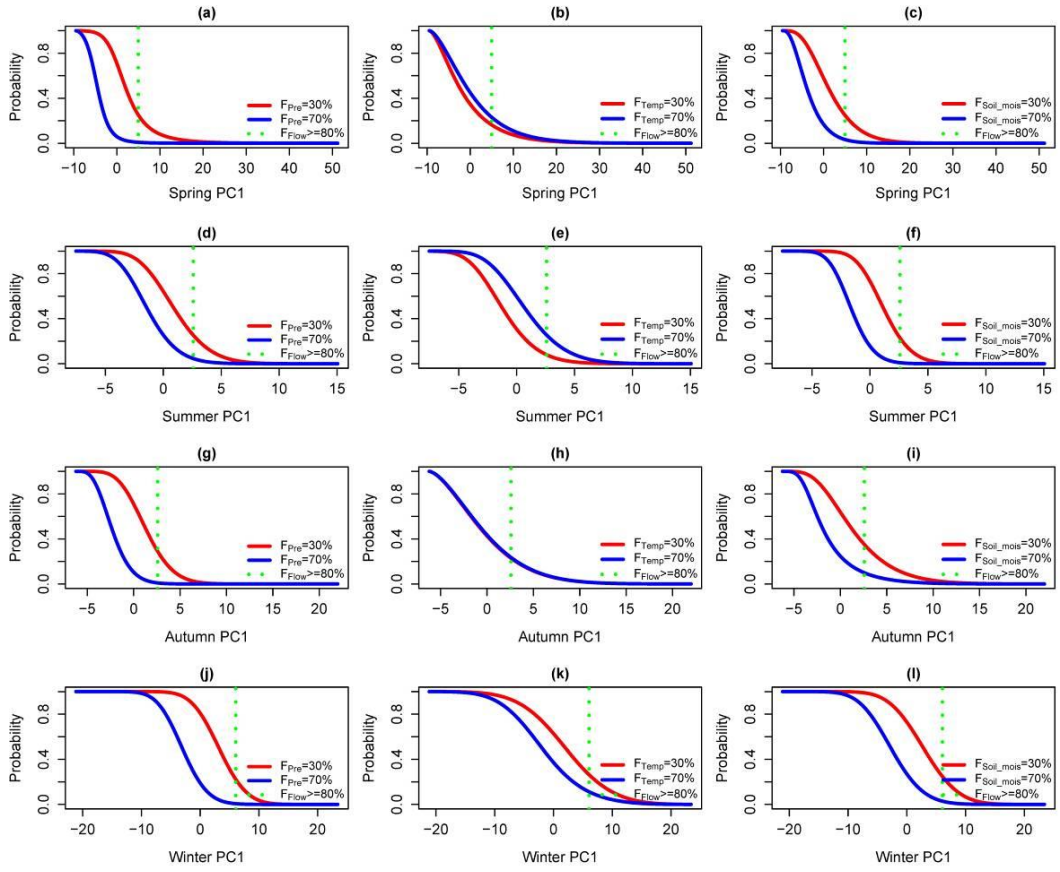

Figure 4.6 The conditional exceedance distribution of streamflow for different seasons under two hydroclimatic scenarios: $F_Y(y)$ = 30% (red line) and $F_Y(y)$ = 70% (blue line), as well as risk (the intersections between the dashed line and two solid curves) of floods concerning a certain streamflow threshold ($F_X(x)_{flood} \geq 80\%$).

4.4.2 Multi-scale relationships

To further identify the frequency bands within which the time series of streamflow and hydroclimatic variables are co-varying (i.e., the multi-scale relationships), the WTC analysis was used in this study. Fig. 4.7 shows the wavelet coherence spectra between streamflow and hydroclimatic variables in four seasons. Colors in Fig. 4.7 illustrate the strength of the coherence, and the red and orange areas within the black lines are significant at the 95% level against red noise. For the multi-scale relationships between streamflow and precipitation, the significant wavelet coherence can be observed in most areas of the spectra for all seasons. The left arrows indicate that the phase relations in these sectors with significant coherence are prominently in-phase (i.e., positive coupling). This demonstrates that at multi-year scales

precipitation generally contributes significantly to the increase of streamflow in this study area during most years. However, there is very weak coherence between streamflow and both precipitation and soil moisture at some specific time scales, e.g., the time scales of 4–8 years during 1950–1980 for spring and around 2–6 years in the 1980s and 1990s for summer, suggesting that streamflow variability is not always sensitive to the changes in precipitation at multi-year scales. It can also be noted that at decadal scales streamflow and precipitation have a stable positive relationship across all years in both spring and winter.

Temperature has quite complex wavelet coherence spectra and the significant areas of coherence are significantly less than those of precipitation, reflecting the weaker influence of temperature on streamflow at multi-year scales in the study area. The phase angles with significant power vary among different seasons, indicating the ambiguous and unstable phase correlations. In spring, the significant coherence between streamflow and temperature occurs at shorter time scales (e.g., 2–4 years). The temperature spectra in summer present significant coherence at the time scales of 10–12 years across almost all years considered. Unlike other variables, the phase angles in spring and summer suggest that the streamflow and temperature are generally in anti-phase, highlighting the negative relationships between them at different time scales, particularly in summer. The wavelet coherence becomes quite weak in autumn. In winter, temperature exhibits strong coherence at shorter time scales during some specific periods and the time scales of 6–10 years during 1955–2003. However, the arrows turn to be in-phase, identifying the positive linkages between temperature and streamflow at these scales.

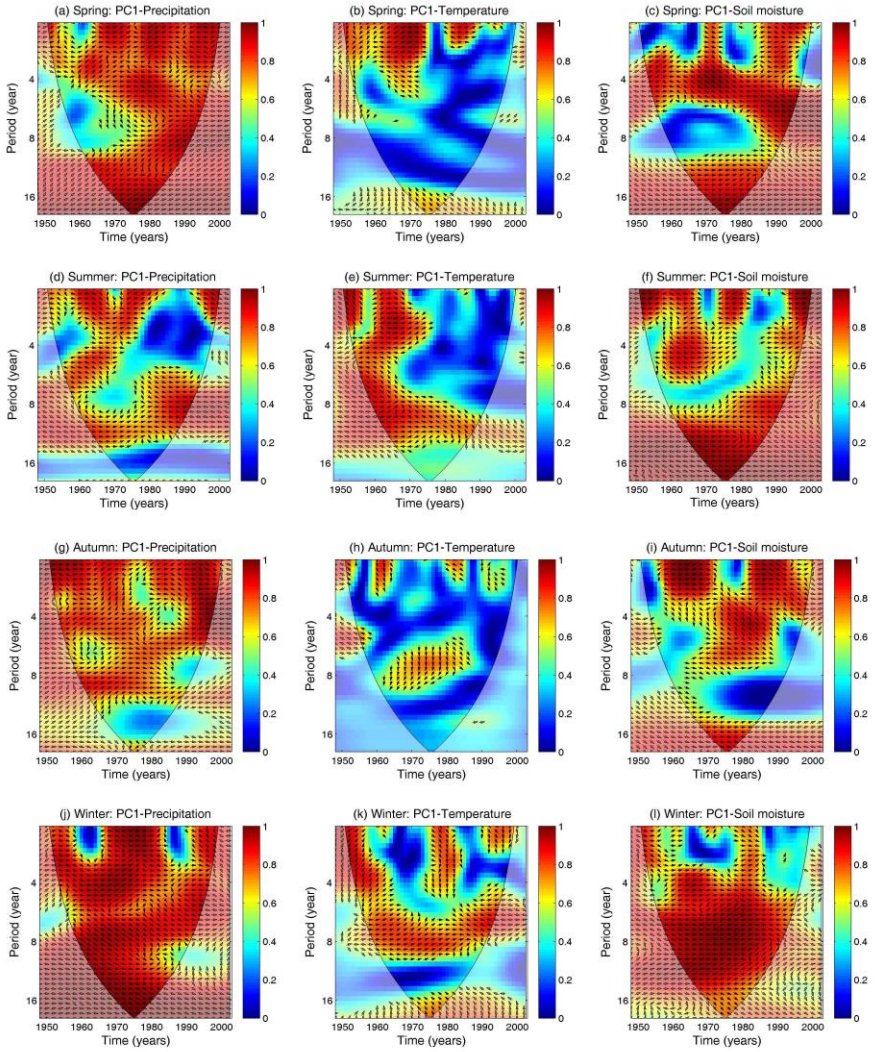

Figure 4.7 The squared wavelet coherence (WTC) and phase between different hydroclimatic variables in four seasons. Figures are color-mapped to show high values (1 being the highest coherence) of squared WTC with red and orange, and low values in blue. The thick black contour is the 5% significance level, and the black line indicates the cone of influence (COI) (to reduce the edge effect). Right-pointing arrows denote that the relationships are in-phase (positive) while left-pointing arrows are for anti-phase signals.

The significant coherency between streamflow and soil moisture can be found in most regions of the WTC maps (Fig. 4.7). In spring, the peak coherence occurs at 4–8 years and longer-term scales (e.g., greater than 10 years) across 1950–2003. In summer, at the high-frequency scales (e.g., 2–8 years) the relationship between streamflow and soil moisture tends to be unstable and the significant coherency differs with time,

while at longer-term scales the coherency shifts to be very homogeneous during the whole time period considered in this study. Significant coupling occurs across periodic components of 2–8 years from 1970–2003 in autumn. Coherency becomes strong at the scales of higher than 4 years in winter. The phase angles of the significant coherency are dominantly in-phase, reflecting that high soil moisture generally produces a positive streamflow response in Baden-Württemberg.

4.4.3 Linkages between streamflow variability and atmospheric circulations

In this section, this study investigated the possible physical mechanism of the linkages between the streamflow and atmospheric circulations in different seasons. For each season, this study used the first principal component of streamflow anomalies over Baden-Württemberg (i.e., PC1 values) to build composite anomaly maps of geopotential height and wind vectors at 850 hPa for both high and low streamflow years. The high and low streamflow events for each season were determined by two thresholds: events not exceeding 30% of the streamflow PC1 (low flow) and events exceeding 70% of the PC1 (high flow).

For spring, the composite map of the Z850 anomalies and wind vectors for the years with high values of the streamflow anomalies shows a center of positive geopotential height anomalies over Greenland and a negative center over northern Europe (Fig. 4.8). This pattern leads to a strong pressure gradient difference between the positive and negative centers. As illustrated in Fig. 4.8, high streamflow anomalies in Baden-Württemberg are related to a cyclonic activity over northern Europe leading to an eastward shift of the Atlantic jet orientation (the wind vectors) that is beneficial for the transport of warm water vapor from the Atlantic Ocean towards Europe, including the study area. This could be bring enhanced precipitation in this area thus results in high streamflow anomalies. However, an opposite pattern is found in the years with low streamflow anomalies (Fig. 4.8b). Northern Europe becomes a center of positive geopotential height anomalies. This pressure gradient induces the dry and cold air from the Scandinavian Peninsula (see the wind sector) to Baden-Württemberg and thus results in reduced precipitation over this region.

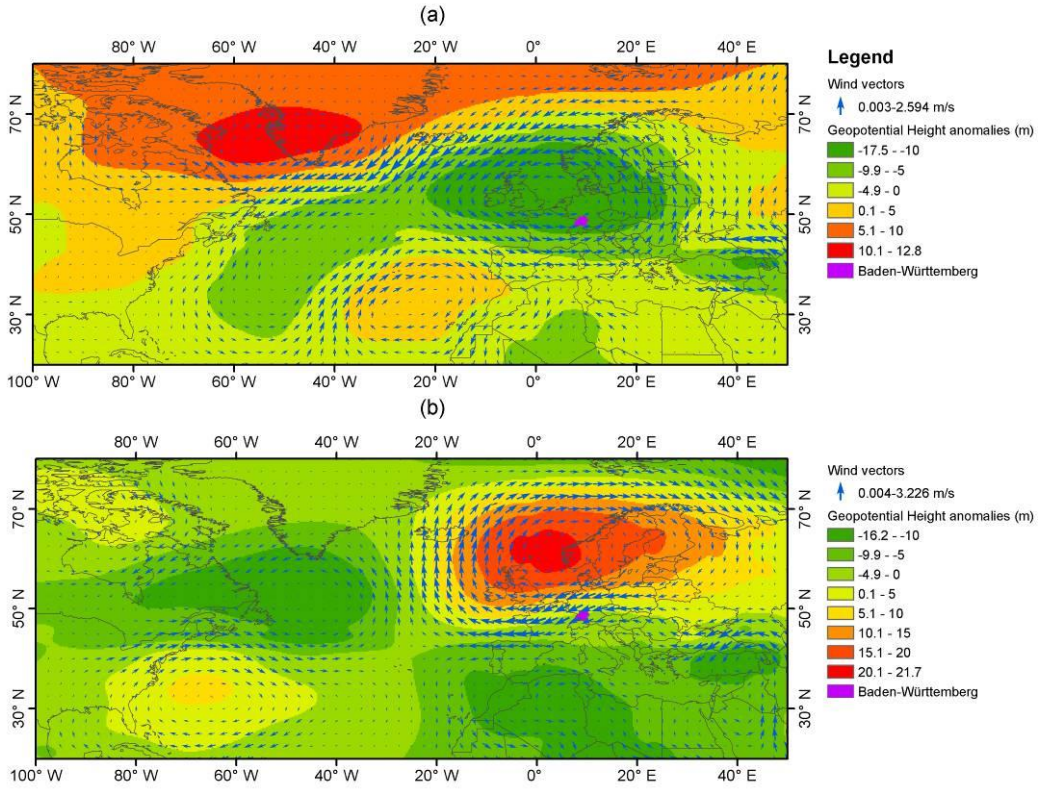

Figure 4.8 The composite anomaly map of the geopotential height and wind vectors (arrows) at 850 hPa in the high (a) and low (b) spring-streamflow years.

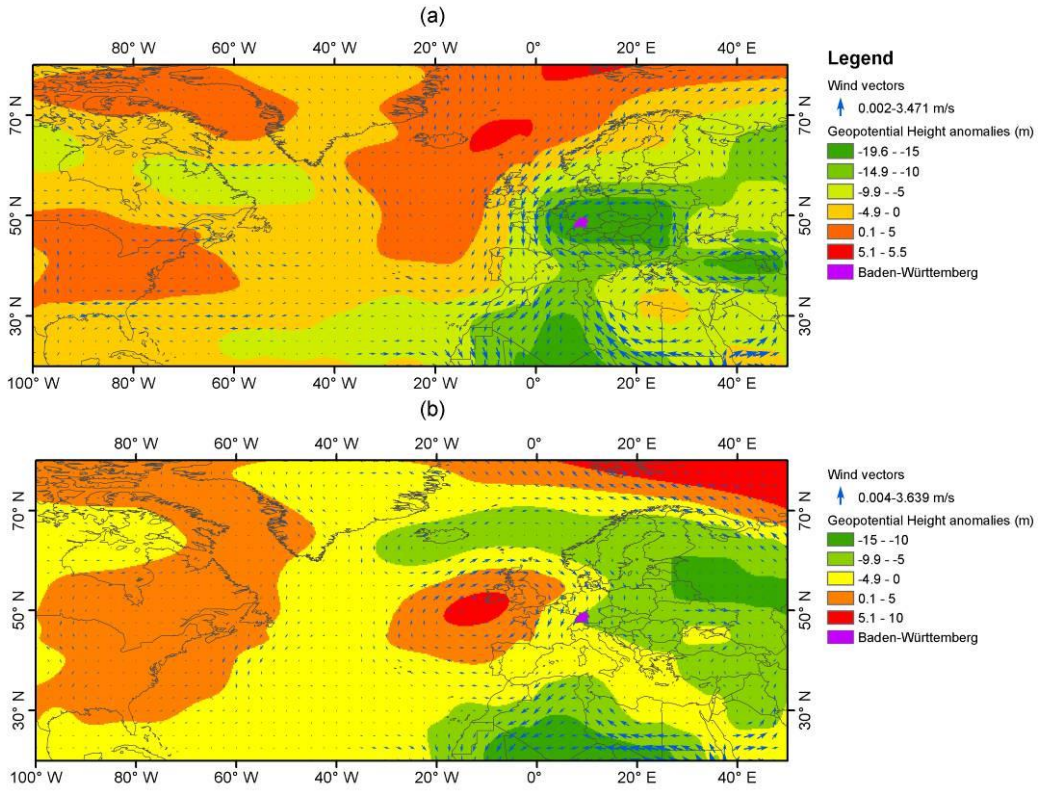

Figure 4.9 The composite anomaly map of the geopotential height and wind vectors (arrows) at 850 hPa in the high (a) and low (b) summer-streamflow years.

Fig. 4.9 shows the composite anomaly maps of the geopotential height and the wind vectors in the high (a) and low (b) summer-streamflow years. For the years of high streamflow anomalies, there is a center of negative geopotential height anomalies over central Europe. A positive center is over the Northern Atlantic Ocean. The study area is found under a cyclonic region in central Europe, which could induce water vapor from the North Atlantic Ocean to Europe including Baden-Württemberg and thus result in intensive precipitation and above-normal streamflow. This map also shows that central Europe is under the effect of the African jet. The warm and dry air from the eastern portion of northern Africa is brought to Europe, but mainly in the southern part. During the years of low summer streamflow anomalies, a center of positive geopotential height anomalies is located the west of Ireland. The anticyclonic activity over this region can result in the reduced precipitation in western Europe, including Baden-Württemberg.

During autumn, the composite map regarding high streamflow anomalies (Fig. 4.10a) shows a center of strong negative geopotential height anomalies in northwest Europe, while a positive center is located in the Arctic Ocean. This pressure gradient results in the movement of moist air from the North Atlantic Ocean towards central Europe, which may enhance precipitation over this region (as a result of high streamflow anomalies). As shown in Fig. 4.10b, the composite map of low streamflow anomalies presents an opposite pattern of the geopotential height anomalies and wind vectors over Baden-Württemberg. In winter (Fig. 4.11), the patterns of the geopotential height anomalies and the wind vectors for the high streamflow anomalies show a very similar structure to that of spring. This pattern induces warm water vapor from the tropical North Atlantic Ocean to most European regions. On the contrary, the composite map of low streamflow anomalies shows an opposite pattern.

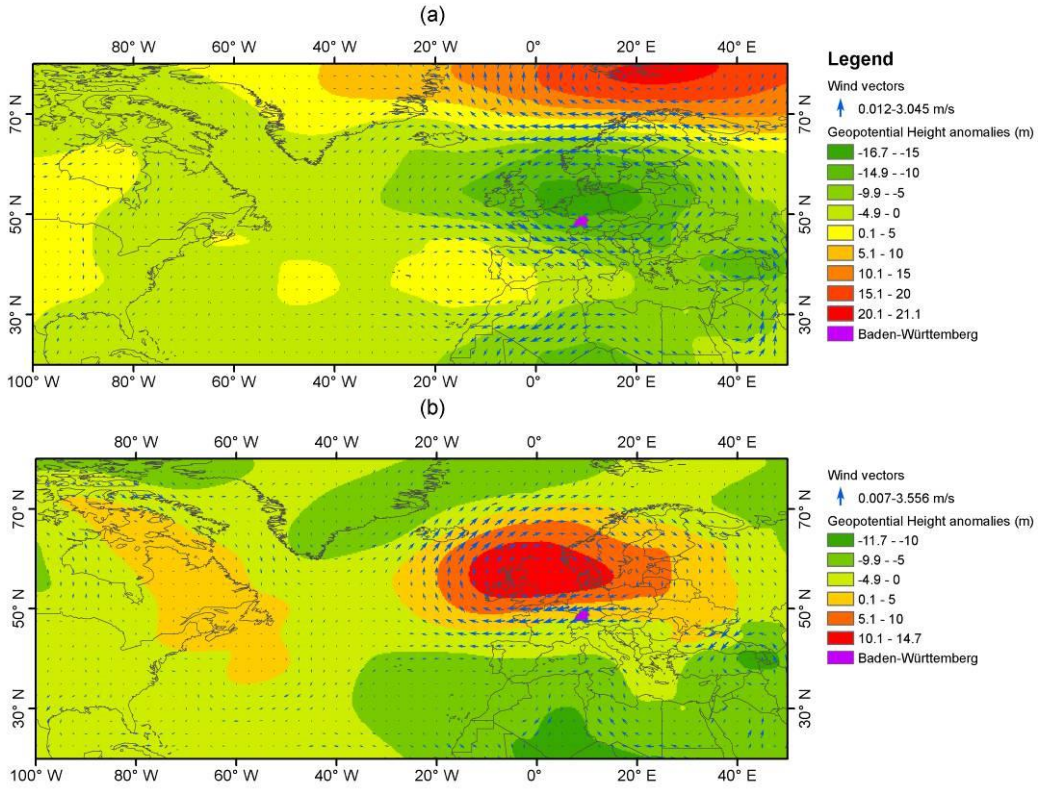

Figure 4.10 The composite anomaly map of the geopotential height and wind vectors (arrows) at 850 hPa in the high (a) and low (b) autumn-streamflow years.

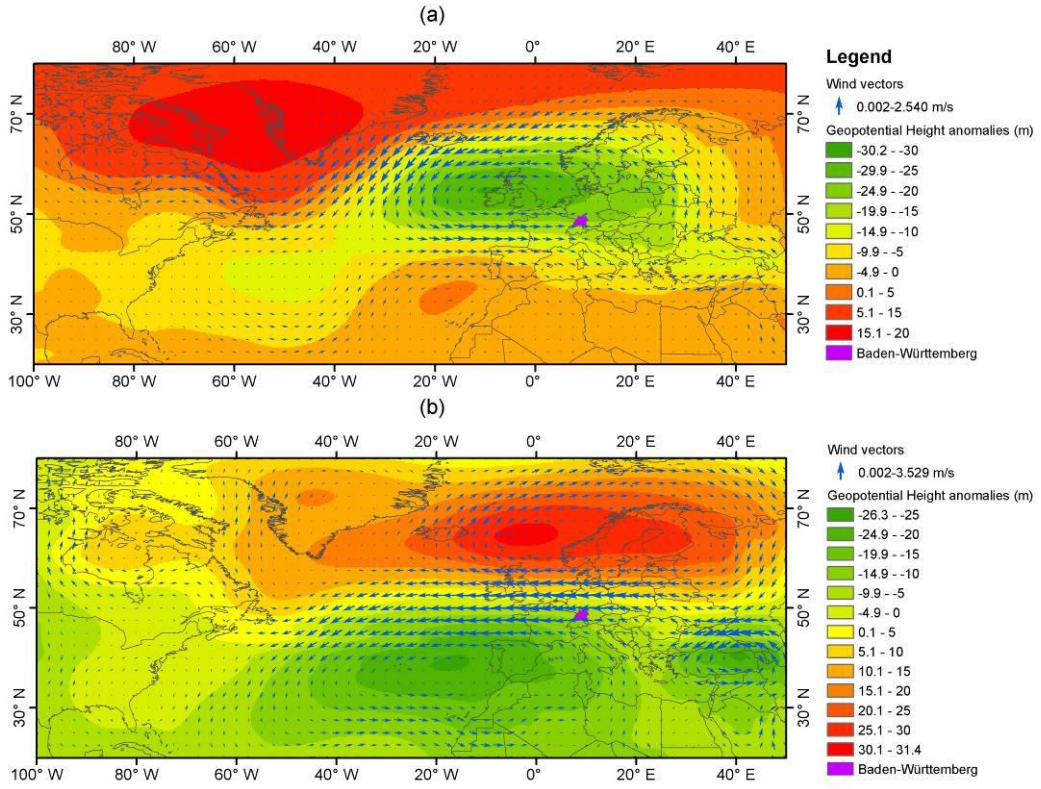

Figure 4.11 The composite anomaly map of the geopotential height and wind vectors (arrows) at 850 hPa in the high (a) and low (b) winter-streamflow years.

4.5 Discussion and conclusions

This study presents a general approach to identify probabilistic and multi-scale relationships between streamflow and hydroclimatic variables (precipitation, temperature and soil moisture) and the potential connections to large-scale atmospheric circulations in Baden-Württemberg, Southwest Germany. First, copulas were employed to construct a bivariate probabilistic model to examine the dependence between streamflow and hydroclimatic variables. Once a joint distribution has been established, the probability of streamflow deficit or flood (defined by certain streamflow thresholds) was evaluated conditioned upon two different given scenarios of hydroclimatic variables across different seasons. It is thus possible to obtain the information about the risk of streamflow deficit events and floods occurring under the given conditions of hydroclimatic variables. This risk-based assessment presents important additional information for the development of hydrological drought mitigation and flood prevention strategies. Based on the established bivariate model, it is also possible to provide a visual comparison of the probabilistic relationships between streamflow and hydroclimatic variables using a proposed method. Our results show that the streamflow is strongly affected by precipitation. According to the estimation of probabilistic relationships and wavelet coherence at different time scales, precipitation generally has a positive effect on streamflow.

It is understandable that precipitation plays a positive role in the changes of streamflow and is largely responsible for the occurrence of floods in this study area (Ruiz-Villanueva et al., 2012). The analysis of the precipitation-streamflow relation also indicates the probabilistic and multi-scale relationships between streamflow and precipitation vary in different seasons. Our results show that temperature has less importance in contributing to changes of streamflow in each season when compared to precipitation and soil moisture. For both probabilistic and multi-scale analyses in spring and summer, temperature plays an inverse role in the changes of streamflow. This is probably attributed to the fact that temperature generally has an influence on the initial soil moisture state via evapotranspiration, particularly in summer

(Haslinger et al., 2014). However, this effect is less significant in winter in this study area as the rate of evapotranspiration is low. In autumn, the changes in temperature have little effect on streamflow, suggesting that precipitation and soil moisture probably have a more significant effect on runoff. In winter, temperature provides a positive contribution to the changes of streamflow by affecting the occurrence of snowfall and snowmelt. A higher temperature generally exacerbates the snowmelt, particularly in mountainous regions such as the Black Forest. On the other hand, an increase of temperature in winter may result in more precipitation in the form of rainfall instead of snowfall, as a consequence of more streamflow.

Streamflow is also sensitive to the changes in soil moisture and there are positive relationships between streamflow and soil moisture across different seasons. However, we cannot find a threshold of the soil moisture affecting the streamflow variability and conclude the detailed mechanism of soil moisture on runoff generation in the study area based on the current data. More extensive studies will focus on this topic based on more measured soil moisture data at some specific catchments in Baden-Württemberg. In addition, future works will also be extended to investigate the influence of spatial variability in climate and soil moisture on runoff generation on a catchment scale.

Wavelet coherency was used to investigate the variability of relationships between streamflow and hydroclimatic variables at multi-year scales in four seasons. Despite varying significantly, strong positive links between streamflow and both precipitation and soil moisture can be found at most temporal scales, particularly at decadal scales. This highlights that in general the changes in precipitation and soil moisture significantly drive the streamflow variability at multi-year scales in Baden-Württemberg. The coupling of temperature and streamflow is not as notable as that of precipitation and soil moisture at different temporal scales, and only at some specific time scales temperature is strongly coupled with streamflow. In spring and summer, these strong relationships are generally opposite, yet turn to be positive in winter.

This study further assessed the connections between streamflow over

Baden-Württemberg and large-scale atmospheric circulations based on composite analysis. In most seasons the high streamflow anomalies over Baden-Württemberg are generally related to westerly atmospheric circulations that can result in the transport of warm water vapor from the Atlantic Ocean towards the study area and enhance the precipitation. This thus leads to more streamflow (Beurton and Thieken, 2009; Ionita et al., 2012a; 2012b; 2015; Petrow and Merz, 2009). It is also possible to find that the atmospheric circulation structures in winter and spring are very similar, particularly for the years with high streamflow anomalies. This suggests that there might be a persistent influence of circulation systems on the climate conditions over Baden-Württemberg from winter to spring. In summer, the cyclonic activity over central Europe causes increased precipitation and thus high streamflow anomalies. The low streamflow anomalies are generally linked to the northerly circulations that induce the movement of cold air from the northern Europe towards this study area and reduces the precipitation. It has also been well reported that the climate variability in Europe is linked to the North Atlantic Oscillation (NAO). The NAO affects the intensity and direction of the wind anomalies and interaction between air masses in the North Atlantic region. It is also one of the most important teleconnection patterns which affects the climate and hydrology over Europe in all seasons (Barnston and Livezey, 1987; Hurrell et al., 2003; Kingston et al., 2006), particularly in winter when the atmosphere is very active and greatly drives the climate dynamics. Rimbu et al (2004) documented that there is generally below-normal precipitation over central Europe during the positive phase of the NAO and opposite precipitation conditions are found during the negative phase of the NAO. Thus this might also influence the streamflow variability over Baden-Württemberg. Moreover, some existing studies also pointed out that El Niño–Southern Oscillation (ENSO) events have a significant influence on the precipitation and streamflow over Europe. The El Niño events are usually associated with the large streamflow in most rivers from Europe while the opposite situation happens during La Niña events (Dettinger and Diaz, 2000). Some previous studies have reported that there is a significant connection between ENSO events and the streamflow variability of the Danube River and Rhine River. Both

rivers flow across the study area. The further work will focus on exploring the specific connections between climate indices and streamflow variability over Baden-Württemberg, particularly on interannual to decadal scales.

Chapter 5: A probabilistic prediction network for hydrological drought identification and environmental flow assessment

5.1 Introduction

Drought, or water deficit, is a natural disaster that takes place in all climate zones (Wilhite and Buchanan-Smith, 2005; Tatli and Türkes, 2011). Relying on evolution of water deficit from precipitation to soil moisture and to streamflow and potential socio-economic consequences, drought is generally characterized as meteorological, agricultural, hydrological and socio-economic (American Meteorological Society (AMS), 2004; Mishra and Singh, 2010; Wilhite and Glantz, 1985). Of these types, hydrological drought is described as the abnormally low flow in rivers and abnormally low levels in groundwater, lakes, and reservoirs (Tsakiris and Vangelis, 2004; Van Loon, 2015). Streamflow, which is a key variable for expressing surface water resources, has being widely used for hydrological analysis (Mishra and Singh, 2010; Nalbantis and Tsakiris, 2009). A hydrological drought event can be defined according to the streamflow deficit compared to normal conditions. In order to quantitatively assess hydrological droughts and to identify their features (e.g., severity, intensity, temporal duration and spatial distribution), several hydrological drought indices based on streamflow have been developed, such as the surface water supply index (SWSI) (Shafer and Dezman, 1982) and the standardized runoff index (SRI) (Shukla and Wood, 2008). Recent developments in characterizing drought status have involved the extraction of information from multiple sources and temporal scales by building up a joint probability distribution model (Hao and Singh, 2015). Copulas could be an ideal tool for this task, because they are flexible to construct the joint dependence structure without any restrictions on the marginal distributions (Nelsen, 2006; Salvadori and De Michele, 2004). In the past few years, copulas have gained popularity in the probabilistic modeling of various hydrological phenomena (Bárdossy and Pegram, 2013; Favre et al., 2004; Li et al., 2013a; 2013b; 2014; Madadgar and Moradkhani, 2013; Maity et al., 2013), including hydrological drought identification

and assessment (e.g., the joint deficit index (JDI) and multivariate standardized drought index (MSDI)) (Hao and AghaKouchak, 2013; Kao and Govindaraju, 2010). However, most studies in hydrology involving copulas generally focused on two- to three-dimensional parametric copula models or empirical copulas because the direct extension of parametric copulas is very limited at higher dimensions (Hao and Singh, 2013; Lopez-Paz et al., 2013). Recent efforts in copula theory have resulted in new approaches, such as vine copulas for modeling the joint dependence structure between different variables. Vine copulas focus on problems with large dimensions. They are based on hierarchical structures that construct a higher-dimensional copula by sequentially employing bivariate copulas as the basic blocks. This has enabled a significant progress in modeling joint distributions from complex multivariate data (Kurowicka and Cooke, 2006; Liu et al., 2015a).

Today, there are increasing recognitions and desires for water resources managers, governments, and decision-makers to consider the water flows required for water resources development and management (e.g., the drinking water supply, irrigation, industrial water demands, drought preparedness, and hydropower generation), and for maintaining the health and ecological functioning of a river ecosystem (including essential ecosystem processes, water quality, disturbed riparian habitats, and species composition and structure) (Mathews and Richter, 2007; Tharme, 2003). This thus results in accelerated development of the approach of environmental flow assessment. Environmental flow assessment is generally defined as an assessment of the certain volume of water required in a river in order to sustain specific and valued features of the ecosystem (King et al., 2003; Tharme and King, 1998). In recent years, a growing variety of methodologies have been developed to assess the environmental flows for different rivers (Mathews and Richter, 2007; Richter et al., 1997; Tharme, 2003; Yin et al., 2011). The simplest environmental flow assessment methodologies focus on using the hydrological data to establish a certain flow rate that should be exceeded or exceeding percentiles from a flow duration curve, based on statistical evaluation of historical monthly or daily flow records. They often refer to the minimum flows indicating that the river ecosystem is at an acceptable level (Cavendish and Duncan,

1986; Tennant, 1976). Later on, other elements of a flow regime that may impact the river ecosystem are considered for the environmental flow assessment such as low and medium flows as well as floods (Hill and Platts, 1991; Junk et al., 1989; Yin et al., 2011). Some methodologies tend to combine the observed hydrological data and use certain hydrological indices and ecological data to examine the environmental flow (Dunbar and Acreman, 2001; Hughes, 2001; Richter et al., 1996). Moreover, several methodologies take a broad understanding of the river ecosystem and provide the environmental flow assessment based on hydrological, hydraulic rating and biological response data (King et al., 2003; Swales and Harris, 1995; Yin et al., 2011). This study seeks to provide an environmental flow assessment method by integrating the concept of hydrological drought. This method involves providing dynamic risk-based information on how much flow is required for drought recovery and the likelihood of the event under different hydrological drought conditions. Given the required flow for drought recovery, it would also be interesting to investigate how possible to obtain this specific flow under various precipitation scenarios, considering that precipitation generally is the main driver of variability in streamflow. In other words, it involves assessing the conditional risk associated with the expected flow for drought recovery under future possible precipitation scenarios. To achieve this, it is necessary to properly account for the joint dependence structure between streamflow and precipitation.

Therefore, the main aim of the study in this chapter is to present a general probabilistic prediction network for hydrological drought examination and environmental flow assessment. This objective is three-fold: (1) to present a copula-based overall drought indicator to describe the hydrological dryness/wetness conditions using high-dimensional vine copulas; (2) to provide a drought-based environmental flow assessment that involves deriving the required flow needed to recover from certain drought conditions, and estimate the associated exceedance probability of this event based on the historical streamflow observations; (3) to quantify the conditional probability associated with the expected streamflow for drought recovery under various precipitation scenarios by building up an appropriate

joint dependence structure between streamflow and precipitation.

5.2 Theoretical background

Although the definition of copula for two variables was given in Chapter 4, this chapter focuses on higher-dimensional (>2-d) copulas. A *n*-dimensional multivariate joint distribution function F for *n*-dimensional given random variables $\mathbf{X} = [x_1,...,x_n]^{\mathrm{T}}$ can be expressed by a copula that satisfies the following condition:

$$F(x_1,...,,x_n) = C(F_1(x_1),...,F_n(x_n)) = C(u_1,...,u_n) \tag{5.1}$$

where F_i, denoted by u_i (i=1,…, n), represents the marginal cumulative distribution function (CDF) of the ith variable. The function C is called a copula function, and its form reflects the joint dependence structure. Two most frequently-used copula families are elliptical copulas and Archimedean copulas.

Elliptical copulas are simply the copulas of elliptically contoured (or elliptical) distributions. Let H be the multivariate CDF of an elliptical distribution, F_i be CDF of the ith margin and F_i^{-1} be the corresponding inverse function (quantile function), i=1,…, n (Yan, 2007). The elliptical copula can be written by:

$$C(u_1,...,u_n) = H[F_1^{-1}(u_1),...,F_n^{-1}(u_n)] \tag{5.2}$$

The most popular elliptical copula is the Gaussian copula. A detailed description of the Gaussian copula is given in Appendix A.

The Archimedean family is very commonly used in hydrological applications due to ease of construction and the variety of choices for the strength of dependence structures (Khedun et al., 2014; Maity et al., 2013). The general form of an Archimedean copula is defined by:

$$C(u_1,...,u_n) = \phi^{-1}[\phi(u_1) + \cdots + \phi(u_n)] \tag{5.3}$$

where the function ϕ is a continuous, strictly decreasing function from [0, 1] to [0, ∞], named the generator of the copula ($\phi(0) = \infty$ and $\phi(1) = 0$). Its inverse ϕ^{-1} is

completely monotonic on [0, ∞]. A generator uniquely (up to a scalar multiple) determines an Archimedean copula (Joe, 1997; Maity et al., 2013; Nelsen, 2006). The details of the Archimedean copulas (i.e., Frank, Gumbel and Joe) used in the current study are given in Appendix A.

Elliptical copulas and Archimedean copulas are quite useful for modeling the two-dimensional joint distribution. However, for higher dimensional applications, the number and expressiveness of families of parametric copulas are more limited by parameter restrictions and computationally intensive formulations (Lopez-Paz et al., 2013). Vine copulas offer a way to solving this issue (Joe, 1997; Kurowicka and Cooke, 2006).

Vine copulas model multivariate data using bivariate copulas as building (basic) blocks. Vine copulas decompose an *n*-dimensional multivariate density into *n*(*n*-1)/2 bivariate copula densities (Liu et al., 2015a). In vine structures, *n*(*n*-1)/2 bivariate pair-copulas are arranged into *n*-1 trees (Brechmann et al., 2013; Kurowicka and Cooke, 2006). This provides great flexibility for modeling multivariate data, as each of the bivariate copulas in the decomposition can belong to a different parametric copula model (Lopez-Paz et al., 2013). Canonical vines (C-vines) and drawable vines (D-vines) are two popular vine copulas. This study uses C-vines for constructing the joint distribution (Aas et al., 2009; Brechmann et al., 2013; Liu et al., 2015a).

The joint density of the *n*-dimensional C-vine is given by:

$$f(x_1,...,x_n) = \prod_{k=1}^{n} f_k(x_k) \times \prod_{i=1}^{n-1} \prod_{j=1}^{n-i} c_{i,i+j|1:(i-1)}(F(x_i \mid x_1,...,x_{i-1}), F(x_{i+j} \mid x_1,...,x_{i-1})) \quad (5.4)$$

where the f_k (k = 1,…, n) indicate the marginal densities, and $c_{i,i+j|1:(i-1)}$ denote the bivariate copula densities. The outer product in the second term runs over the *n*-1 trees and root nodes *i*, whereas the inner product refers to the *n*-*i* pair copulas in each tree *i* = 1,…, *n*-1 (Liu et al., 2015a).

As an example, a structure of a five-dimensional C-vine is illustrated (Fig. 5.1). The multivariate density of x_1, x_2, x_3, x_4, and x_5 can be written as follows:

$$f_{12345} = f_1 \cdot f_2 \cdot f_3 \cdot f_4 \cdot f_5 \cdot c_{12} \cdot c_{13} \cdot c_{14} \cdot c_{15} \cdot c_{23|1} \cdot c_{24|1} \cdot c_{25|1} \cdot c_{34|12} \cdot c_{35|12} c_{45|123} \qquad (5.5)$$

where $c_{1,2}(F_1(x_1,), F_2(x_2))$ is simply written as c_{12}.

This study considered a copula (Gaussian) from the elliptical copula family and four copulas (Clayton, Frank, Gumbel and Joe) from the Archimedean copula family as the potential bivariate pair-copulas (building blocks) used to establish the C-vine model (the bivariate copulas are given in Appendix A). The appropriate model structure for the C-vine was determined using R package *CDvine* (Schepsmeier and Brechmann, 2015).

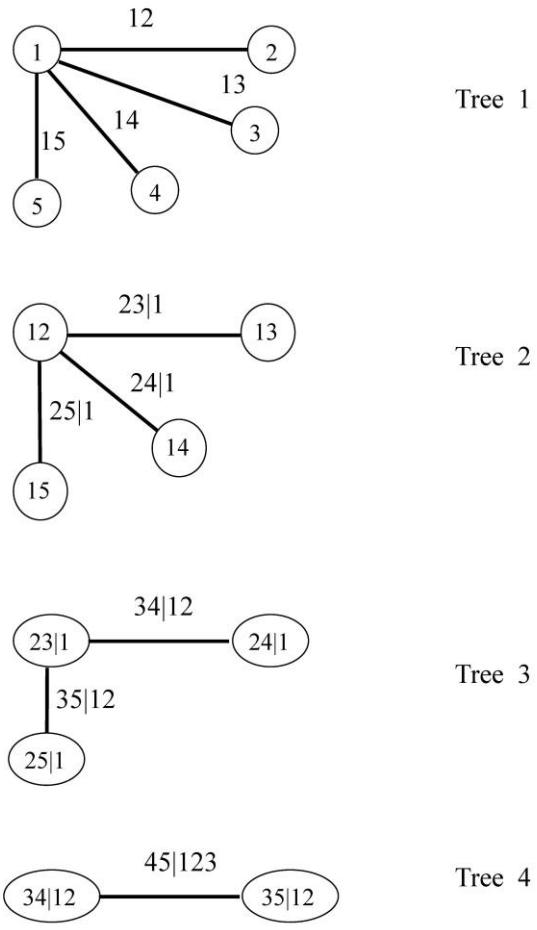

$f_{12345}=f_1 \cdot f_2 \cdot f_3 \cdot f_4 \cdot f_5 \cdot c_{12} \cdot c_{13} \cdot c_{14} \cdot c_{15} \cdot c_{23|1} \cdot c_{24|1} \cdot c_{25|1} \cdot c_{34|12} \cdot c_{35|12} \cdot c_{45|123}$

Figure 5.1 Graphical structure of C-vine for five variables with four trees. The node names are shown in circles, and the edge names appear close to the edges in the trees.

5.3 Case study and data

This study considered two catchments in Germany to demonstrate the performance of the presented methodology. The first catchment (CM I) is the Treene River Basin, which has a size of 481 km² (Guse et al., 2014). The second catchment (CM II) has an area of 1092 km² and is part of the Glan River Basin (Hellebrand et al., 2009). The locations of theses catchments are shown in Fig. 5.2. The choice of these catchments was determined by the need to conduct hydrological drought studies for regions where streamflow was minimally affected by human activities.

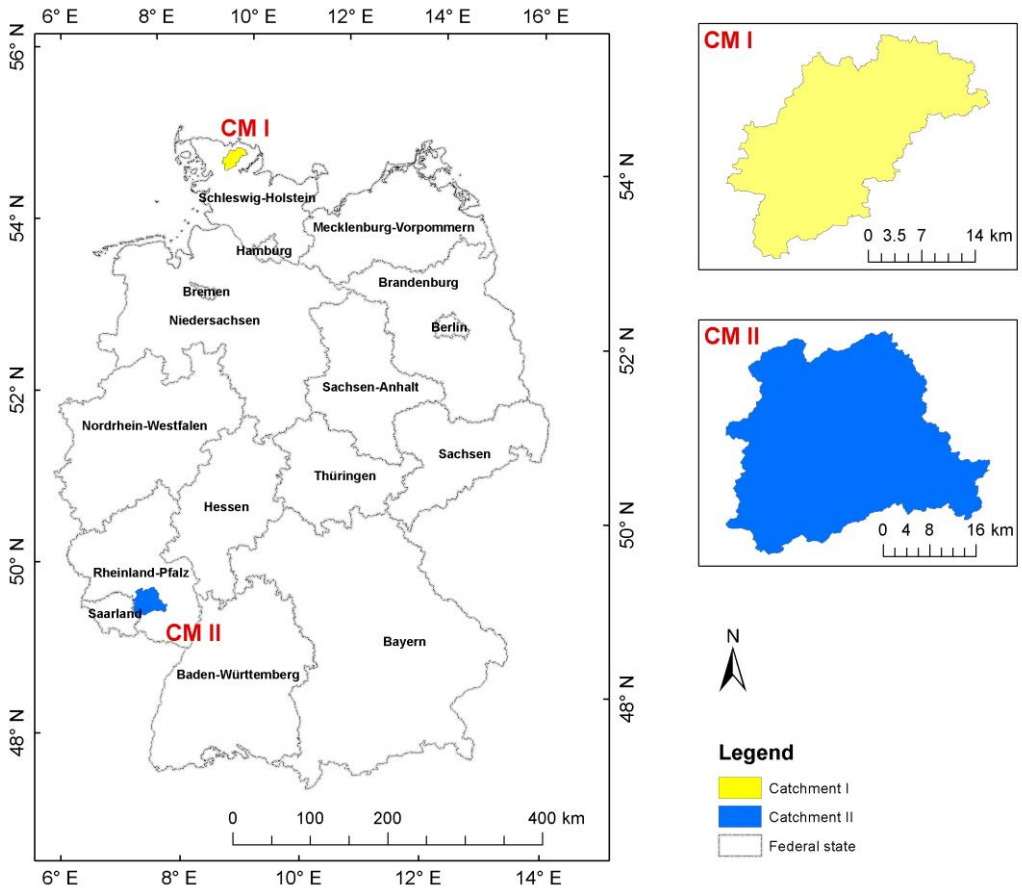

Figure 5.2 Locations of the two catchments used for this study.

Monthly streamflow data covering the period 1974–2013 for CM I was provided by the department of hydrology and water resources management, Kiel University. For CM II, monthly streamflow records available from 1957 to 2012 were obtained from Landesamt für Umwelt, Wasserwirtschaft und Gewerbeaufsicht Rheinland-Pfalz. Monthly catchment-averaged precipitation time series for each catchment were

extracted from a 1 km gridded precipitation dataset available from the Deutscher Wetterdienst (DWD).

5.4 Model development and results

In this section, this study first illustrates the definition of the joint streamflow drought indicator (JSDI). This involves data preprocessing, determining the marginal distributions, estimating an appropriate high-dimensional vine copula parameter to establish the joint distribution, and the Kendall distribution transformation. A schematic diagram of this general probability prediction network is summarized in Fig. 5.3.

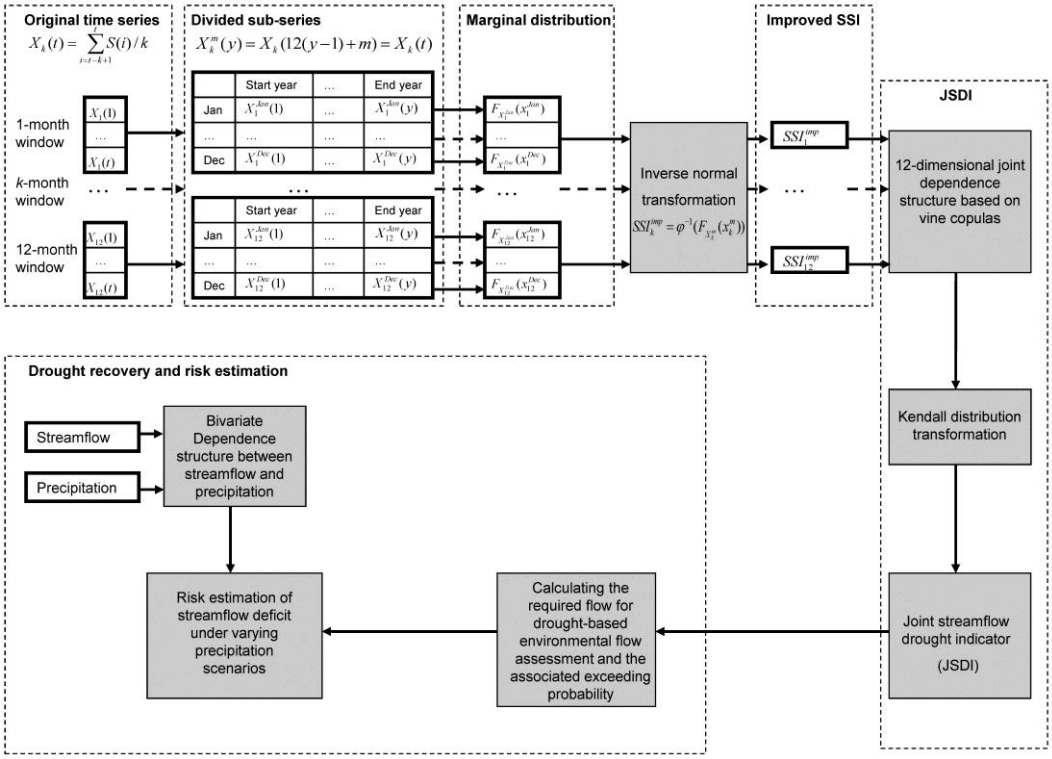

Figure 5.3 Schematic diagram of the probabilistic prediction network for identifying hydrological drought and drought-based environmental flow assessment.

5.4.1 Data preprocessing

Referring to the definition of the SI (the version of this algorithm for streamflow is called the standardized streamflow index, simply SSI), the concept of the time

window length is also used to generate the monthly streamflow time series with a given *k*-month time window (Kao and Govindaraj, 2010; Mirabbasi et al., 2013). Let *S(t)* be the observed monthly streamflow at time *t* (Δt=1 month); the averaged value $X_k(t) = \sum_{i=t-k+1}^{t} S(i)/k$ indicates the mean streamflow for a given *k*-month time window corresponding to time *t*. Before calculating the drought indicator, this study investigated two important characteristics of the monthly streamflow time series with a given *k*-month time window. First of all, there may be strong seasonal patterns in the original streamflow time series. To illustrate this, this study used the continuous wavelet transform (CWT), which is widely used to detect the periodic features of hydroclimatic variables (Liu et al., 2013; 2015c; Özger et al., 2009; Zhao et al., 2012). As shown in Fig. 5.4, a significant annual periodic pattern can be observed for both catchments used in the current study.

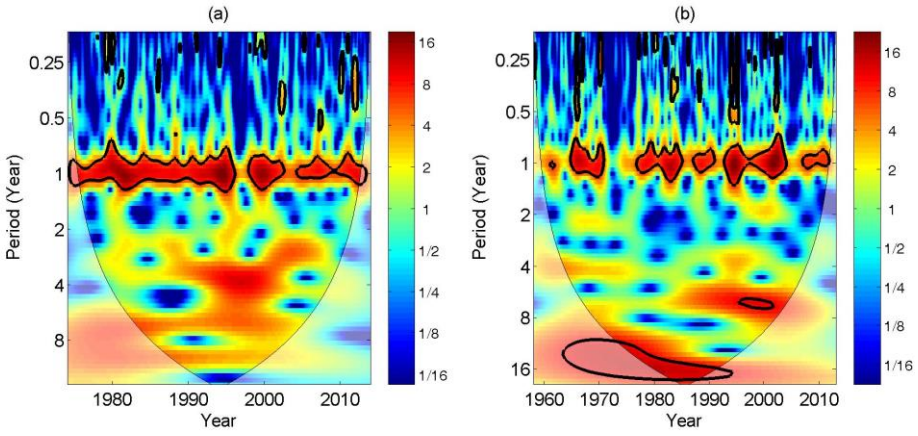

Figure 5.4 Continuous wavelet power spectrum for detecting seasonality patterns in the monthly streamflow time series of CM I (a), and CM II (b). The low wavelet power is shown in blue and high power in red and orange. The thick contours indicate the 5% significance level. The black line indicates the cone of influence (COI) (to reduce the edge effect).

In addition, the averaged method may result in the overlap of the generated time series for a given *k*-month time window. For example, the X_4 (4-month window) of May 2000 has 3 months in common with X_4 of April 2000 (i.e., February, March and April 2000). The overlap may lead to significant auto-correlation within the time series. With an increased width for the time windows, this problem will be accumulated and

become more severe. This study examined the auto-correlation of the monthly streamflow time series with a given *k*-month time window for each of the two catchments (the results are given in Table 5.1. It can be found that significant auto-correlation indeed exists in the samples and higher auto-correlation coefficients can be observed in larger time windows.

Table 5.1 Autocorrelation of the mean streamflow time series with the time windows from 1- to 12-months for each catchment.

lag months	1-month	2-month	3-month	4-month	5-month	6-month	7-month	8-month	9-month	10-month	11-month	12-month
						CM I						
1	0.629	0.804	0.856	0.883	0.898	0.909	0.922	0.936	0.949	0.961	0.972	0.977
2	0.376	0.454	0.556	0.616	0.658	0.695	0.738	0.788	0.836	0.881	0.917	0.934
3	0.110	0.151	0.195	0.273	0.342	0.415	0.496	0.589	0.689	0.780	0.848	0.879
4	-0.103	-0.113	-0.099	-0.058	0.029	0.131	0.250	0.387	0.535	0.672	0.773	0.817
5	-0.277	-0.311	-0.310	-0.278	-0.212	-0.097	0.047	0.216	0.398	0.568	0.693	0.749
6	-0.362	-0.399	-0.395	-0.367	-0.311	-0.218	-0.072	0.105	0.299	0.478	0.613	0.676
7	-0.302	-0.338	-0.338	-0.317	-0.270	-0.196	-0.087	0.069	0.244	0.410	0.536	0.600
8	-0.134	-0.157	-0.163	-0.149	-0.116	-0.066	0.005	0.101	0.231	0.360	0.463	0.520
9	0.062	0.066	0.074	0.083	0.098	0.121	0.151	0.191	0.244	0.319	0.388	0.436
10	0.236	0.285	0.305	0.313	0.313	0.307	0.298	0.288	0.280	0.282	0.312	0.350
						CM II						
1	0.540	0.768	0.842	0.873	0.893	0.906	0.919	0.932	0.945	0.958	0.970	0.976
2	0.286	0.394	0.533	0.610	0.660	0.702	0.743	0.789	0.837	0.884	0.922	0.940
3	0.099	0.131	0.183	0.283	0.365	0.440	0.521	0.610	0.707	0.799	0.869	0.900
4	-0.085	-0.086	-0.072	-0.030	0.068	0.176	0.296	0.433	0.578	0.713	0.812	0.856
5	-0.197	-0.239	-0.245	-0.221	-0.160	-0.036	0.117	0.289	0.470	0.635	0.755	0.810
6	-0.260	-0.306	-0.318	-0.296	-0.243	-0.147	0.013	0.200	0.394	0.569	0.699	0.762
7	-0.228	-0.269	-0.273	-0.250	-0.196	-0.113	0.004	0.173	0.355	0.522	0.648	0.713
8	-0.115	-0.128	-0.121	-0.090	-0.043	0.023	0.105	0.209	0.352	0.492	0.603	0.665
9	0.060	0.080	0.109	0.140	0.175	0.213	0.258	0.312	0.381	0.476	0.561	0.616
10	0.237	0.311	0.351	0.377	0.394	0.405	0.414	0.426	0.443	0.468	0.519	0.567

However, in the traditional SI model, the seasonal differences and significant auto-correlation that would cause the fitting of probability distributions to be biased were not considered (the SI model fits the whole series of $X_k(t)$ using a gamma distribution, as given by McKee et al. (1993). With these issues considered, the X_k values were further grouped by their ending months m (month of $S(t)$) to form X_k^m

sub-series (*m* indicates January, February, …, December) (Kao and Govindaraj, 2010; Kuhn et al., 2007; Mirabbasi et al., 2013). Eventually, the series $X_k(t)$ were subdivided into 12 sub-series using:

$$X_k^m(y) = X_k(12(y-1)+m) = X_k(t) \tag{5.6}$$

where *y* is the year index, *y*=1, 2,…, *m*=1 (January), 2 (February), …, 12 (December) is the month index, and *t* is the time index *t*=12(*y*–1)+*m*. For instance, $X_4^{November}$ indicates the 4-month (time window) mean streamflow averaged from August to November. In this way, samples in each X_k^m set are grouped annually and will be non-overlapping when $k \leq 12$ (note that longer time windows, i.e., $k > 12$, are not considered in the current study, because the adopted samples will start to overlap with each other and are no longer independent). By conducting this data preprocessing, the samples in the same group X_k^m are subjected to the same seasonal effects (spanning for the same months of the year), and the seasonal variation could be reflected (Kuhn et al., 2007). Moreover, the auto-correlation within the samples is considerably reduced.

5.4.2 Marginal distribution selection

For probabilistic drought analysis, the first step is to fit the marginal distributions to each group in X_k^m (namely, $u_k^{January} = F_{X_k^{January}}(x_k^{January})$, $u_k^{February} = F_{X_k^{February}}(x_k^{February})$, …, $u_k^{December} = F_{X_k^{December}}(x_k^{December})$). Several probability distributions that are widely used in hydro-meteorology were considered in this study: normal, gamma, Weibull, lognormal and exponential. The method of maximum likelihood estimation was employed to estimate the parameters of each distribution (Gyasi-Agyei, 2013). In order to test the appropriateness of the probability distributions, two formal goodness-of-fit tests were performed: the Kolmogorov-Smirnov test (K-S test) and the chi-squared test (chi2 test) (more details about these tests can be found in

(Bagdonaviciu and Nikulin, 2011; Khedun et al., 2014; Massey, 1951). The K-S test and chi2 test return the *p* value, which should be greater than the significance level of α (herein α=0.05) to accept the null hypothesis (passing the test). For each catchment, there are 144 sub-series (cases) of X_k^m to be fitted, relating to 12 different ending months (*m*=January, February, …, December) and 12 time integration windows (*k* = 1, 2,…, 12). The total sum of individual numbers of cases that passed the K-S and chi2 tests were obtained. The theoretical distribution with the highest sum was considered to be the most appropriate. As illustrated in Table 5.2, the gamma distribution was identified to be the most appropriate distribution for both catchments, and was hence adopted. With the fitted distributions (i.e., the u_k^m) for each group X_k^m, one can calculate the improved SSI values similar to original SSI (McKee et al., 1993), namely SSI_k^{imp}. This can be obtained by deriving the inverse normal according to: $\varphi^{-1}(u_k^m)$: $SSI_k^{imp} = \varphi^{-1}(u_k^m) = \varphi^{-1}(F_{X_k^m}(x_k^m))$.

Table 5.2 Goodness-of-fit tests of different theoretical distributions for each catchment. Numbers of cases that are accepted by the K-S test and the chi-squared test at the 5% significance level are given. The distributions with the maximum total numbers are shown in bold.

Distribution	CM I			CM II		
	K-S	Chi-squred	in total	K-S	Chi-squred	in total
Gaussian	142	124	266	136	119	255
Gamma	144	125	**269**	143	129	**272**
Weibull	143	122	265	142	128	270
log-normal	144	107	251	144	127	271
exponential	0	142	142	0	93	93

Nonetheless, it can be found that both the lognormal and Weibull distributions also perform well in comparison to the gamma distribution. This study will discuss the effects of different theoretical distributions on the performance of the JSDI in Section 5.4.6.

5.4.3 Joint distribution and copula parameter estimation

The JSDI involves evaluation of the overall hydrological drought condition, and it aims to capture drought features at various temporal resolutions. Unlike the single SSI_k^{imp} (e.g., SSI 1-month or 6-month), this is done without focusing on a certain time window. This means that all different time windows from 1- to 12-months (i.e., the $SSI_1^{imp}, SSI_2^{imp}, ... SSI_{12}^{imp}$) are considered together when developing the JSDI. A copula-based joint distribution paves the path for this achievement. Therefore, in this study, a 12-dimensional joint function is modeled to join the multivariate margins for all time windows (u_k^{imp}, k=1, 2, ..., 12) based on the copula algorithm. First, the margins u_k^{imp} (herein, u_1^{imp} is the union of $\{u_1^{January}, u_1^{February}, ..., u_1^{December}\}$, …, u_{12}^{imp} is the union of $\{u_{12}^{January}, u_{12}^{February}, ..., u_{12}^{December}\}$) for a given k-month window can be given by the corresponding $\varphi(SSI_k^{imp})$ values. This study then used the C-vine copulas to construct the joint dependence of the multivariate margins with window sizes from 1-month to 12-months. In order to build up the C-vine copula, Gaussian, Clayton, Frank, Gumbel, and Joe copulas were used as the potential pair-copulas. Based on well-fitted marginal distributions, a 12-d C-vine copula was employed to join the margins and fit the joint dependence. This was determined by using a approach introduced by Schepsmeier and Brechmann (2015) (i.e., the *CDvine* package), as mentioned above. Figs. 5.5 and 5.6 show the graphical mode of the 12-d C-vine model for each catchment.

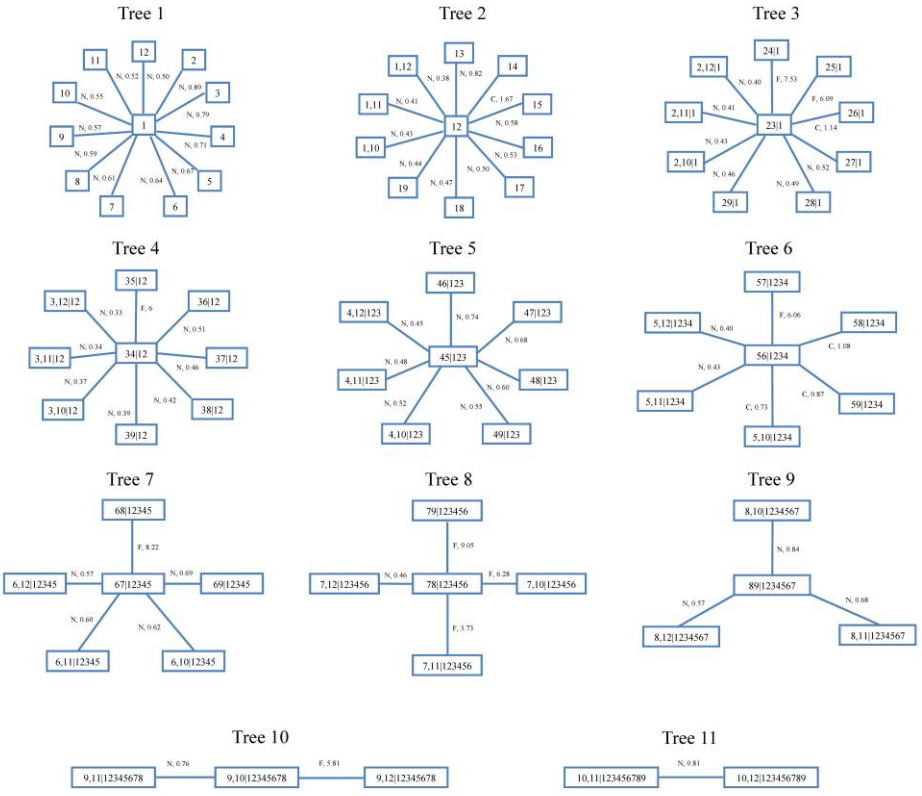

Figure 5.5 The 12-d C-vine for CM I, with the well-fitted bivariate copulas and the corresponding parameters. The numbers 1–12 denote the improved SSI time series on the time windows of 1–12 months, respectively. C, F, G, J, and N denote Clayton, Frank, Gumbel, Joe, Normal (Gaussian) bivariate copulas with their associated parameters.

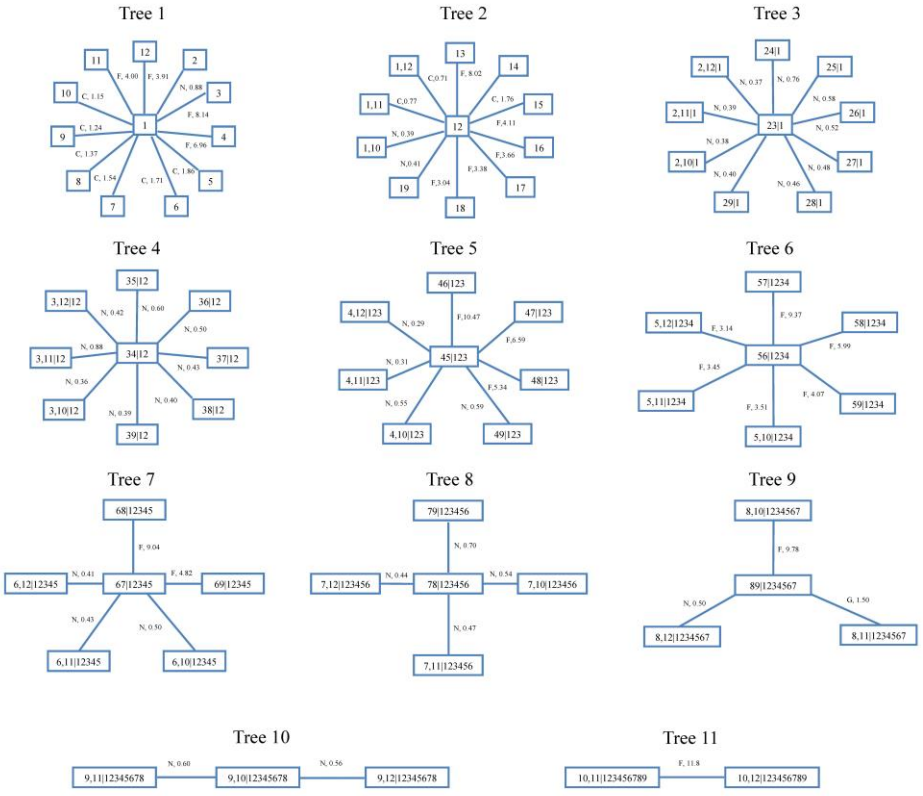

Figure 5.6 The 12-d C-vine for CM II, with the well-fitted bivariate copulas and the corresponding parameters. The numbers 1–12 denote the improved SSI time series on the time windows of 1–12 months, respectively. C, F, G, J, and N denote Clayton, Frank, Gumbel, Joe, Normal (Gaussian) bivariate copulas with their associated parameters.

5.4.4 Kendall distribution transformation

So far, the well-fitted C-vine copula $C_{U_1,U_2,...,U_{12}}$ for each catchment has been obtained, which is the cumulative joint probability $P[U_1 \le u_1^{imp}, U_2 \le u_2^{imp}, ..., U_{12} \le u_{12}^{imp}] = s$ for given 12-variate margins (i.e., u_1^{imp}, u_2^{imp}, ..., u_{12}^{imp}). Following Kao and Govindaraj (2010), the distribution function of copulas, Kendall distribution function K_C, was used to generate the probability measures of the copula values less than or equal to a given s (i.e., $K_C(s) = P[C_{U_1,U_2,...,U_{12}}(U_1, U_2, ..., U_{12}) \le s]$) (Nelsen et al., 2003; Nelsen, 2006).

Although an analytical expression of K_C might not exist for vine copulas, it is possible to use the empirical Kendall distribution function K_C. An explicit description of the empirical Kendall distribution function can be found in Genest et al. (2011) and Nelsen et al. (2003). This study computed the empirical Kendall distribution function K_C by using the R function *Kn* in the *copula* package (Hofert et al., 2013). The empirical Kendall distribution function $K_C(s)$ based on streamflow margins $\{u_1^{imp}, u_2^{imp}, ..., u_{12}^{imp}\}$ for each catchment is shown in Fig. 5.7. Similar to the definition of SI (McKee et al., 1993), the JSDI can be computed by taking the inverse normal $\varphi^{-1}(K_C(s))$. Then, the definition of JSDI can be given as follows:

$$JSDI = \varphi^{-1}(K_C(s)) \tag{5.7}$$

here, negative JSDI values ($0 < K_C < 0.5$) indicate the overall dryness status, zero values ($K_C = 0$) represent normal status, and positive JSDI values ($0.5 < K_C < 1$) represent overall wetness status. The JSDI evaluates the overall dryness/wetness status based on the dependence structure of streamflow margins regarding different temporal windows.

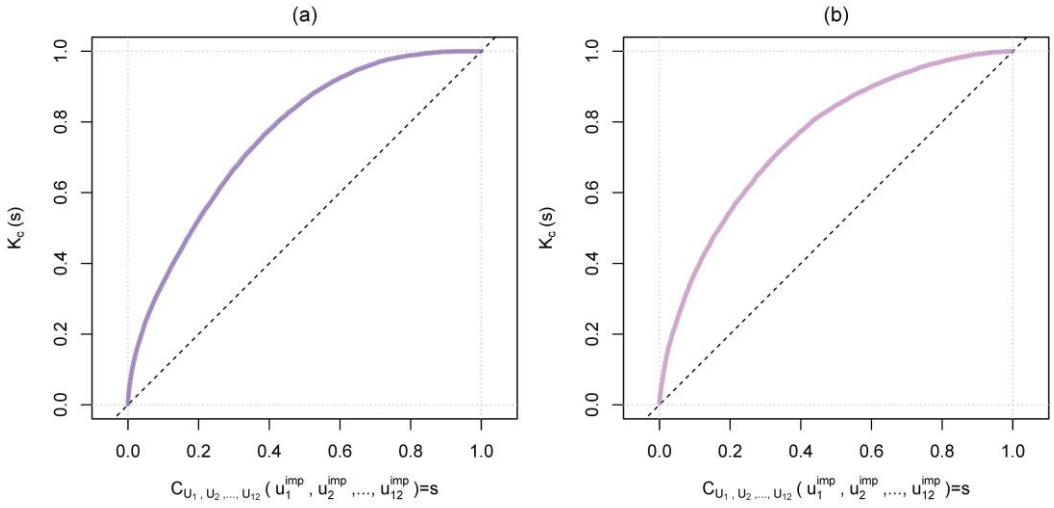

Figure 5.7 Kendall distribution functions of the 12-d C-vine copulas for CM I (a) and CM II (b).

5.4.5 JSDI performance

According to the calculation procedure above, this study obtained the monthly JSDI time series that identify the hydrological drought conditions for each catchment. Fig. 5.8 illustrates the visual comparison of the monthly time series of JSDI, improved 1-month (SSI_1^{imp}) and 12-month (SSI_{12}^{imp}) SSI with the corresponding observed streamflow time series at the two catchments. As shown in Fig. 5.8 it appears that the JSDI generally combines the strengths of the short-term drought index (e.g., the SSI_1^{imp}) in capturing the drought onset and long-term drought index (e.g., the SSI_{12}^{imp}) in reflecting the drought duration or persistence. Therefore, it provides a more comprehensive evaluation of drought and could be more competitive than other traditional hydrological drought indices (e.g., the SSI). This attractive feature is attributed to the fact that the JSDI describes the overall drought conditions based on the joint temporal dependence structure. Another advantage of the JSDI compared to the SSI is that it provides a month-by-month potential assessment for drought-based environmental flow assessment due to the property of the joint dependence structure. This will be further explored in Section 5.4.7.

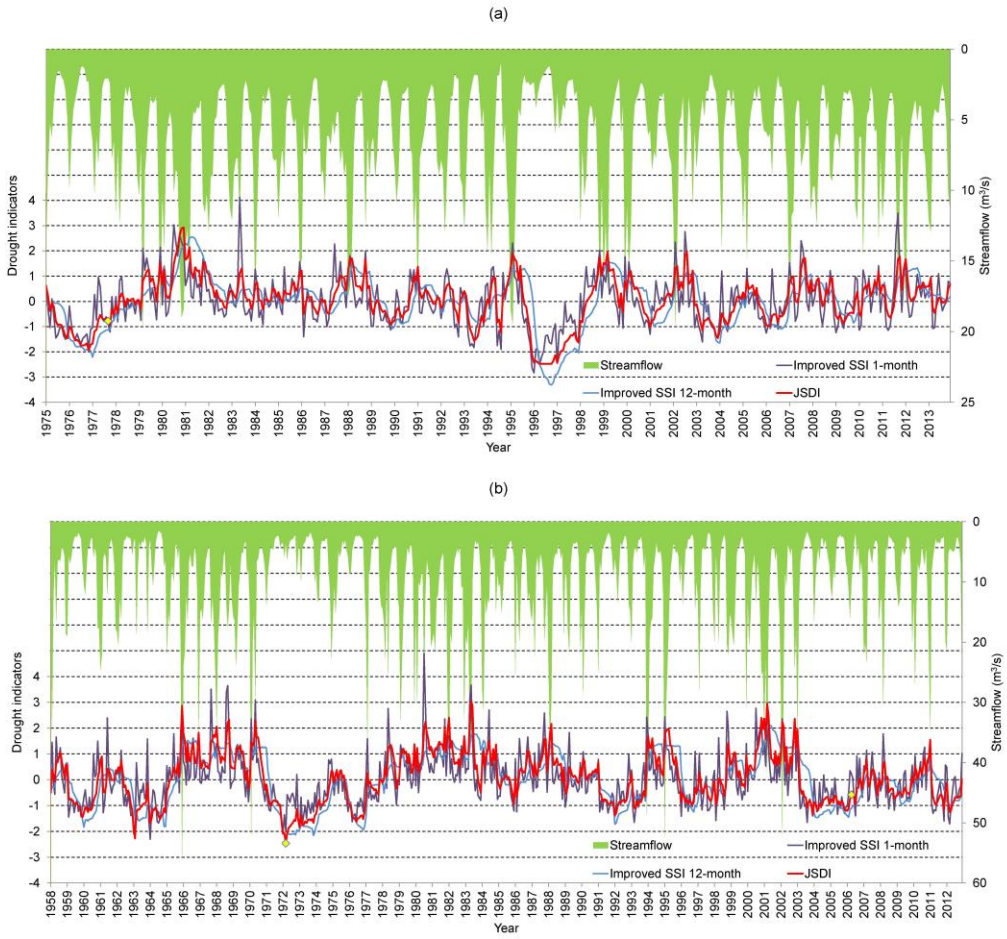

Figure 5.8 Time series of monthly streamflow, improved SSI 1-month, 12-month and JSDI for each catchment: CM I (a), and CM II (b). The yellow diamond-shapes indicate the selected events for the analyses in Table 5.3.

5.4.6 Sensitivity of marginal distributions

When computing the JSDI presented above, the gamma distribution was used to model the margins. As shown in Table 5.2, it can also be seen that the Weibull and log-normal distributions provide close performance to gamma. This evokes an investigation of interest that involves the examining of the sensitivity of varying marginal distributions in evaluating the hydrological drought status using the JSDI. This study therefore fitted the margins using the Weibull and log-normal separately. Again, C-vine copulas were used to construct the joint dependence of the margins. Fig. 5.9 shows a comparison of various JSDI curves generated by varying copulas with Weibull and log-normal marginal distributions for each catchment. It can be seen that the JSDI time series using the Weibull and log-normal distributions are in close

agreement with those of using gamma, while it seems there is a slight difference to evaluate the extreme conditions.

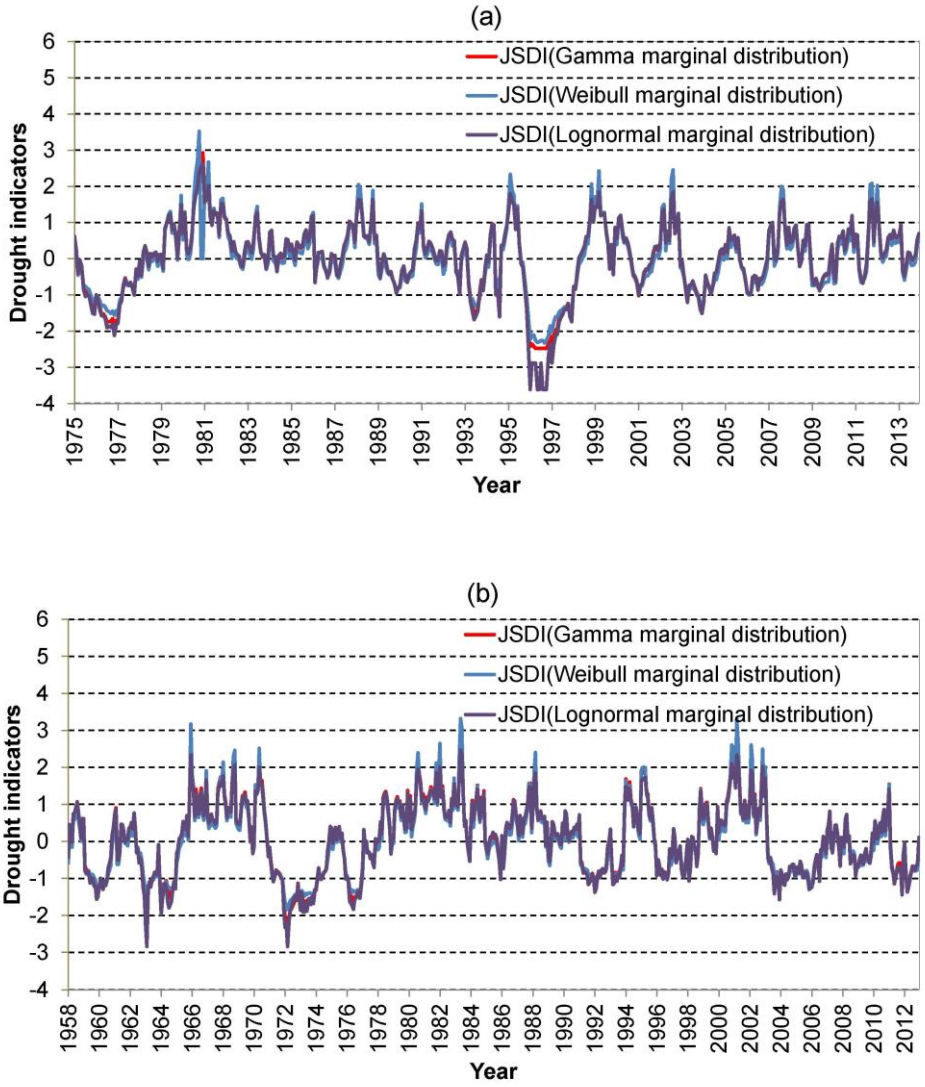

Figure 5.9 Comparison of the monthly JSDI time series generated from different marginal distributions for each catchment: CM I (a), and CM II (b).

5.4.7 Drought-based environmental flow assessment

This section illustrates the drought-based environmental flow assessment method based on the JSDI model, which refers to producing dynamic information on how much environmental flow (the required mean flow of the future *n*-month) is required for drought recovery and the likelihood of the occurrence of this event under different

initial drought situations. It should be mentioned that the environmental flow here is dynamic and referred to the required flow to recover from various initial drought situations to expected hydrological dryness/wetness conditions.

Table 5.3 Required average flow in the future 1 to 12 months in order to reach normal conditions (K_c=0.5) and moderate wet conditions (K_c=0.7) for the selected events, and the corresponding probabilities of these events for each catchment.

	Selected events	1 month	2 months	3 months	4 months	5 months	6 months	7 months	8 months	9 months	10 months	11 months	12 months
							CM I						
Target flow for normal condition	1977/09	8.660	7.150	7.390	7.890	8.210	8.090	7.990	7.550	7.100	6.700	6.440	6.252
Probability		0.127	0.360	0.448	0.515	0.513	0.551	0.520	0.518	0.515	0.519	0.505	0.500
Target flow for moderate wet condition		16.180	10.680	9.740	9.900	9.630	9.610	9.330	8.600	8.150	7.610	7.330	7.166
Probability		0.003	0.091	0.191	0.270	0.318	0.332	0.309	0.332	0.314	0.332	0.315	0.300
							CM II						
Target flow for normal condition	1972/03	50.050	28.440	20.590	16.070	13.560	11.690	10.340	9.320	9.200	8.970	9.130	9.269
Probability		0.000	0.002	0.004	0.008	0.013	0.024	0.052	0.114	0.230	0.380	0.463	0.500
Target flow for moderate wet condition		66.420	36.040	25.950	20.450	16.810	14.280	12.680	11.540	11.340	10.970	10.930	11.130
Probability		0.000	0.000	0.000	0.001	0.002	0.005	0.012	0.032	0.087	0.192	0.275	0.300
Target flow for normal condition	2006/04	21.480	12.760	9.650	7.980	6.620	6.080	5.920	6.410	7.260	8.090	8.910	9.260
Probability		0.011	0.043	0.087	0.131	0.222	0.309	0.419	0.540	0.569	0.577	0.537	0.500
Target flow for moderate wet condition		38.400	20.910	15.010	11.790	10.070	8.530	8.090	8.480	9.360	10.060	10.710	11.142
Probability		0.000	0.001	0.005	0.013	0.028	0.084	0.155	0.270	0.320	0.353	0.340	0.300

As an illustration (Table 5.3), this study considered two expected conditions: a normal condition ($K_C = 0.5$) and a moderate wet condition ($K_C = 0.7$) in the current study (note that it is flexible to consider any expected hydrological condition of interest). The detailed algorithms and procedures for this computation are described in

Appendix B.

For the moderate-dryness initial situation (e.g., the selected event in September 1977 at CM I), the environmental flow target (8.66 m^3/s) to recover from the drought to the normal condition ($K_C = 0.5$) in the future 1 month was obtained and the corresponding exceedance probability shows the chance of this event is low (lower than 0.2). However, the risk of drought is decreasing for longer future months and becomes very stable three months later. It is expected that the amount of environmental flow target is higher for achieving the moderate wet level ($K_C = 0.7$) when compared to the normal condition and the probability thus is much lower (higher risk of drought). With respect to the extreme-dryness initial situation, there was a severe drought at CM II in March 1972 (see Fig. 5.8b) and it thus needs to receive a large amount of flow (50.05 m^3/s) to drive the drought to normal condition in the next month. The exceedance probability clearly shows that the possibility of drought recovery in next month at this catchment is close to zero based on the historical streamflow data. The actual streamflow in April 1972 was only 6.28 m^3/s (see Fig. 5.8), which confirms the persistence of drought. The required monthly mean flow is generally dropping. The potential for drought recovery is slowly rising as the months increase but still seems significantly low (lower than 0.1) even after seven months. It could be understood that the chance to achieve wetter conditions ($K_C = 0.7$) is almost impossible during the following months. In April 2006 at CM II, there was a prolonged drought. It required a flow amount of 21.48 m^3/s in order to reach normal status in the following 1 month. The corresponding exceedance probability indicates that it is very unlikely to happen. For the future four months, the chance of drought recovery is still less than 20%. This suggests that it is very likely that this catchment could persistently suffer the very dry condition in the coming four months, but the probability is getting higher after four months later. As expected, the possibility to reach the defined moderate wet level is much lower in the following months compared to the expected normal condition. In this manner, the copula-based

prediction algorithm provides a feasible way to dynamically measure the quantitative environmental flow targets and account for the risk.

5.4.8 Conditional dependence between streamflow and precipitation

This study has so far investigated the probability of the required flow for drought-based environmental flow assessment in the future months based on the historical streamflow data. Generally, precipitation has a significant influence on streamflow, and one might also be interested in knowing how possible it is that the required flow can be obtained for drought recovery ($K_C = 0.5$ or JSDI=0) under different precipitation scenarios. In this section, the current study first examined the joint dependence structure between precipitation and streamflow. Then, this study identified the conditional probability under different precipitation scenarios based on the established dependence structure. Note that the precipitation data used here are the time series of catchment-averaged monthly precipitation as introduced in Section 5.3.

5.4.8.1 Bivariate dependence structure between streamflow and precipitation

To model the joint dependence between streamflow and precipitation, the current study first grouped the observed time series of monthly precipitation (*P(t)*) and streamflow (*S(t)*) according to the base month (the given month to be assessed to form individual sub-series over future 12 months). That is to say, the observed monthly precipitation series *P(t)*) were subdivided into 12 sub-series using: $P_{bmonth}^{fmonth}(y) = \sum_{i=1}^{fmonth} P(12(y-1)+bmonth+i)$ (where *y*=1, 2, …, is the year index, *bmonth*=1 (January), 2(February),…, 12(December), is the base month to be assessed, and *fmonth*=1, 2, …, 12, is the number of the future months). For the observed monthly streamflow (*S(t)*), the sub-series are $S_{bmonth}^{fmonth}(y) = \sum_{i=1}^{fmonth} S(12(y-1)+bmonth+i)/\,fmonth$, which relates to the mean streamflow in the following future months. For instance, P_{10}^{3} denotes the future 3-month accumulated precipitation starting from November (base month is October),

and S_4^{11} represents the future 11-month mean streamflow starting from May (base month is April). As an illustration, this study selected one event from the Table 5.3, i.e., the event in March 1972 (extreme-dryness initial situation) at CM II. Taking this event as an example, the corresponding precipitation sub-series with the given base month (March) and the number of future months (e.g., future three months) is P_3^3, and the streamflow sub-series with the same base month and future three months is S_3^3. Before identifying the bivariate distribution ($C(u_p, u_s)$) between these two groups of sub-series, it is important to fit appropriate marginal functions to the precipitation (u_p) and streamflow (u_s) sub-series. Again, the five theoretical probability distributions as mentioned in Section 5.4.2 were compared. The most appropriate one for each sub-series was determined by the smallest statistics (the corresponding *p* value should be greater than the significance level of α as well) from the chi-squared test. Once the best fitting marginal distributions are obtained, a proper bivariate copula function is needed to join the margins and model the joint dependence structure. Five bivariate copulas (i.e., Gaussian, Clayton, Frank, Gumbel, and Joe copulas) mentioned above were tested for this low-dimensional (i.e., 2-d) application. The Cramér-von Mises approach was used to test the goodness-of-fit of the copulas considered. This goodness-of-fit test computes the Cramér-von Mises statistics S_n as a measure of distance between the empirical and parametric copulas. More details about this test can be found in Chapter 4. Table 5.4 gives the goodness-of-fit statistics (S_n) of different 2-d copulas for this selected event over the future 1 to 12 months.

Table 5.4 The Cramér–von Mises statistics (S_n) of different copulas (2-dimendional) for a selected event (in March 1972) at CM II in the following 1 to 12 months. The S_n statistics that are accepted by the Cramér–von Mises test at a significance level of 5% are indicated by *. The one with smallest S_n statistic (shown in bold) is the most appropriate copula.

Copula	1 month	2 months	3 months	4 months	5 months	6 months	7 months	8 months	9 months	10 months	11 months	12 months
Clayton	0.201	0.110	0.072	0.063	0.026*	0.039*	0.050*	0.076	0.089	0.103	0.064	0.078
Frank	0.049*	0.046*	0.038*	0.022*	0.025*	0.022*	0.028*	0.031*	0.027*	0.019*	0.016*	**0.016***
Gumbel	0.026*	0.024*	0.023*	0.022*	0.031*	0.038*	0.040	0.023*	0.031*	**0.012***	0.018*	0.024*
Joe	**0.022***	**0.023***	0.041*	0.060	0.088	0.114	0.111	0.060	0.077	0.024*	0.056	0.060
Gaussian	0.045	0.034	0.027*	**0.016***	**0.015***	**0.015***	**0.022***	**0.020***	**0.026***	0.017*	**0.013***	0.020*

5.4.8.2 Risk estimation of streamflow deficit under varying precipitation scenarios

Once the copula-based joint distribution ($C(u_p, u_s)$) has been obtained, the conditional distributions of streamflow under given precipitation scenarios can be examined. The conditional CDF of $S \le s$ (streamflow) given $P = p$ (precipitation) can be expressed as follows (Zhang et al., 2007):

$$F_{S \le s|P=p}(s, p) = \frac{\partial C(u_s, u_p)}{\partial u_p} \tag{5.9}$$

Then, the conditional probability of reaching or exceeding the required mean flow (obtained from Section 5.4.7) under given precipitation scenarios can be calculated by $(1 - \frac{\partial C(u_s, u_p)}{\partial u_p})$. Therefore, one can now know the probability of attaining the required flow under the given precipitation conditions for the study catchments. Three given precipitation scenarios corresponding to three thresholds were considered in this study: events at the 20th, 50th and 80th quantiles of the precipitation data (i.e., $u_P = 20\%, u_P = 50\%$ and $u_P = 80\%$). Note that any precipitation scenario of interest can be considered, as long as the copula-based joint distribution has been established. Fig. 5.10 shows the exceedance probabilities (the intersections between the red line and three blue curves) associated with individual required flow values (the red line) for drought recovery ($K_C = 0.5$ or JSDI=0), conditioned upon three given

precipitation scenarios (blue curves) for the considered event (the event in March 1972 at CM II) in the future 1–12 months. In this figure, it can be seen that streamflow is sensitive to the changes in precipitation scenarios (the difference between three blue curves), although the sensitivity varies for different future months. These exceedance probabilities help to identify the possibility of reaching the required flow for drought recovery (i.e., the condition of JSDI=0) under different precipitation conditions. Thus, it also provides a risk estimation of hydrological drought. For instance, even given a potentially abundant precipitation scenario ($u_P = 80\%$) in the future five months for the considered event at CM II (Fig. 5.10), one can find out that the probability of gaining the required mean flow that would bring dry condition to normal is still very low (close to zero). This information would be important for developing appropriate water supply planning in order to balance the water demand in the following months at this catchment. It can also be seen (Fig. 5.10f–l) that there is a very low probability of getting the required flow for drought recovery in the following 6–12 months under the scarce precipitation condition ($u_P = 20\%$). For the potentially more sufficient precipitation scenarios ($u_P = 50\%$ and $u_P = 80\%$), the chance of obtaining the required flow increases. Moreover, it should be mentioned that different initial conditions and catchments could reflect varying risk patterns.

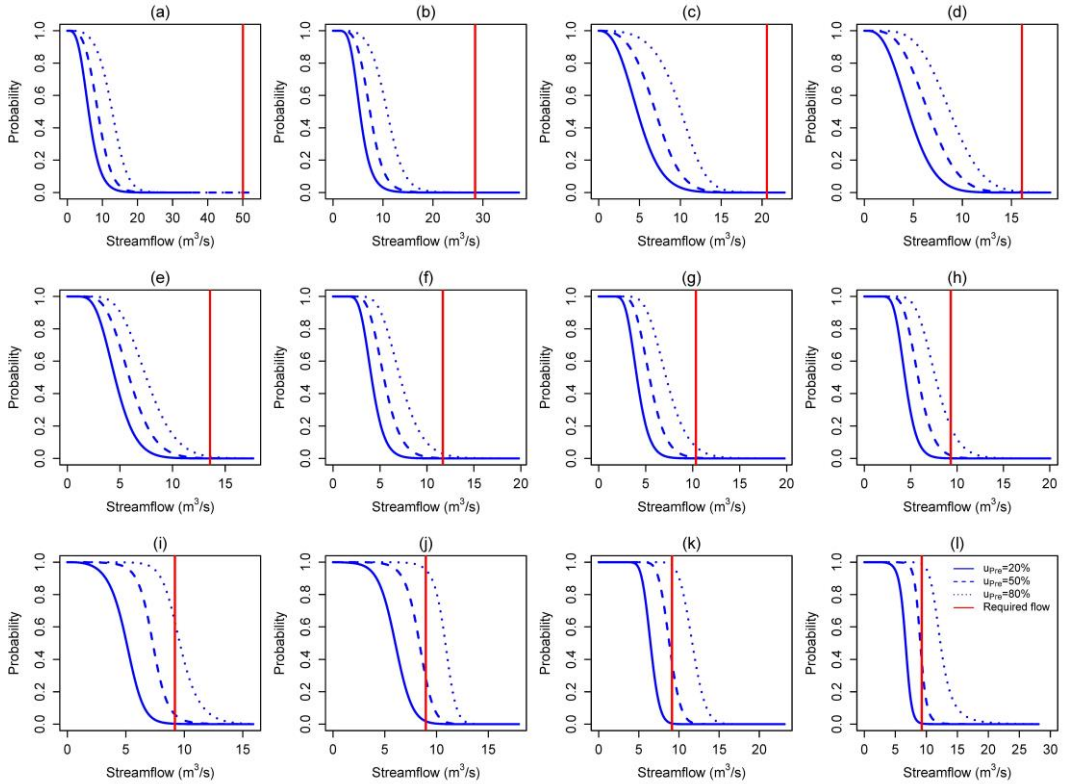

Figure 5.10 The conditional probability of streamflow for the future 1 to 12 months (a-l) under three precipitation scenarios: $u_P = 20\%, u_P = 50\%$ and $u_P = 80\%$, as well as the specific required flow for drought recovery ($K_C = 0.5$ or JSDI=0), for CM II with the selected event (in March 1972).

5.5 Summary and conclusions

This chapter presents a general probabilistic prediction network for hydrological drought identification and drought-based environmental flow assessment by exploiting the strength of a copula-based joint distribution model. This general network is comprised of three major parts. First, the JSDI was presented to describe the hydrological dryness/wetness conditions based on the monthly streamflow data. The development of JSDI involves grouping the original streamflow data on various time windows from 1- to 12-months, determining the marginal distributions, the establishment of the joint distribution model, and Kendall distribution transformation. This study proposed using high-dimensional (12-d) vine copulas to build up the joint dependence structure between 12 different margins. This drought indicator provides

an overall description of the hydrological dryness/wetness status based on various temporal resolutions. The second part of the network is to expand the application domain of the JSDI for drought-based environmental flow assessment. Based on the joint dependence, the JSDI is capable of dynamically predicting the required flow for drought recovery under different drought conditions and giving the associated exceedance probability that shows the likelihood of this event. Finally, the third part is to estimate the conditional probability of streamflow deficit under varying precipitation scenarios by establishing the joint dependence structure between streamflow and precipitation. In this part, the idea of copula (bivariate copula) was used again to model this bivariate joint dependence structure. According to the conditional probability analysis that relies on the historical precipitation and streamflow data, one can assess the chance of gaining the required environmental flow for drought recovery under the different precipitation scenarios.

To demonstrate the usefulness and applicability of this network, this study used the streamflow and precipitation data from two different catchments in Germany. Our results show that the vine copulas could account for the multivariate joint distribution model well in developing the JSDI. The JSDI provides a very applicable algorithm for assessing hydrological dryness/wetness conditions and it is able to effectively capture drought onset and persistence. It could thus be more competitive and flexible than other conventional hydrological drought indices (e.g., the SSI). In addition, the results also confirmed that the presented network can allow for estimating the amount of environmental flow required for drought recovery in the future months and interpreting the risk of this event based on the historical observed streamflow. By constructing the joint dependence between precipitation and streamflow, one can derive the probability of obtaining the required flow conditioned upon on different precipitation scenarios.

This general network can potentially help decision-makers in water resources management by providing valuable insight toward assessing hydrological drought status. Moreover, the generated risk-evaluation information based on this network can

be useful for developing appropriate water supply plans for environmental flow assessment by integrating the drought information. This approach is also promising for use in other basins worldwide under different climate regimes. Future efforts could extend this network by incorporating more hydrological variables (e.g., soil moisture) and constructing the conditional dependence with both precipitation and soil moisture in order to better address hydrological droughts.

Chapter 6: Overall conclusions and perspectives

In this dissertation, an assessment of the linkages and interactions between vegetation, climate, streamflow, and drought was addressed. To achieve this, a three-step strategy with individual specific objectives was applied. First, this study evaluated the long-term variations in vegetation and climatic variables and their scale-dependent relationships by using Rhineland-Palatinate as a case study area with a classification of different vegetation types and precipitation regimes. This was accomplished in Chapter 3. In this chapter, a hybrid approach by combining the DWT and MK trend tests was implemented to examine the temporal trends in the time series of NDVI, temperature and precipitation in Rhineland-Palatinate and their coherence at various time-scales. On the basis of this combined method, one can obtain which time-scales are dominantly responsible for the trends found in the original data and find out the certain time-scales which represent the strongest correlation between NDVI and both temperature and precipitation. In this case study, the proposed DWT-MK approach indeed paves a way to extracting time-scale information in the original NDVI and climatic parameters. This is beneficial for understanding the scale-dependent characteristics and trend structures of those variables and identifying how the correlations between NDVI and climatic parameters were affected by different time-scales. The results provided detailed information about the dominant periodic modes affecting the trends in the NDVI and climatic variables and presented their correlations at different time-scales, which would be valuable for forecasting future hydroclimatic and vegetation conditions and helpful for making efficient water resources management and reasonable agricultural strategies. However, several limitations of this study should also be mentioned. For instance, other climatic variables (i.e., the maximum temperature, minimum temperature, and relative humidity) closely related to vegetation growth have not been examined, and correlations between vegetation and climatic variables in growing season were not investigated.

In the second step, this study presents an investigation of the probabilistic and multi-scale relationships between streamflow and hydroclimatic variables (precipitation, temperature and soil moisture) over Baden-Württemberg based on their joint dependence structure constructed by copula functions. In light of this, one can gain the information about the risk of occurring streamflow deficit events and floods under the different conditions of hydroclimatic variables. This is given in Chapter 4. Moreover, the multi-year relationships between streamflow and hydroclimatic variables were detected by the means of wavelet coherency technique, which generates a visual and clear map of coherence pattern between those variables. This chapter further explored the potential links of streamflow variability and large-scale atmospheric circulations in this study area. It can be inferred that the high streamflow anomalies over Baden-Württemberg are generally related to strong westerly atmospheric circulations that play an important role in inducing the warm and moist air from the North Atlantic Ocean towards the study area and thus enhancing the precipitation, while the low streamflow anomalies are generally related to the northerly circulations. These findings would provide useful knowledge for understanding the seasonal streamflow variability and the prediction of streamflow in Baden-Württemberg. This probability-based analysis method is also applicable for other regions worldwide.

This final step involves proposing a general probabilistic prediction network to identify the hydrological drought and drought recovery and environmental flow assessment, as shown in Chapter 5. This network first presented a multivariate streamflow drought index (i.e., the JSDI) for describing the hydrological droughts using high-dimensional copula functions. It can provide a risk-based assessment for the drought recovery. This chapter used the data from two different catchments in Germany to demonstrate the usefulness and applicability of this framework. The results indicate that the proposed methodology can effectively capture drought onset and persistence in the hydrological droughts as compared to traditional hydrological drought indices (e.g., the SSI). Moreover, by using this network, one can also know the amount of environmental flow required for drought recovery in the future months

and how possible is it. The general probabilistic network can potentially facilitate the decision-makers in water resources management by providing a valuable insight toward assessing hydrological drought status. Moreover, the generated risk-evaluation information based on this network can be helpful for developing appropriate water supply plans to reduce the drought risk likely to occur in future. This prediction framework is also promising for application to other basins worldwide under different climate regimes. Future efforts could extend this network by joining more hydrological variables (e.g., the soil moisture) and constructing the conditional dependence with both precipitation and soil moisture in order to better address hydrological droughts.

Appendix A

This appendix lists the bivariate copulas employed in the current study in detail. They are given for the bivariate case (Mendes and Souza, 2004).

1. Gaussian (Normal) copula

The Gaussian copula is an elliptical copula and can be written by:

$$C_\rho(u_1,u_2)=\int_{-\infty}^{\Phi^{-1}(u_1)}\int_{-\infty}^{\Phi^{-1}(u_2)}\frac{1}{2\pi(1-\rho^2)^{1/2}}\exp\left\{-\frac{s^2-2\rho st+t^2}{2(1-\rho^2)}\right\}dsdt \qquad \text{(A1)}$$

where u_1 and u_2 are the margins of random variable varying from 0 to 1. Φ^{-1} denotes the inverse of the standard Gaussian distribution function and ρ is the copula parameter (the linear correlation coefficient).

2. Clayton copula

The Clayton copula is given as:

$$C(u_1,u_2)=(u_1^{-\theta}+u_2^{-\theta}-1)^{-1/\theta} \qquad \text{(A2)}$$

The generator is $\phi(\tau)=(\tau^{-\theta})/\theta$.

where θ ($\theta\in(0,\infty)$) is the copula function parameter and τ is Kendall's coefficient between two variables.

3. Frank copula (Zhang and Singh, 2007)

The Frank copula can be formulated as:

$$c(u_1,u_2)=-\frac{1}{\theta}\ln[1+\frac{(\exp(-\theta u_1)-1)(\exp(-\theta u_2)-1)}{(\exp(-\theta)-1)}],\theta\neq 0 \qquad \text{(A3)}$$

And its generator is $\phi(t)=-\ln\left(\frac{\exp(-\theta t)-1}{\exp(-\theta)-1}\right)$.

where θ is the copula function parameter and *t* is the specific values of u_1 or u_2 varying from 0 to 1. Note that the parameters u_1 , u_2 and θ will have the same

definitions in the following copula function.

4. Gumbel copula

The Gumbel copula (i.e., Gumbel-Hougard copula) is given by:

$$c(u_1,u_2)=\exp\left\{-[(-\ln u_1)^{\theta}+(-\ln u_2)^{\theta}]^{1/\theta}\right\},\theta\in[1,\infty) \quad \text{(A4)}$$

with the generator: $\phi(t)=(-\ln t)^{\theta}$.

5. Joe copula

The formulation of Joe copula is expressed as follows:

$$c(u_1,u_2)=1-[(1-u_1)^{\theta}+(1-u_2)^{\theta}-(1-u_1)^{\theta}(1-u_2)^{\theta}]^{1/\theta},\theta\geq 1 \quad \text{(A5)}$$

with the generator: $\phi(t)=-\ln[1-(1-t)^{\theta}]$

Appendix B

Algorithm and procedure for computing the required flow (the environmental flow target) and the associated exceedance probability based on vine copulas.

The consideration of high-dimensional margins in the JSDI computations provides a way to examining the month-by-month future environmental flow assessment. S_n^f is defined as the future *n*-month mean flow (*n*=1,…12), and S_g^p indicates the historical monthly flow for the past *g* months. It should be emphasized that, based on the definition of JSDI, this study focuses on evaluating the mean flow of the future *n*-month rather than the individual flow in each future *n*-month which will require to make more extra assumptions. For instance, to obtain the required flow in the future second month (*n*=2), it is necessary to assume a value of prior flow in the future first month (*n*=1) because the JSDI is calculated based on the average values of flow for a given *n*-month time window as described in Section 5.4.1. To assess S_n^f, it is necessary to obtain the past 12–*n* months observations S_1^p,…, S_{12-n}^p, considering that the maximum temporal length of JSDI is 12 months. Kao and Govindaraju (2010) described the main procedure to compute the expected S_n^f based on empirical copula, and here this study introduces the vine copulas to achieve this computation instead of the original empirical joint function.

1. Assume an initial guess of S_n^f.

2. Compute the flow margins u_n^m by the assumed S_n^f, u_{n+1}^m by $(S_n^f + S_1^p)$, .., and u_{12}^m by $(S_n^f + \sum_{i=1}^{12-n} S_i^p /(12-n))$. The month when S_n^f occurs is the ending month used in the improved SSI procedure.

3. Following the Section 5.4.3 and 5.4.4, use the vine copulas to model the joint

dependence structure of $C_{U_n,\ldots,U_{12}}(u_n^m,\ldots,u_{12}^m)$ and the associated K_C.

4. Reset the S_n^f and repeat step 2, and 3 until $K_C = 0.5$ (normal condition) or $K_C = 0.7$ (moderate wet condition). One can pre-define a range of flow values for S_n^f based on historical observations, in order to reduce computation time and effort.

5. If $K_C = 0.5$ (normal condition) or $K_C = 0.7$ (moderate wet condition), the obtained S_n^f represents the required mean flow corresponding to a certain environmental flow target over the following *n* months. $(1-u_n^m)$ will be the associated exceedance probability of this event.

It is worth emphasizing that, because there are no extra assumptions about the future flow, it is inevitable that a truncated dependence model $C_{U_n,\ldots,U_{12}}(u_n^m,\ldots,u_{12}^m)$ are adopted to compute the corresponding JSDI values in the study. When *n* reaches 12, copula $C_{U_{12}}(u_{12}^m)$ and K_C will decay to the margin u_{12}^m because no available historical monthly flow joins the computation. Thereby, S_{12}^f refers to 0.5 (for the targeted normal condition) and 0.7 (for the targeted moderate wet condition) of $F_{X_{12}^m}$.

References

Aas, K., Czado, C., Feigessi, A., Bakken, H., 2009. Pair-Copula Construction of Multiple Dependence. Insurance Math. Econom., 44 (2), 182–198, doi: 10.1016/j.insmatheco.2007.02.001.

Alexandersson, H., 1986. A homogeneity test applied to precipitation data. J. Climatol. 6, 661–675.

American Meteorological Society (AMS) (2004). Statement on meteorological drought. Bull. Am. Meteorol. Soc., 85, 771–773.

Arking, A., 1964. Latitudinal distribution of cloud cover from TIROS I11 photographs. Science, 143, 569–572.

Aubert, D., Loumagne, C., Oudin, L., 2003. Sequential assimilation of soil moisture and streamflow data in a conceptual rainfallrunoff model, J. Hydrol., 280, 145–161.

Bárdossy, A., Li, J., 2008. Geostatistical interpolation using copulas. Water Resour. Res., 44, W07412, doi:10.1029/2007WR006115.

Bardossy, A. and Filiz, F., 2005. Identification of flood producing atmospheric circulation patterns. J. Hydrol. 313, 48–57.

Bárdossy, A., Li J., 2008. Geostatistical interpolation using copulas, Water Resour. Res., 44, W07412, doi:10.1029/2007WR006115.

Bárdossy, A., Pegram, G., 2013. Interpolation of precipitation under topographic influence at different time scales. Water Resour. Res., 49, 4545–4565, doi:10.1002/wrcr.20307.

Barnston, A.G., Livezey, R.E., 1987. Classification, seasonality, and persistence of low-frequency atmospheric circulation patterns. Mon. Weather. Rev., 115,1083–1126.

Bedford, T., Cooke, R. M., 2002. Vines–a new graphical model for dependent random variables. Ann. Statist., 30(4), 1031–1068, doi:10.1214/aos/1031689016.

Beurton, S., Thieken, A.H., 2009. Seasonality of floods in Germany. Hydrolog. Sci. J.,

54(1), 62–76.

Bjerknes, J., 1959. Atmospheric telecoriectioiis froin the eqclatarial Pacific. Mon. Wea. Rev., 97, 163–172.

Borak, J. S., Lambin, E. F., Strahler, A. H., 2000. The use of temporal metrics for land cover change detection at coarse spatial scales. Int. J. Remote Sens. 21, 1415−1432.

Bouwer, L. M., Vermaat, J. E., Aerts, J. C. J. H., 2006. Winter atmospheric circulation and river discharge in northwest Europe. Geophys. Res. Lett., 33, L06403, doi:10.1029/2005GL025548.

Brechmann, E. C., Hendrich, K., Czado, C., 2013. Conditional copula simulation for systemic risk stress testing. Insurance Math. Econom., 53(3), 722–732, doi:10.1016/j.insmatheco.2013.09.009.

Brocca, L., Melone, F., Moramarco, T., 2008. On the estimation of antecedent wetness conditions in rainfall-runoff modeling. Hydrol. Process., 22, 629–642.

Brocca, L., Melone, F., Moramarco, T., Morbidelli, R., 2009. Antecedent wetness conditions based on ERS scatterometer data. J. Hydrol., 364, 73–87, doi:10.1016/j.jhydrol.2008.10.007.

Brovkin, V., 2002. Climate–vegetation interaction. J. Phys., 4, 57–72.

Buishand, T.A., 1982. Some methods for testing the homogeneity of rainfall records. J. Hydrol., 58, 11–27.

Burrows, C.J., 1990. Processes of vegetation change. Unwin Hyman, London, United Kingdom.

Cavendish, M.G., Duncan, M.I., 1986. Use of the instream flow incremental methodology: a tool for negotiation. Environ. Impact Assess. Rev., 6, 347–363.

Cayan, D.R., Riddle, L.G., Aguado, E.. 1993. The Influence of Precipitation and Temperature on Seasonal Streamflow in California. Water Resour. Res., 29, 1127–1140. http://dx.doi.org/10.1029/92WR02802

Chen, M., P. Xie, Janowiak, J. E., Arkin, P. A., 2002. Global land precipitation: A 50-yr monthly analysis based on gauge observations. J. Hydrometeorol., 3, 249–266.

Choi, T.-M., Yu, Y., Au, K.-F., 2011. A hybrid SARIMA wavelet transform method for sales forecasting. Decis. Support Syst. 51 (1), 130–140.

Chuai, X. W., Huang, X. J., Wang, W. J. Bao, G., 2013. NDVI, temperature and precipitation changes and their relationships with different vegetation types during 1998–2007 in Inner Mongolia, China. Int. J. Climatol., 33, 1696–1706.

Cui, L.L., Shi, J., 2010. Temporal and spatial response of vegetation NDVI to temperature and precipitation in eastern China. J. Geogr. Sci., 20(2), 163–176, DOI: 10.1007/s11442-010-0163-4.

Cunderlik, J. M., Burn, D. H., 2004. Linkages between regional trends in monthly maximum flows and selected climate variables. J. Hydrol. Eng., 9(4), 246–256.

Daubechies, I., 1990. The wavelet transform, time-frequency localization and signal analysis. IEEE Trans. Inf. Theory, 36 (5), 961–1005.

de Artigas, M.Z., Elias, A.G., de Campra, P.F., 2006. Discrete wavelet analysis to assess long-term trends in geomagnetic activity. Phys. Chem. Earth, 31 (1–3), 77–80.

de Beurs, K.M., Henebry, G.M., 2005. A statistical framework for the analysis of long image time series. Int. J. Remote Sens., 26, 1551–1573.

De Michele, C., Salvadori, G., Vezzoli, R., Pecora, S., 2013. Multivariate assessment of droughts: Frequency analysis and dynamic return period. Water Resour. Res., 49, 6985–6994, doi:10.1002/wrcr.20551.

Dettinger, M.D., Diaz, H.F., 2000. Global characteristics of streamflow seasonality. J. Hydrometeor., 1, 289–310.

Dong, C., Menzel, L., 2016. Improving the accuracy of MODIS 8-day snow products with in situ temperature and precipitation data. J. Hydrol. (accepted).

Dong, X., Nyren, P., Patton, B., Nyren, A., Richardson, J., Maresca, T., 2008. Wavelets for agriculture and biology: a tutorial with applications and outlook. Bioscience, 58(5), 445–453.

Dunbar, M.J., Acreman, M.C., 2001. Applied hydro-ecological science for the twenty-first century, in Hydro-ecology: Linking Hydrology and Aquatic Ecology, edited by Acreman, M.C., pp. 1–17, Publication No. 266. IAHS Press, Centre for

Ecology and Hydrology, Wallingford, UK.

Fan, Y., van den Dool, H., 2004. Climate Prediction Center global monthly soil moisture data set at 0.5 resolution for 1948 to present. J. Geophys. Res., 109, D10102, doi:10.1029/2003JD004345.

Fan, Y., van den Dool, H., 2008. A global monthly land surface air temperature analysis for 1948–present. J. Geophys. Res., 113, D01103, doi:10.1029/2007JD008470.

Fang, K.T., Kotz, S., Ng, K.W., 1990. Symmetric Multivariate and Related Distributions. Chapman & Hall Ltd.

Favre, A.-C., El Adlouni, S., Perreault, L., Thiémonge, N., Bobée, B., 2004. Multivariate hydrological frequency analysis using copulas. Water Resour. Res., 40, W01101, doi:10.1029/2003WR002456.

Ficklin, D.L., Luo, Y.Z., Luedeling, E., Zhang, M.H., 2009. Climate change sensitivity assessment of a highly agricultural watershed using SWAT. J. Hydrol., 374 (1–2), 16–29.

Forkel, M., Carvalhais, N., Verbesselt, J., Mahecha, M.D., Neigh, C.S., Reichstein, M. 2013. Trend Change Detection in NDVI Time Series: Effects of Inter-Annual Variability and Methodology. Remote Sens. 5, 2113-2144.

Fujinami, H., Yasunari, T. and Watanabe, T., 2015. Trend and interannual variation in summer precipitation in eastern Siberia in recent decades. Int. J. Climatol., doi: 10.1002/joc.4352

Gan, T.Y., 1998. Hydroclimatic trends and possible climatic warming in the Canadian Prairies. Water Resour. Res. 34(11), 3009–3015.

Genest, C., Favre, A., 2007. Everything you always wanted to know about copula modeling but were afraid to ask. J. Hydrol. Eng., 12(4), 347–368, doi:10.1061/(ASCE)1084-0699.

Genest, C., Nešlehová, G., Ziegel, J., 2011. Inference in multivariate Archimedean copula models, Test, 20, 223–256.

Genest, C., Rémillard, B., 2008. Validity of the parametric bootstrap for goodness-of-fit testing in semiparametric models. Annales de l'Institut

Henri-Poincaré, 44(6), 1096–1127.

Gitelson, A.A., 2004. Wide dynamic range vegetation index for remote quantification of biophysical characteristics of vegetation. J. Plant Physiol., 161, 165–173, DOI: 10.1078/0176-1617-01176.

Gleick, P., Water in Crisis, Oxford University Press, New York, 1993.

Grinsted, A., Moore, J.C., Jevrejeva, S., 2004. Application of the cross wavelet transform and wavelet coherence to geophysical time series. Nonlinear Process Geophys., 11(5/6), 561–566.

Guo, X., 2003, Relationships between NDVI and climatological variability in the prairie ecozone of Canada. Prairie perspective, geographical essays 6, pp. 32–46.

Guse, B., Reusser, D. E., Fohrer, N., 2014. How to improve the representation of hydrological processes in SWAT for a lowland catchment – temporal analysis of parameter sensitivity and model performance. Hydrol. Process., 28, 2651–2670. doi: 10.1002/hyp.9777.

Gyasi-Agyei, Y., 2013. Evaluation of the effects of temperature changes on fine timescale rainfall. Water Resour. Res., 49, 4379–4398, doi:10.1002/wrcr.20369.

Hamed, K.H., Rao, A.R., 1998. A modified Mann–Kendall trend test for autocorrelated data. J. Hydrol., 204 (1–4), 182–196.

Hamlet, A. F., Lettenmaier, D. P., 2007. Effects of 20th century warming and climate variability on flood risk in the western U.S. Water Resour. Res., 43, W06427, doi:10.1029/2006WR005099

Hansen, J., Ruedy, R., Sato, M., Lo K., 2010. Global surface temperature change. Rev. Geophys., 48, RG4004,doi:10.1029/2010RG000345.

Hao, Z, AghaKouchak, A., 2013. Multivariate standardized drought index: a parametric multi-index model. Adv. Water Resour., 57, 12–18. doi:10.1016/j.advwatres.2013.03.009.

Hao, Z., Singh, V. P., 2013. Modeling multisite streamflow dependence with maximum entropy copula. Water Resour. Res., 49, 7139–7143, doi:10.1002/wrcr.20523.

Haslinger, K., Koffler, D., Schoner, W., Laaha, G., 2014. Exploring the link between

meteorological drought and streamflow: Effects of climatecatchment interaction. Water Resour. Res., 50, 2468–2487, doi:10.1002/ 2013WR015051.

He, Y., Guo, X., Dixon, P., Wilmshurst, J. F., 2012. NDVI variation and its relation to climate in Canadian ecozones. Can. Geogr.-Geogr. Can., 56, 492–507.

Hellebrand H., Van Den Bos, R., Hoffmann, L., Juilleret, J., Krein, A., Pfister, L., 2009. Spatio-temporal variability of behavioural patterns in hydrology in meso-scale basins of the Rhineland Palatinate (1972–2002). Clim. Change, 93(1–2), 223–242.

Hellebrand, H., Van Den Bos, R., Hoffmann, L., Juilleret, J., Krein, A., Pfister, L., 2009. Spatio-temporal variability of behavioural patterns in hydrology in meso-scale basins of the Rhineland Palatinate (1972-2002). Clim. Chang, 93(1–2), 223–242.

Helsel, D.R., Hirsch, R.M., 1992. Statistical methods in waterresources. Studies in Environmental Science. Elsevier, Amsterdam, pp. 522.

Hill, M., Platts, W.S., 1991. Ecological and geomorphological concepts for instream and out-of-channel flow requirements. Rivers, 2, 319–343.

Hirsch, R.M., Slack, J.R., 1984. A nonparametric trend test for seasonal data with serial dependence. Water Resour. Res. 20(6), 727–732.

Hirsch, R.M., Slack, J.R., Smith, R.A., 1982. Techniques of trend analysis for monthly water quality data. Water Resour. Res., 18(1), 107–121.

Hofert, M., Kojadinovic, I., Machler, M., Yan, J., 2014. Package copula, <URL: http://nacopula.r-forge.r-project.org/>.

Holben, B. N., 1986. Characteristics of maximum-value composite image from temporal AVHRR data. Int. J. Remote Sens., 7, 1417−1434.

Hollinger, S.E., Isard, S.A., Welford, M.R., 1993. A New Soil Moisture Drought Index for Predicting Crop Yields. In: Preprints, Eighth Conf. on Applied Climatology, Anaheim, CA, Amer. Meteor. Soc., pp. 187–190.

Horion, S., Cornet, Y., Erpicum, M., Tychon, B., 2013. Studying interactions between climate variability and vegetation dynamic using a phenology based approach. Int. J. Appl. Earth Obs. Geoinf., 20, 20–32.

Horton, R., 1933. The role of infiltration in the hydrologic cycle. Transactions of the American Geophysical Union, 14, 446-460.

Huang, S.H., Krysanova, V., Hattermann, F., 2015. Projections of climate change impacts on floods and droughts in Germany using an ensemble of climate change scenarios. Reg. Environ. Chang., doi:10.1007/s10113-014-0606-z.

Hughes, D.A., 2001. Providing hydrological information and data analysis tools for the determination of ecological instream flow requirements for South African rivers. J. Hydrol., 241,140–151.

Hurrell, Y. Kushnir, G. Ottersen, M. Visbeck, Eds. 2003: The North Atlantic Oscillation: Climatic significance and environmental effect. Geophys Monogr., Vol. 134, Amer. Geophys.Union, 279 pp.

Ichii, K., Kawabrata, A., Yamaguchi, Y., 2002. Global correlation analysis for NDVI and climate variables and NDVI trends: 1988–1990. Int. J. Remote Sens., 23, 3873–3878,

Intergovernmental Panel on Climate Change (IPCC), 2007. Climate Change 2007: The Physical Science Basis,edited by S. Solomon et al., Cambridge Univ. Press, New York.

Ionita, M, Boroneant, C,, Chelcea, S., 2015. Seasonal modes of dryness and wetness variability over Europe and their connections with large scale atmospheric circulation and global sea surface temperature. Clim. Dyn., doi:10.1007/s00382-015-2508-2.

Ionita, M., Lohmann, G., Rimbu, N., Chelcea, S., 2012. Interannual variability of Rhine River streamflow and its relationship with large-scale anomaly patterns in spring and autumn. J. Hydrometeorol., 13 (1), 172–188.

Ionita, M., Lohmann, G., Rimbu, N., Chelcea, S., Dima, M., 2011. Interannualto decadal summer drought variability over Europe and its relationshipto global sea surface temperature. Clim. Dyn., 38(1–2), 363–377, DOI:10.1007/s00382-011-1028-y.

IPCC, 2008, 2009. climate change and water. Intergovernmental Panel on Climate Change Technical Paper VI. IPCC Secretariat, Geneva.

IPCC, 2013. Climate Change 2013: The Physical Science Basis. Contribution of Working Group I to the Fifth Assessment Report of the Intergovernmental Panel on Climate Change. Cambridge University Press, Cambridge, United Kingdom and New York, NY, USA, 1535 pp.

Jacobeit, J., Glaser, R., Luterbacher, J., Wanner, H., 2003. Links between flood events in Central Europe since AD 1500 and large-scale atmospheric circulation modes. Geophys. Res. Lett., 30, 1172–1175.

Jha, M., Z., Pan, E. S., Takle, Gu, R., 2004. Impacts of climate change on streamflow in the Upper Mississippi River Basin: A regional climate model perspective. J. Geophys. Res., 109, D09105, doi:10.1029/2003JD003686.

Joe, H., 1997. Multivariate Models and Dependence Concepts. Chapman and Hall, London.

Julien, Y, Sobrino, J. A., 2010. Comparison of Cloud-reconstruction Methods for Time Series of Composite NDVI Data. Remote Sens. Environ.,114, 618–625.

Jung, H.Y., Choi, Y., Oh, J.H., Lim, G.H., 2002. Recent trends in temperature and precipitation over South Korea. Int. J. Climatol., 22, 1327–1337.

Junk, W.J., Bayley, P.B., Sparks, R.E., 1989. The flood pulse concept in river-floodplain systems. Can. Spec. Publ. Fish. Aquat. Sci., 106, 110–127.

Kalnay, E., Kanamitsu, M., Kistler, R., Collins, D., Deaven, D., Gandin, L., Iredell, M., Saha, S., White, G., Woolen, J., Zhu, Y., Chelliah, M., Ebisuzaki, W., Higgins, W., Janowiak, J., Mo, K.C., Kopelewski, C., Wang, J., Leetmaa, A., Reynolds, R., Jeene, R., Joseph, D., 1996. The NCEP/NCAR 40-year Reanalysis Project. Bull. Am. Meteorol. Soc. 77, 437–471.

Kao, S.-C., Govindaraju, R. S., 2010. A copula-based joint deficit index for droughts. J. Hydrol., 380, 121–134, doi:10.1016/j.jhydrol.2009.10.029.

Karl, T., Quinlan, F., Ezell, D. S., 1987. Drought termination and amelioration—Its climatological probability. J. Clim. Appl. Meteorol., 26(9), 1198–1209.

Kawabata, A., Ichii, K., Yamaguchi, Y., 2001. Global monitoring of interannual changes in vegetation activities using NDVI and its relationships to temperature and precipitation. Int. J. Remote Sens., 22, 1377–1382,

Kendall, M.G., 1975. Rank Correlation Methods, fourth ed. Charles Griffin, London.

Khedun, C. P., Mishra, A. K., Singh, V. P., Giardino, J. R., 2014. A copula-based precipitation forecasting model: Investigating the interdecadal modulation of ENSO's impacts on monthly precipitation. Water Resour. Res., 50, 580–600, doi:10.1002/2013WR013763.

Kim, S., 2004. Wavelet analysis of precipitation variability in northern California, USA. KSCE J. Civ. Eng., 8 (4), 471–477.

King, J., Brown, C., Sabet, H., 2003. A scenario-based holistic approach to environmental flow assessments for rivers. River Res. Appl., 19, 619–639.

King, J., Brown, C., Sabet, H., 2003. A scenario-based holistic approach to environmental flow assessments for rivers. River Res. Appl., 19, 619–639, doi:10.1002/rra.709.

Kingston, D. G., Lawler, D. M., McGregor, G. R., 2006. Linkages between atmospheric circulation, climate and streamflow in the northernNorth Atlantic:Research prospects. Prog. Phys. Geogr., 30, 143–174.

Kletti, L.L. Stefan, H.G., 1997. Correlations of Climate and Streamflow in Three Minnesota Streams. Clim. Change, 37, 575–600.

Kuhn, G., Khan, S., Ganguly, A.R.,. Branstetter, M.L., 2007. Geospatial-temporal dependence among weekly precipitation extremes with applications to observations and climate model simulations in South America. Adv. Water Resour., 30, 2401–2423. doi:10.1016/j.advwatres.2007.05.006.

Kulkarni, J.R., 2000. Wavelet analysis of the association between the Southern Oscillation and the Indian summer monsoon. Int. J. Climatol. 20 (1), 89–104.

Kurowicka, D. and Cooke, R., 2006. Uncertainty Analysis with High Dimensional Dependence Modelling, Wiley, Chichester.

Kurowicka, D., 2011. Introduction: Dependence Modeling. In Dependence Modeling, Vine Copula Handbook, World Scientific Publishing, Singapore.

Laux, P., Vogl, S., Qiu, W., Knoche, H. R., Kunstmann, H., 2011. Copula-based statistical refinement of precipitation in RCM simulations over complex terrain. Hydrol. Earth Syst. Sci., 15, 2401–2419, doi:10.5194/hess-15-2401-2011.

Laux, P., Vogl, S., Qiu, W., Knoche, H. R., Kunstmann, H., 2011. Copula-based statistical refinement of precipitation in RCM simulations over complex terrain. Hydrol. Earth Syst. Sci., 15, 2401–2419, doi:10.5194/hess-15-2401-2011.

Li, C., Singh, V. P., Mishra, A. K., 2013a. A bivariate mixed distribution with a heavy-tailed component and its application to single-site daily rainfall simulation. Water Resour. Res., 49, doi:10.1002/wrcr.20063.

Li, C., Sinha, E., Horton, D. E., Diffenbaugh, N. S., Michalak, A. M., 2014. Joint bias correction of temperature and precipitation in climate model simulations. J. Geophys. Res. Atmos., 119, 13,153–13,162, doi:10.1002/2014JD022514.

Li, C., Singh, V. P., Mishra, A. K., 2013b. Monthly river flow simulation with a joint conditional density estimation network. Water Resour. Res., 49, 3229–3242, doi:10.1002/wrcr.20146.

Liu, W.T., Kogan, F.N., 1996. Monitoring regional drought using the vegetation condition index. Int. J. Remote Sens., 17, 2761–2782.

Liu, Z., Menzel, L., Dong, C., Fang, R., 2015a. Temporal dynamics and spatial patterns of drought and the relation to ENSO: a case study in Northwest China. Int. J. Climatol., doi: 10.1002/joc.4526.

Liu, Z., Zhou, P., Zhang, F., Liu, X. Chen, G., 2013. Spatiotemporal characteristics of dryness/wetness conditions across Qinghai Province, Northwest China. Agric. For. Meteorol., 182–183, 101–108.

Liu, Z., Zhou, P., Zhang, Y., 2015b. A probabilistic wavelet-support vector regression model for streamflow forecasting with rainfall and climate information input. J. Hydrometeor., doi: 10.1175/JHM-D-14-0210.1.

Liu, Z., Zhou, P., Chen, G., Guo, L., 2014. Evaluating a coupled discrete wavelet transform and support vector regression for daily and monthly streamflow forecasting. J. Hydrol., 519, 2822–2831, doi:10.1016/j.jhydrol.2014.06.050.

Liu, Z., Zhou, P., Chen, X., Guan, Y., 2015c. A multivariate conditional model for streamflow prediction and spatial precipitation refinement. J. Geophys. Res. Atmos., doi: 10.1002/2015JD023787.

Luce, C. H., Holden Z. A., 2009. Declining annual streamflow distributions in the

Pacific Northwest United States, 1948–2006. Geophys. Res. Lett., 36, L16401, doi:10.1029/2009GL039407.

Ma, H., Yang, D., Tan, S.K., Gao, B., Hu, Q., 2010. Impact of climate variability and human activity on streamflow decrease in the Miyun Reservoir catchment. J. Hydrol., 389, 317–324.

Madadgar, S., Moradkhani, H., 2013. A Bayesian framework for probabilistic seasonal drought forecasting. J. Hydrometeorol., 14, 1685–1705, doi:10.1175/JHM-D-13-010.1.

Maity, R., Ramadas, M., Govindaraju, R. S., 2013. Identification of hydrologic drought triggers from hydroclimatic predictor variables. Water Resour. Res., 49, 4476–4492, doi:10.1002/wrcr.20346.

Mallat, S.G., 1989. A theory for multiresolution signal decomposition: the wavelet representation. IEEE Trans. Pattern Anal. Mach. Intell., 11(7), 674–693.

Mann, H.B., 1945. Nonparametric tests against trend. Econometrica, 13, 245–259.

Mao, D., Wang, Z., Luo, L., Ren, C., 2012. Integrating AVHRR and MODIS data to monitor NDVI changes and their relationships with climatic parameters in Northeast China. Int. J. Appl. Earth Obs. Geoinf., 18, 528–536.

Martínez, B., Gilaber,t M.A., 2009. Vegetation dynamics from NDVI time series analysis using the wavelet transform. Remote Sens. Environ., 113(9), 1823–1842.

Massey, F. J., 1951. The Kolmogorov-Smirnov test for goodness of fit. Amer. Stat. Assoc., 46(253), 68–78, doi:10.1080/01621459.1951.10500769.

Mathews, R., Richter, B. D., 2007. Application of the Indicators of Hydrologic Alteration Software in Environmental Flow Setting. J. Am. Water Resour. Assoc., 43, 1400–1413. doi: 10.1111/j.1752-1688.2007.00099.x.

McKee, T.B., Doesken, N.J., Kleist, J., 1993. The Relationship of Drought Frequency and Duration to Time Scales, Paper Presented at 8th Conference on Applied Climatology. American Meteorological Society, Anaheim, CA

McKee, T.B., Doesken, N.J., Kleist, J., 1995. Drought monitoring with multiple time scales. Presented at the Eighth Conference on Applied Climatology, Dallas, TX. Am. Meteorol. Soc., 233–236.

McNeil, A. J., Nešlehová, J., 2009. Multivariate Archimedean copulas, d-monotone functions and l1-norm symmetric distributions. Ann. Stat., 37(5b), 3059–3097.

Mendes, B.V.M., Souza, R.M., 2004. Measuring financial risks with copulas. Int. Rev. Financ. Anal., 13 (1), 27–45.

Mengistu, S. G., I. F. Creed, R. J. Kulperger, Quick, C. G., 2013. Russian nesting dolls effect—Using wavelet analysis to reveal nonstationary and nested stationary signals in water yield from catchments on a northern forested landscape. Hydrol. Processes, 27, 669–686, doi:10.1002/hyp9552.

Meyer, S.J., Hubbard, K.G., 1995. Extending the Crop-specific Drought Index to Soybean. In: Preprints, Ninth Conf. on Applied Climatology, Dallas, TX, Amer. Meteor. Soc., pp. 258–259.

Miao, L., Luan, Y., Luo, X., Liu, Q., Moore, J.C., Nath, R., He, B., Zhu, F., Cui, X.,2013. Analysis of the Phenology in the Mongolian Plateau by Inter-Comparison of Global Vegetation Datasets. Remote Sens., 5, 5193-5208.

Miao, L., Ye, P., He, B., Chen, L., Cui, X., 2015. Future Climate Impact on the Desertification in the Dry Land Asia Using AVHRR GIMMS NDVI3g Data. Remote Sens., 7, 3863-3877.

Mirabbasi, R., Anagnostou, E.N., Fakheri-Fard, A., Dinpashoh, Y., Eslamian, S., 2013. Analysis of meteorological drought in northwest Iran using the joint deficit index. J. Hydrol., 492, 35–48.

Mishra, A.K., Singh, V.P., 2010. A review of drought concepts. J. Hydrol., 391 (1–2), 202–216.

Misiti, M., Misiti, Y., Oppenheimer, G., Poggi, J.M., 1997. Wavelet Toolbox Users Guide. MathWorks, USA, pp. 626.

Nalbantis, I., Tsakiris, G., 2009. Assessment of hydrological drought revisited. Water Resour. Manag., 23, 881–897.

Nalley, D., Adamowski, J., Khalil, B., 2012. Using discrete wavelet transforms to analyze trends in streamflow and precipitation in Quebec and Ontario (1954–2008). J. Hydrol., 475, 204–228.

Nalley, D., Adamowski, J., Khalil, B., Ozga-Zielinski, B., 2013. Trend detection in

surface air temperature in Ontario and Quebec, Canada during 1967–2006 using the discrete wavelet transform. Atmos. Res., 132–133, 375–398.

Nelsen, R.B., 2006. An Introduction to Copulas. Springer, New York.

Nelsen, R.B., Quesada-Molina, J.J., Rodríguez-Lallena, J.A., Úbeda-Flores, M., 2003. Kendall distribution functions. Stat. Probab. Lett., 65, 263–268.

New, M, Hulme, M., Jones, P. D., 2000. Representing twentieth century space-time climate variability. Part II: Development of 1901-96 monthly grids of terrestrial surface climate. J. Clim., 13, 2217–2238.

Nijssen, B., Schnur, R., Lettenmaier, D.P., 2001. Global retrospective estimation of soil moisture using the variable infiltration capacity land surface model. 1980–93. J. Clim., 14, 1790–1808.

Özger, M., Mishra, A., Singh, V., 2009. Low frequency drought variability associated with climate indices. J. Hydrol., 364(1–2), 152–162.

Palmer, W.C., 1965. Meteorologic Drought. US Department of Commerce, Weather Bureau, Research Paper No. 45, p. 58.

Pan, M., Yuan, X., Wood, E. F., 2013. A probabilistic framework for assessing drought recovery. Geophys. Res. Lett., 40, 3637–3642, doi:10.1002/grl.50728.

Park, H.-S., Sohn, B. J., 2010. Recent trends in changes of vegetation over East Asia coupled with temperature and rainfall variations. J. Geophys. Res., 115, D14101, doi:10.1029/2009JD012752.

Partal, T., 2010. Wavelet transform-based analysis of periodicities and trends of Sakarya basin (Turkey) streamflow data. River Res. Appl., 26 (6), 695–711.

Partal, T., Küçük, M., 2006. Long-term trend analysis using discrete wavelet components of annual precipitations measurements in Marmara region (Turkey). Phys. Chem. Earth, 31 (18), 1189–1200.

Penna, D., Tromp-van Meerveld, H.J., Gobbi, A., Borga, M., Dalla, Fontana G., 2011.The influence of soil moisture on threshold runoff generation processes in an alpine headwater catchment. Hydrol. Earth Syst. Sci., 15, 689–702.

Percival, D.B., 2008. Analysis of geophysical time series using discrete wavelet transforms: an overview. In: Donner, R.V., Barbosa, S.M. (Eds.), Nonlinear Time

Series Analysis in the Geosciences–Applications in Climatology, Geodynamics, and Solar-terrestrial Physics. Springer, Berlin/Heidelberg.

Petrow, T., Merz, B., 2009. Trends in flood magnitude, frequency and seasonality in Germany in the period 1951–2002. J. Hydrol., 371(1–4), 129–141, doi:10.1016/j.jhydrol.2009.03.024.

Petrow, T., Zimmer, J., Merz, B., 2009. Changes in the flood hazard in Germany through changing frequency and persistence of circulation patterns. Nat. Hazards Earth Syst. Sci., 9, 1409–1423.

Piao, S. L., Ciais, P., Huang, Y., Shen, Z., Peng, S., Li, J., et al., 2010. The impacts of climate change on water resources and agriculture in China. Nature, 467, 43–51.

Piao, S.L., Fang, J.Y., Ji, W., Guo, H., Ke, J.H., Tao, S., 2004. Variation in a satellite-based vegetation index in relation to climate in China. J. Veg. Sci., 15: 219–226.

Piao, S.L., Mohammat, A., Fang, J.Y., Cai, Q., Feng, J.M., 2006. NDVIbased increase in growth of temperate grasslands and its responses to climate changes in China. Glob. Environ. Chang., 16, 340–348,

Pielke, R. A., Avissar, R., Raupach, M., Dolman, A. J., Zeng, X., Denning, A. S. (1998), Interactions between the atmosphere and terrestrial ecosystems: influence on weather and climate. Glob. Change Biol., 4, 461–475, doi: 10.1046/j.1365-2486.1998.t01-1-00176.x

Pisoft, P., Kalvova, J., Brazdil, R., 2004. Cycles and trends in the Czech temperatures series using wavelet transform. Int. J. Climatol., 24, 1661–1670.

Popivanov, I., Miller, R.J., 2002. Similarity search over time-series data using wavelets. In: Proceedings 18th International Conference on Data Engineering, pp. 212–221.

Qin, N.X., Chen, X., Fu, G.B., Zhai, J.Q., Xue, X.W., 2010. Precipitation and temperature trends for the Southwest China, 1960–2007. Hydrol. Processes, 24(25), 3733–3744.

Rees, M., Condit, R., Crawley, M., Pacala, S., Tilman, D., 2001. Long-term studies of vegetation dynamics. Science, 293, 650–655.

Ren, X., Li, S. J., Lv, C., Zhang, Z. Y., 2014. Sequential dependence modeling using Bayesian theory and D-vine copula and its application on chemical process risk prediction. Ind. Eng. Chem. Res., 2014, 53(38), 14788–14801, doi: 10.1021/ie501863u.

Richter, B., Baumgartner, J., Wigington, R. Braun D., 1997. How much water does a river need? Freshwater Biol., 37, 231–249. doi: 10.1046/j.1365-2427.1997.00153.x

Richter, B.D., Baumgartner, J.V., Powell, J., Braun, D.P., 1996. A method for assessing hydrological alteration within ecosystems. Conserv. Biol., 10(4), 1163–1174.

Rimbu, N., Dima, M., Lohmann, G., Stefan, S., 2004. Impacts of the North Atlantic Oscillation and the El Niño-Southern Oscillation on Danube river flow variability. Geophys. Res. Lett., 31, L23203.doi:10.1029/2004GL020559

Ritter, M. E., 2006. The Physical Environment: an Introduction to Physical Geography. < http://www.earthonlinemedia.com/ebooks/tpe_3e/title_page.html >.

Rodgers, A, Streluk, A., 2003. Precipitation. Chicago, IL: Heinemann Library.

Ruiz-Villanueva, V., Borga, M., Zoccatelli, D., Marchi, L., Gaume, E., Ehret, U., 2012. Extreme flood response to short-duration convective rainfall in South-West Germany. Hydrol. Earth Syst. Sci., 16, 1543-1559, doi:10.5194/hess-16-1543-2012.

Running, S.W., Nemani, R., 1988. Relating seasonal patterns of the AVHRR vegetation index to simulated photosynthesis and transpiration of forests in different climates. Remote Sens. Environ., 24, 347−367.

Salvadori, G., De Michele, C., 2004. Frequency analysis via copulas: Theoretical aspects and applications to hydrological events. Water Resour. Res., 40, W12511, doi:10.1029/2004WR003133.

Sang, Y. F., Wang, Z., Liu, C., 2013. Discrete wavelet-based trend identification in hydrologic time series. Hydrol. Process., 27, 2021–2031.

Sang, Y.F., D. Wang, J.C. Wu, Q.P. Zhu, L. Wang, 2009, The relation between periods' identification and noises in hydrologic series data, J. Hydrol., 368(1–4), 165–177.

Schepsmeier, U., Brechmann, E. C., 2015. Package CDVine, <http://CRAN.R-project.org/package=CDVine>.

Schröter, K., Kunz, M., Elmer, F., Mühr, B., and Merz, B., 2015. What made the June 2013 flood in Germany an exceptional event? A hydro-meteorological evaluation, Hydrol. Earth Syst. Sci., 19, 309-327, doi:10.5194/hess-19-309-2015,.

Shafer, B.A., Dezman, L.E., 1982. Development of a Surface Water Supply Index (SWSI) to Assess the Severity of Drought Conditions in Snowpack Runoff Areas. In: Preprints, Western SnowConf., Reno, NV, Colorado State University, pp. 164–175.

Shafer, B.A., Dezman, L.E., 1982. Development of a Surface Water Supply Index (SWSI) to assess the severity of drought conditions in snowpack runoff areas. Proceedings of the Western Snow Conference, pp. 164–175.

Shukla, S., Wood, A.W., 2008. Use of a standardized runoff index for characterizing hydrologic drought. Geophys. Res. Lett., 35, L02405. doi:10.1029/2007GL032487.

Sklar, A., 1959. Fonctions de Répartition à n Dimensions et Leurs Marges. Publ. Inst. Stat. Univ. Paris, 8, 229–231.

Stewart, I. T., Cayan, D. R., Dettinger, M. D., 2005. Changes toward earlier streamflow timing across western North America. J. Clim., 18, 1136–1155.

Swales, S., Harris, J.H., 1995. The expert panel assessment method (EPAM): a new tool for determining environmental flows in regulated rivers, In The Ecological Basis for River Management, edited by Harper DM, and Ferguson, A.J.D., pp. 125–134, John Wiley & Sons: New York.

Syed, T. H., Webster, P. J., Famiglietti, J. S., 2014. Assessing variability of evapotranspiration over the Ganga river basin using water balance computations. Water Resour. Res., 50, 2551–2565, doi:10.1002/2013WR013518.

Tatli, H., Türkes, M., 2011. Empirical Orthogonal Function analysis of the palmer drought indices. Agric. For. Meteorol., 151(7), 981–991.

Tennant, D.L., 1976. Instream flow requirements for fish, wildlife, recreation and related environmental resources. Fisheries, 1, 6–10.

Tharme, R. E., 2003. A global perspective on environmental flow assessment: emerging trends in the development and application of environmental flow methodologies for rivers. River Res. Applic., 19, 397–441. doi: 10.1002/rra.736.

Tharme, R.E., King, J.M., 1998. Development of the Building Block Methodology for Instream Flow Assessments, and Supporting Research on the Effects of Different Magnitude Flows on Riverine Ecosystems. Water Research Commission Report, No. 576/1/98.

Torrence, C., Compo, G.P., 1998. A practical guide to wavelet analysis. Bull. Am. Meteorol. Soc., 79, 61–78.

Tourre, Y. M., Jarlan, L., Lacaux, J. P., Rotela, C. H., Lafaye, M., 2008. Spatio-temporal variability of NDVI–precipitation over southernmost South America: possible linkages between climate signals and epidemics. Environ. Res. Lett., 3, 044008.

Townshend, J.R.G., 1994, Global data sets for land applications from the advanced very high resolution radiometer: an introduction. Int. J. Remote Sens., 15, 3319–3332.

Tsakiris, G., Vangelis, H., 2004. Towards a drought watch system based on spatial SPI. Water Resour. Manag., 18, 1–12.

Tucker, C.J., Pinzon, J. E., Brown, M. E., Slayback, D., Pak, E. W., Mahoney, R., Vermote, E., El Saleous, N., 2005. An Extended AVHRR 8-km NDVI Data Set Compatible with MODIS and SPOT Vegetation NDVI Data. Int. J. Remote Sens., 26(20), 4485–5598.

Türkes¸ , M., Tatli, H., 2009. Use of the standardized precipitation index (SPI) and a modified SPI for shaping the drought probabilities over Turkey. Int. J. Climatol., 29, 2270–2282

Udelhoven, T., Stellmes, M., del Barrio, G., Hill, J., 2009. Assessment of rainfall and NDVI anomalies in Spain (1989–1999) using distributed lag models. Int. J. Remote Sens, 30(8):1961–1976

Van Loon, A. F., 2015. Hydrological drought explained. WIREs Water, 2, 359–392, doi: 10.1002/wat2.1085

Van Rooy, M.P., 1965. A rainfall anomaly index independent of time and space. Notos, 14, 43.

Wang W, Anderson BT, Phillips N, Kaufmann RK, Potter C,Myneni RB (2006) Feedbacks of vegetation on summertime climate variability over the North American grasslands. Part I: statistical analysis. Earth Interactions, 10, 1–27.

Wang, G., Sun, S., and Mei, R., 2011. Vegetation dynamics contributes to the multi-decadal variability of precipitation in the Amazon region. Geophys. Res. Lett., 38, L19703.

Wang, J., Price, K.P., Rich, P.M., 2001. Spatial patterns of NDVI in response to precipitation and temperature in the central Great Plains. Int. J. Remote Sens., 22, 3827–3844.

Warrach-Sagi, K., Wulfmeyer, V., Grasselt, R., Ament, F., Simmer, C., 2008. Streamflow simulations reveal the impact of the soil parameterization. Meteorol. Z., 17, 751–762.

Weiss, J.L., Gutzler, D.S., Coonrod, J.E.A., Dahm, C.M., 2004. Seasonal and interannual relationships between vegetation and climate in central New Mexico, USA. J. Arid. Environ. 57, 507–534.

Vicente-Serrano, S. M., Pérez-Cabello, F., Lasanta, T., 2008. Assessment of radiometric correction techniques in analyzing vegetation variability and change using time series of Landsat images. Remote Sens. Environ., 112, 3916−3934.

Vicente-Serrano, S., López-Moreno, J., Beguería, S., Lorenzo-Lacruz, J., Azorin-Molina, C., Morán-Tejeda, E., 2012. Accurate Computation of a Streamflow Drought Index. J. Hydrol. Eng., 17(2), 318–332.

Wilhite, D.A., Buchanan-Smith, M., 2005. Drought as Hazard: Understanding the Natural and Social Context, in Proceeding of Drought and Water Crises: Science, Technology, and Management Issues, edited by Whilhite, D.A., pp. 3–29, CRC Press, Boca Raton, FL.

Wilhite, D.A., Glantz, M.H., 1985. Understanding the drought phenomenon: the role of definitions. Water Int., 10, 111–120.

Wu, H., Hayes, M.J., Welss, A., Hu, Q., 2001. An evaluation the standardized

precipitation index, the China-Z index and the statistical Z-score. Int. J. Climatol., 21, 745–758.

Yan, J., 2007. Enjoy the joy of copulas: with a package copula. J. Stat. Softw., 21(4), 1–21.

Yin, X.-A., Yang, Z.-F., Petts, G. E., 2011. Reservoir operating rules to sustain environmental flows in regulated rivers. Water Resour. Res., 47, W08509, doi:10.1029/2010WR009991.

Zehe, E., Graeff, T., Morgner, M., Bauer, A., Bronstert, A., 2010. Plot and field scale soil moisture dynamics and subsurface wetness control on runoff generation in a headwater in the Ore Mountains. Hydrol. Earth Syst. Sci., 14, 873-889, doi:10.5194/hess-14-873-2010.

Zhang, L., 2005. Multivariate hydrological frequency analysis and risk mapping, Ph.D. thesis, La. State Univ., Baton Rouge.

Zhang, L., Singh, V. P., 2007. Bivariate rainfall frequency distributions using Archimedean copulas. J. Hydrol., 332 (1–2), 93–109. doi:10.1016/ j.jhydrol.2006.06.033.

Zhang, L., Singh, V., 2006. Bivariate flood frequency analysis using the copula method. J. Hydrol. Eng., 11(2), 150–164, doi:10.1061/(ASCE)1084-0699(2006)11:2(150).

Zhang, Q., Xu, C.-Y., Becker, S., Jiang, T., 2006. Sediment and runoff changes in the Yangtze River basin during past 50 years. J. Hydrol., 331, 511–523

Zhang, X., Friedl, M. A., Schaaf, C. B., Strahler, A. H., Hodges, J. C. F., Gao, F., 2003. Monitoring vegetation phenology using MODIS. Remote Sens. Environ., 84, 471−475.

Zhang, X., Friedl, M. A., Schaaf, C. B., Strahler, A. H., Hodges, J. C. F., Gao, F., 2003. Monitoring vegetation phenology using MODIS. Remote Sens. Environ., 84, 471−475.

Zhang, Y., Hirabayashi, Y., Liu, S., 2012. Catchment-scale reconstruction of glacier mass balance using observations and global climate data: case study of the Hailuogou catchment, south-eastern Tibetan Plateau. J. Hydrol., 444–445,

146–160

Zhang, Y., Wei, H., Nearing, M.A., 2011. Effects of antecedent soil moisture on runoff modeling in small semiarid watersheds of southeastern Arizona. Hydrol. Earth Syst. Sci. Discuss., 8 (3), 6227–6256. http://dx.doi.org/10.5194/hessd-8-6227-2011.

Zhao, G., Mu, X., Hoermann, G., Fohrer, N., Xiong, M., Su, B.D., Li, X., 2012. Spatial patterns and temporal variability of dryness/wetness in the Yangtze River Basin, China. Quat. Int., 282, 5–13.

Zhou, L., Kaufmann, R. K., Tian, Y., Myneni, R. B., Tucker, C. J., 2003. Relation between interannual variations in satellite measures of northern forest greenness and climate between 1982 and 1999, J. Geophys. Res., 108(D1), 4004, doi:10.1029/2002JD002510.

Zhu, Z., Bi, J., Pan, Y., Ganguly, S., Anav, A., Xu, L., Samanta, A., Piao, S., Nemaniand, R. R., Myneni, R.B., 2013. Global data sets of vegetation leaf area index (LAI)3g and fraction of photosynthetically active radiation (FPAR)3g derived from global inventory modeling and mapping studies (GIMMS) Normalized Difference Vegetation Index (NDVI3g) for the period 1981 to 2011. Remote Sens., 5, 927–48.

Erklärung

Ich erkläre hiermit, dass ich die vorgelegte Dissertation selbst verfasst und mich keiner anderen als der von mir ausdrücklich bezeichneten Quellen und Hilfen bedient habe. Ich erkläre auch, dass ich an keiner anderen Stelle ein Prüfungsverfahren beantragt bzw. die Dissertation in dieser oder anderer Form bereits anderweitig als Prüfungsarbeit verwendet oder einer anderen Fakultät als Dissertation vorgelegt habe.

Heidelberg, February 25, 2016

Zhiyong Liu

Eidesstattliche Versicherung gemäß § 8 der Promotionsordnung der Naturwissenschaftlich-Mathematischen Gesamtfakultät der Universität Heidelberg

1. Bei der eingereichten Dissertation zu dem Thema

Improved Understanding of the Linkages and Interactions between Vegetation, Climate, Streamflow and Drought: Case Studies in Germany

handelt es sich um meine eigenständig erbrachte Leistung.

2. Ich habe nur die angegebenen Quellen und Hilfsmittel benutzt und mich keiner unzulässigen Hilfe Dritter bedient. Insbesondere habe ich wörtlich oder sinngemäß aus anderen Werken übernommene Inhalte als solche kenntlich gemacht.

3. Die Arbeit oder Teile davon habe ich wie folgt/bislang nicht[1)] an einer Hochschule des In- oder Auslands als Bestandteil einer Prüfungs- oder Qualifikationsleistung vorgelegt.

Titel der Arbeit: _____

Hochschule und Jahr: _____

Art der Prüfungs- oder Qualifikationsleistung: _____

4. Die Richtigkeit der vorstehenden Erklärungen bestätige ich.

5. Die Bedeutung der eidesstattlichen Versicherung und die strafrechtlichen Folgen einer unrichtigen oder unvollständigen eidesstattlichen Versicherung sind mir bekannt.

Ich versichere an Eides statt, dass ich nach bestem Wissen die reine Wahrheit erklärt und nichts verschwiegen habe.

Heidelberg March 03, 2016
Ort und Datum

Zhiyong Lin
Unterschrift

[1)] Nicht Zutreffendes streichen. Bei Bejahung sind anzugeben: der Titel der andernorts vorgelegten Arbeit, die Hochschule, das Jahr der Vorlage und die Art der Prüfungs- oder Qualifikationsleistung.

12/2012